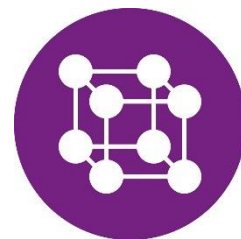




POLITECHNIKA POZNAŃSKA



Wydział Inżynierii Materiałowej i Fizyki Technicznej
Instytut Fizyki
Zakład Fizyki Molekularnej

Paulina Błaszkwicz

*Optymalizacja procesu syntezy i funkcjonalizacji nanocząstek złota
oraz określenie istotnych do zastosowań biomedycznych parametrów
fotofizycznych nanocząstek i ich układów hybrydowych z wybranymi
barwnikami*

Rozprawa doktorska

Promotor
prof. dr hab. Alina Dudkowiak

Promotor pomocniczy
dr inż. Michał Kotkowiak

Poznań 2022

*Serdecznie dziękuję
prof. dr hab. Alinie Dudkowiak
za przekazaną wiedzę, opiekę naukową
oraz cenną pomoc podczas realizacji pracy*

*Serdecznie dziękuję
dr inż. Michałowi Kotkowiak
za pomoc w realizacji części praktycznej pracy
oraz liczne dyskusje, cenne uwagi i wskazówki*

Spis skrótów i oznaczeń

Oznaczenie	Opis
AgNO ₃	azotan srebra
C-481	barwnik laserowy – 7-N,N-dimetyloamino-4-trifluorometylo-1,2-benzopiran (C ₁₄ H ₁₄ F ₃ NO ₂)
C-510	barwnik laserowy – 2,3,5,6-1H,4H-tetrahydro-9-(3-pirydylo)chinolizino[9,9a,1-gh]kumaryna (C ₂₀ H ₁₈ N ₂ O ₂)
C ₆ H ₈ O ₆	kwask askorbinowy
DCM	barwnik laserowy – pyran 4-(dicyjanometyleno)-2-metylo-6-(4-dimetyloaminostyryl)-4H-piran (C ₁₉ H ₁₇ N ₃ O)
DLS	dynamiczne rozpraszanie światła (ang. dynamic light scattering)
DPBF	wygaszacz tlenu singletowego – 1,3-difenylobenzofuran (C ₂₀ H ₁₄ O)
DPPC	1,2-dipalmitoilo-sn-glicero-3-fosfocholina (C ₄₀ H ₈₀ NO ₈ P)
DPPG	1,2-dipalmitoilo-sn-glicero-3-fosfo- <i>rac</i> -(1-glicerol) (C ₃₈ H ₇₄ O ₁₀ PNa)
FIT	technika całkowania skończonego (ang. finite integration technique)
FRET	försterowskie rezonansowe przekazywanie energii (ang. Förster Resonance Energy Transfer)
HAuCl ₄	kwask chlorozłotowy(III)
LIOAS	czasowo-rozdzielna laserowo-indukowana spektroskopia optoakustyczna (ang. time-resolved laser-induced optoacoustic spectroscopy)
LSPR	zlokalizowany powierzchniowy rezonans plazmonowy (ang. localized surface plasmon resonance)
NaBH ₄	borowodorek sodu
Na ₃ C ₆ H ₅ O ₇	cytrynian trisodowy
NaOH	wodorotlenek sodu
NPs	nanocząstki o kształcie kulistym (ang. nanoparticles)
NRs	prętopodobne nanocząstki (ang. nanorods)
NSET	nanocząstkowe powierzchniowe przekazywanie energii (ang. nanoparticle surface energy transfer)
PDD	diagnostyka fotodynamiczna (ang. photodynamic diagnostic)
PDT	terapia fotodynamiczna (ang. photodynamic therapy)
PEG-SH	poli(tlenek etylenu) z grupą tiolową
Pheide	feoforbid <i>a</i>

PTT	terapia fototermiczna (ang. photothermal therapy)
TEM	transmisyjna mikroskopia elektronowa (ang. transmission electron microscopy)
TEOS	ortokrzemian tetraetylu ($\text{Si}(\text{OC}_2\text{H}_5)_4$) (ang. tetraethyl orthosilicate)

Spis treści

Streszczenie	6
Abstract	9
1. Wstęp	11
2. Forma rozprawy doktorskiej oraz wkład doktoranta	17
3. Badane materiały oraz zastosowane techniki pomiarowe	19
4. Krótki opis badań	22
5. Podsumowanie	28
Literatura	30
Dorobek naukowy doktorantki	33
Załączniki	41
Oświadczenia współautorów o wkładzie w publikacje naukowe doktorantki	41
Przedruk publikacji [Błaszkiwicz, JL 2017]	47
Przedruk publikacji [Błaszkiwicz, JPCC 2020]	56
Przedruk publikacji [Błaszkiwicz, JPCC 2019]	71
Przedruk publikacji [Tim, JML 2022]	83

Streszczenie

Rozprawę doktorską stanowią spójne tematycznie, cztery artykuły naukowe, w których opisano wyniki badań sfunkcjonalizowanych nanocząstek oraz mieszanin hybrydowych typu sfunkcjonalizowane nanocząstki/barwniki. Przeprowadzone badania miały na celu zsyntezowanie i sfunkcjonalizowanie polimerem lub ditlenkiem krzemu nanocząstek złota o różnym kształcie, a następnie wytworzenie ich mieszanin z barwnikami laserowymi lub fotouczulaczem II generacji. Ww. układy scharakteryzowano określając wielkość nanostruktur, grubość ich otoczki i właściwości spektroskopowe oraz wyznaczając istotne dla zastosowań biomedycznych parametry fotofizyczne (m.in. wydajności emisji fluorescencji, wydajności generowania tlenu singletowego oraz konwersji energii wzbudzenia na ciepło). Ponadto, dla wybranych nanocząstek umieszczonych w modelowej błonie biologicznej zbadano jak obecność nanocząstek i lokalny wzrost temperatury, indukowany światłem, wpływają na oddziaływania pomiędzy składnikami błony i jej organizację.

Badania przeprowadzono wykorzystując techniki spektroskopowe i mikroskopowe, technikę Langmuira oraz metody obliczeniowe do weryfikacji wyników eksperymentalnych lub modeli teoretycznych.

Wyniki badań układów złożonych z sfunkcjonalizowanych polimerem, kulistych nanocząstek i barwników laserowych pokazały, że zmodyfikowany model nanocząstkowego powierzchniowego przekazywania energii, uwzględniający zmianę zdolności absorpcyjnej zależną od wielkości nanocząstek, jest podejściem najlepiej opisującym proces przekazywania energii w badanych układach, a wartość całki przekrywania determinuje wydajność tego procesu. Ponadto, powierzchnia otoczki polimerowej nanocząstek nie oddziałuje z barwnikami, jej grubość wpływa na efektywność dynamicznego superwygaszania emisji fluorescencji, a obserwowane zmiany wydajności fluorescencji barwników sugerują, że badane układy można wykorzystać do obrazowania kumulacji nanocząstek w układach biologicznych.

Dla układów typu sfunkcjonalizowane nieorganiczną krzemionką, prętopodobne nanocząstki z fotouczulaczem II generacji przeanalizowano proces przekazywania energii i jego wpływ na konkurencyjne procesy emisji fluorescencji oraz generowania tlenu singletowego. W badanych układach obserwowano dynamiczny mechanizm wygaszania fluorescencji oraz zależną od grubości otoczki efektywność wydzielania tlenu singletowego. Podjęto próbę skorelowania wzrostu wydajności generowania tlenu

singletowego z obliczoną wydajnością rozpraszania nanocząstek i zasugerowano, że w mieszaninach hybrydowych możliwe jest „pułapkowanie” przez barwniki dodatkowego światła rozproszonego przez nanocząstki, co powoduje zwiększenie ich skuteczności terapeutycznej.

Ze względu na terapeutyczny potencjał nanocząstek prętopodobnych z otoczką krzemionkową, oszacowano ich wydajność konwersji energii wzbudzenia na ciepło. Badania pokazały, że nanocząstki zamieniają, w czasie krótszym niż 200 ns, ok. 87-95% energii na ciepło (w zależności od grubości otoczki). Wyniki eksperymentalne porównano z obliczeniami teoretycznymi odpowiednich właściwości optycznych nanocząstek. Po raz pierwszy pokazano, że metodę optoakustyczną można wykorzystać do precyzyjnego oszacowania ilości energii zamienianej na ciepło przez nanocząstki, który to parametr ma istotne znaczenie dla ich potencjalnych zastosowań w fototermicznej terapii. Dodatkowo, metoda ta charakteryzuje się wysoką czułością i uniwersalnością, umożliwiając dopasowanie długości fali do zakresu spektralnego pasma zlokalizowanego powierzchniowego rezonansu plazmonowego.

Zbadano również nanocząstki prętopodobne, otoczone nietoksycznym polimerem, w modelowych błonach biologicznych utworzonych z fosfolipidów. Określono wpływ obecności i fotoaktywacji nanocząstek na stabilność i elastyczność monowarstwy lipidowej oraz zmiany jej morfologii i organizacji. Zdolność nanocząstek do generowania ciepła powoduje lokalny wzrost temperatury w ich otoczeniu, w wyniku indukowanego światłem efektu fototermicznego, zmieniając oddziaływania pomiędzy składnikami błony, co może wpływać na jej przepuszczalność i/lub integralność oraz wymaga dalszych badań w celu ustalenia mechanizmów transportu substancji leczniczych w błonach komórkowych oraz optymalnych warunków do stosowania nanocząstek w terapii fototermicznej.

Podczas prowadzonych badań opracowano i zoptymalizowano metody syntezy oraz funkcjonalizacji nanocząstek złota o różnych kształtach i rodzajach otoczek, wykorzystując materiały charakteryzujące się niską cytotoksycznością. W wyniku odpowiedniej funkcjonalizacji otrzymano nanocząstki stabilne w czasie. Natomiast, dobór warunków syntezy pozwolił na uzyskanie prętopodobnych nanocząstek wykazujących maksimum pasma ekstynkcji w obszarze 660 nm, tj. w zakresie tzw. okna terapeutycznego i pasma absorpcji wyselekcjonowanego fotouczulacza. Dla wytworzonych, sfunkcjonalizowanych nanocząstek i ich układów hybrydowych z

barwnikami określono parametry fotofizyczne istotne dla potencjalnych zastosowań w fotodynamicznej terapii, diagnostyce lub terapii fototermicznej.

Abstract

The dissertation consists of four thematically coherent scientific articles that describe the results of research on functionalized nanoparticles and hybrid mixtures of functionalized nanoparticles/dyes. The research carried out aimed at synthesizing and functionalizing gold nanoparticles of various shapes with a polymer or silicon dioxide, and then producing their mixtures with laser dyes or a second-generation photosensitizer. The aforementioned systems were characterized by determining the size of the nanostructures, the thickness of their coating, and spectroscopic properties, as well as the photophysical parameters relevant for biomedical applications (including efficiencies of fluorescence emission, singlet oxygen generation, and excitation energy to heat conversion). In addition, for selected nanoparticles introduced into a model biological membrane, we investigated how the presence of nanoparticles and a local increase in temperature, induced by light, affect the interactions between membrane components and their organization.

The study was carried out using spectroscopic and microscopic techniques, the Langmuir technique, and computational methods to verify experimental results or theoretical models.

The results of the study of systems composed of polymer-functionalized, spherical nanoparticles and laser dyes showed that the modified model of nanoparticle surface energy transfer, which takes into account the change in absorptivity depending on the size of the nanoparticles, is the approach that best describes the process of energy transfer in the studied systems, and the value of the spectral donor-acceptor overlap integral determines the efficiency of the process. In addition, the surface of the polymer coating of the nanoparticles does not interact with the dyes, its thickness affects the efficiency of dynamic super-quenching of fluorescence emission, and the observed changes in the fluorescence efficiency of the dyes suggest that the studied systems can be used for imaging the accumulation of nanoparticles in biological systems.

For systems of the type of inorganic silica-functionalized nanorods with a second-generation photosensitizer, the energy transfer process and its effect on the competing processes of fluorescence emission and singlet oxygen generation were analyzed. The dynamic mechanism of fluorescence quenching and the thickness-dependent efficiency of singlet oxygen release were observed in the studied systems. An attempt was made to correlate the increase in singlet oxygen generation efficiency with the calculated

scattering yields of the nanoparticles, and it was suggested that in hybrid mixtures it is possible for dyes to "trap" additional light scattered by nanoparticles, resulting in an increase in their therapeutic efficacy.

On the basis of the therapeutic potential of silica-coated nanorods, their efficiency in converting excitation energy into heat was estimated. The study showed that nanoparticles convert, in less than 200 ns, about 87-95% of the energy into heat (depending on the thickness of the coating). The experimental results were compared with theoretical calculations of the relevant optical properties of the nanoparticles. It was shown for the first time that the optoacoustic method can be used to accurately estimate the amount of energy converted to heat by nanoparticles, a parameter that is important for their potential applications in photothermal therapy. In addition, the method has high sensitivity and versatility, allowing the wavelength to match the spectral bandwidth of the localized surface plasmon resonance.

Nanorods coated with a nontoxic polymer were also investigated in biological model membranes formed from phospholipids. The effects of the presence and photoactivation of nanoparticles on the stability and flexibility of the lipid monolayer, as well as changes in its morphology and organization, were determined. The ability of nanoparticles to generate heat causes a local increase in temperature in their surroundings as a result of the light-induced photothermal effect altering the interactions between membrane components, which may affect membrane permeability and/or integrity, and requires further research to determine the mechanisms of transport of therapeutic substances in cell membranes and the optimal conditions for using nanoparticles in photothermal therapy.

During the conducted research, methods for the synthesis and functionalization of gold nanoparticles with different shapes and types of coatings, using materials characterized by low cytotoxicity, were developed and optimized. As a result of appropriate functionalization, stable nanoparticles over time were obtained. However, the selection of synthesis conditions made it possible to obtain nanorods that exhibit an extinction band maximum located in the 660 nm region, i.e., in the range of the so-called therapeutic window and the absorption band of the selected photosensitizer. Photophysical parameters relevant to potential applications in photodynamic therapy, diagnostics, or photothermal therapy were determined for synthesized functionalized nanoparticles and their hybrid systems with dyes.

1. Wstęp

Rozwój metod i możliwości wytwarzania nanomateriałów implikują postęp w zakresie udoskonalania i stosowania nowych procedur medycznych. Na wielu płaszczyznach prowadzone są badania interdyscyplinarne mające na celu znalezienie skutecznych metod diagnostycznych i/lub terapeutycznych wykorzystujących m.in. nanocząstki metaliczne [1,2] (np. złota [3], srebra [4]) lub magnetyczne [5]. Określenie właściwości fotofizycznych nanocząstek oraz zbadanie ich oddziaływań z materiałem biologicznym dostarcza istotnych informacji, pozwalających stworzyć coraz lepsze systemy dostarczania leków lub szczepionek oraz zidentyfikować wystąpienie potencjalnych skutków ubocznych. W pracy Błaszkiwicz i Kotkowiak [6], dokonano przeglądu literatury związanej z wykorzystaniem nanocząstek w różnych formach terapii z jednoczesną oceną skuteczności tych metod. Z przeprowadzonej analizy wynika, że nanocząstki są zdolne do poprawy indeksu terapeutycznego, m.in. w przypadku wykorzystania łączonych metod (np. terapii fotodynamicznej i fototermicznej), podczas ablacji falami radiowymi lub zastosowania hipertermii magnetycznej, hipertermii ultradźwiękowej czy chemioterapii [3,6,7].

Szczególnie interesującym obiektem badań są nanocząstki metali szlachetnych, których właściwości optyczne w zakresie widzialnym zdeterminowane są występowaniem zlokalizowanego plazmonowego rezonansu powierzchniowego (LSPR) [8]. W przypadku metalicznych nanocząstek, rezonansowe wzbudzenie wolnych elektronów przez promieniowanie elektromagnetyczne o określonej długości fali powoduje pojawienie się silnych pasm, charakterystycznych dla plazmonów powierzchniowych, obserwowanych w widmie ekstynkcji [9–11]. W zależności od warunków syntezy można uzyskać nanocząstki o różnym kształcie, wykazujące rezonans plazmonowy w określonych obszarach spektralnych [12–15]. Umożliwia to, stworzenie układu z odpowiednio dobranym barwnikiem i uzyskanie wzmocnienia emisji lub wzrost wydajności generowania tlenu singletowego, w wyniku oddziaływania pomiędzy barwnikiem a nanocząstką.

Struktura nanocząstki i jej funkcjonalizacja, zapewnia ochronę przed przedwczesną degradacją leku oraz determinuje jej powierzchnię właściwą, co stwarza możliwość transportowania wysokich stężeń leków do komórek docelowych. Natomiast, kształt nanostruktury wpływa na zdolność do uwalniania substancji aktywnej w odpowiednim miejscu [16–20]. W celu zwiększenia stopnia powinowactwa do określonych struktur

komórki, nanocząstki są funkcjonalizowane np. polimerami o różnej długości łańcucha węglowodorowego z aminową, karboksylową czy tiolową grupą funkcyjną lub tlenkami nieorganicznymi (np. SiO_2 , TiO_2), a także kwasami np. foliowym, oleinowym lub peptydami czy też DNA [6]. Poprawia to biokompatybilność nanocząstek i/lub stabilność kompleksów (koniugatów) będących nośnikami leków oraz zmniejsza ich cytotoksyczność [21]. Odpowiednia funkcjonalizacja nanocząstek, przeznaczonych do biomedycznych zastosowań, pozwala również na wyeliminowanie niektórych problemów, takich jak: agregacja nanocząstek, zwiększona kumulacja w ważnych organach (np. w wątrobie, nerkach i śledzionie), zbyt szybkie wydalanie z organizmu, brak selektywności wnikania do komórek zmienionych chorobowo, stabilność w temperaturze wyższej niż fizjologiczna (np. zastosowanie laserów i/lub hipertermia powodują lokalne podwyższenie temperatury, co może modyfikować ich właściwości) [10,22].

Do tej pory pojawiło się wiele doniesień naukowych związanych z wykorzystaniem nanocząstek metalicznych w zastosowaniach biomedycznych. Pierwszą, która przeprowadziła systematyczne badania zdolności generowania tlenu singletowego przez kompleksy hybrydowe, w skład których wchodziły nanocząstki srebra (Ag-NPs), była grupa Planasa i wsp. [23,24]. Przygotowano kompleksy nanocząstek (o tych samych średnicach i różnej grubości powłoki SiO_2) z barwnikiem, który został chemicznie dołączony do ich powierzchni. Dla określonej grubości powłoki, zaobserwowano wzrost wydajności generowania tlenu singletowego oraz intensywności fosforescencji barwnika w wyniku oddziaływania z Ag-NPs@ SiO_2 [19,25]. Chociaż wykazano, że dzięki funkcjonalizacji powierzchni NPs można uzyskać korzystniejsze parametry fotofizyczne kompleksu, istotne dla zastosowań diagnostycznych lub terapeutycznych, wiele fundamentalnych pytań dotyczących mechanizmu zwiększenia wydajności kwantowej wytwarzania tlenu singletowego pozostało bez odpowiedzi. Abadeer i in. [26] opisali metodę wytwarzania powłoki SiO_2 , o kontrolowanej grubości, na prętopodobnych nanocząstkach złota (Au-NRs). Dla barwnika kowalencyjnie przyłączonego do sfunkcjonalizowanych Au-NRs (Ag-NRs@ SiO_2), zbadano wpływ odległości między donorem a akceptorem energii na intensywność emisji fluorescencji barwnika. W pracy Fanga i in. [27] wykorzystano zieleń indocyjaninową, która absorbuje światło w zakresie bliskiej podczerwieni i jest doskonałym środkiem kontrastowym do obrazowania oraz barwnikiem do potencjalnego stosowania w terapii fototermicznej lub fotodynamicznej. Zaobserwowano wzmocnienie emisji luminescencji dla kompleksu barwnika z Au-

NRs@SiO₂, który można potencjalnie wykorzystać jako nowej generacji sondę fluorescencyjną do poprawy obrazowania tkanek. Natomiast, Xu i in. [22] sfunkcjonalizowali Au-NRs polimerem (PEG-SH – poli(tlenek etylenu) z grupą tiolową) i utworzyli kompleksy z chlorynami. Pokazali, że po wzbudzeniu światłem laserowym (kontrolując czas ekspozycji) z kompleksu barwnik/Au-NRs@PEG-SH uwalniane są chloryn, które następnie w komórkach patologicznych mogą zapoczątkować reakcję fotodynamiczną.

Do badania oddziaływań w błonach biologicznych wykorzystuje się membrany biomimetyczne jako układy modelowe. Jednym z najprostszych modeli membrany jest monowarstwa lipidowa wytworzona techniką Langmuira. Technika ta jest często stosowana do badań i oceny oddziaływania leków z modelową błoną biologiczną oraz do określania sposobu transportu i penetracji błony przez substancje farmakologicznie aktywne. Wprowadzenie do monowarstwy nanocząstek pozwala na określenie ich wpływu na organizację i zmiany właściwości błony, a ich funkcjonalizacja może dostarczyć informacji o oddziaływaniach ze środowiskiem lipidowym. Lin i in. [28] wykorzystali technikę Langmuira do badania oddziaływań nanocząstek o różnym kształcie w monowarstwie lipidowej, utworzonej z 1,2-dipalmitoilo-sn-glicero-3-fosfocholiny (DPPC). Zauważyli, że podczas sprężania warstwy, nanocząstki wykazują różną zdolnością penetracji i w różnym stopniu zaburzają warstwy DPPC. W pracy Torrano i in. [29] opisano oddziaływanie naładowanych nanocząstek złota (Au-NPs) z monowarstwami DPPC lub utworzonymi z ujemnie naładowanego fosfolipidu (DPPG – 1,2-dipalmitoilo-sn-glicero-3-fosfo-*rac*-(1-glicerolu). W przypadku monowarstwy DPPG–Au-NPs dominowały oddziaływania elektrostatyczne, a jej sprężystość, w zakresie ciśnień powierzchniowych odpowiadających rzeczywistym błonom komórkowym, zależała od ładunku NPs. Podczas gdy, w monowarstwie DPPC istotne zmiany w organizacji błony obserwowano tylko dla ujemnie naładowanych Au-NPs, w tym spadek elastyczności warstwy. Matshaya i in. [30] zbadali oddziaływania hydrofobowych, pokrytych kwasem oleinowym magnetycznych nanocząstek z nasyconymi lub nienasyconymi fosfolipidami. Obserwowano wyraźne zmniejszenie średniej powierzchni przypadającej na molekułę w przypadku warstw z nasyconych lipidów, a jej zwiększenie – podczas oddziaływania z nienasyconymi lipidami. Badania te potwierdzają, że istotne znaczenie dla oddziaływań ze składnikami błon biologicznych ma zarówno kształt jak i sposób funkcjonalizacji nanocząstek.

W badaniach opisanych w rozprawie doktorskiej, do funkcjonalizacji nanocząstek złota o kulistym kształcie (Au-NPs) oraz nanoprętów złota (Au-NRs) zastosowano hydrofilowy polimer z grupą tiolową (PEG-SH). Polimer ten wybrano ze względu na jego brak zdolności do adsorpcji białek na powierzchni oraz możliwość tworzenia wiązania kowalencyjnego ze złotem (Au-S), jak również w celu uzyskania wysokiej stabilności w roztworach [31] oraz biokompatybilności [32] sfunkcjonalizowanych nanocząstek. Au-NRs były także funkcjonalizowane nietoksyczną otoczką krzemionkową (SiO_2), która wpływa również na ich stabilność w roztworach alkoholowych oraz indeks terapeutyczny (względne bezpieczeństwo leku), definiowany jako stosunek ilości leku wywołującego efekt terapeutyczny do ilości wywołującej toksyczność. Istotne jest również, że SiO_2 w organizmach żywych degradowuje się do kwasu krzemowego i może być z nich łatwo usuwany [26,33,34].

Do badań wykorzystano także barwniki stosowane w laserach jako ośrodek czynny. Najpopularniejszymi barwnikami laserowymi są kumaryny, fluoresceiny i rodaminy charakteryzujące się wysoką wydajnością emisji fluorescencji, co pozwala rozpatrywać je jako potencjalne znaczniki fluorescencyjne. Szeroka dostępność i wybór barwników laserowych, stwarza możliwość dopasowania obszaru emisji barwnika do pasma LSPR nanocząstek złota i wytworzenia modelowych układów mieszanych (hybrydowych), w których można prześledzić proces przekazywania energii pomiędzy barwnikiem pełniącym rolę donora, a nanocząstką – akceptorem energii. Badania na prostych modelach i możliwość wyznaczenia istotnych parametrów fotofizycznych dla układów typu barwnik laserowy – nanocząstka, stanowiły inspirację i wstęp do rozwijania badań nad układami hybrydowymi dla potencjalnych zastosowań biomedycznych, w tym dla terapii fotodynamicznej (PDT) lub fototermicznej (PTT). Interesującym obiektem dalszych badań były układy złożone z barwnika-fotouczulacza i nanocząstek złota jako potencjalne, organiczno-nieorganiczne fotouczulacze III generacji. Metaliczne nanostruktury zdolne są do wzmacniania lub wygaszania emisji fluorescencji barwników znajdujących się w ich otoczeniu, modyfikując wydajność innych procesów dezaktywacji energii zachodzących z udziałem stanów singletowych i trypletowych barwnika. Najważniejszym wyznacznikiem przydatności układu w PDT jest zdolność do wydajnego obsadzenia stanu trypletowego barwnika, za pośrednictwem którego możliwa jest interakcja z materiałem biologicznym i/lub tlenem molekularnym oraz wytworzenie rodników organicznych i/lub reaktywnych form tlenu. Kluczowym zatem było poszukanie związków organicznych (barwników) spełniających wymagania doskonałych

fotouczulaczy i wykazujących pasma absorpcji/fluorescencji w obszarze pasma LSPR nanocząstek. Z tego punktu widzenia dobrymi kandydatami mogą być pochodne chlorofili [35]. Jednakże ich hydrofobowe właściwości powodują słabą rozpuszczalność w wodzie, a zatem ograniczają ich możliwość zastosowania w układach biologicznych. W takim przypadku, jednym z najbardziej obiecujących rozwiązań dostarczania leków [23,24] jest wytworzenie kompleksów (koniugatów) złożonych z hydrofobowych barwników połączonych kowalencyjnie z nanocząstkami, pełniącymi rolę nośników fotouczulaczy, w celu stworzenia rozpuszczalnego w wodzie układu zdolnego do indukowania reakcji fotodynamicznej.

PTT wykorzystuje związki lub materiały charakteryzujące się wysoką wydajnością konwersji energii promieniowania elektromagnetycznego na ciepło. Podstawą jej efektywnego działania jest zniszczenie komórek nieprawidłowych (chorobowo zmienionych) poprzez znaczący lokalny wzrost temperatury, następujący po naświetleniu światłem. Nanocząstki metaliczne ze względu na ich właściwości optyczne oraz zdolności do lokalnego generowania ciepła mogą być potencjalnie wykorzystywane w PTT. Ich oddziaływanie z promieniowaniem z zakresu widzialnego (do bliskiej podczerwieni) prowadzi do wzbudzenia plazmonów powierzchniowych (pasmo LSPR), co powoduje lokalny wzrost natężenia pola elektromagnetycznego, który generuje wzrost temperatury [6,36]. Lokalny wzrost temperatury stwarza warunki do selektywnego oddziaływania z komórkami (materiałem biologicznym), do których uprzednio wprowadzono nanocząstki metaliczne lub z komórkami znajdującymi się w ich bliskim otoczeniu. Z tego względu, istotny wydaje się opis na poziomie molekularnym oddziaływania nanocząstek z modelowymi błonami komórkowymi. Różne techniki wytwarzania modelowych błon oraz metody charakteryzowania umożliwiają określenie parametrów termodynamicznych i zmian organizacji ich składników np. pod wpływem oświetlenia nanocząstek wbudowanych w błony.

Badania, opisanie w rozprawie doktorskiej, miały na celu optymalizację procesu syntezy i dwóch różnych sposobów funkcjonalizacji nanocząstek złota o różnym kształcie oraz określenie właściwości i parametrów fotofizycznych sfunkcjonalizowanych nanocząstek i ich układów hybrydowych z wybranymi barwnikami, które są istotne dla ich potencjalnych zastosowań biomedycznych. Wyniki badań umożliwiły wyjaśnienie i zrozumienie procesów indukowanych światłem zachodzących na poziomie molekularnym oraz ich wpływ na zdolności fotouczulające i/lub fototermiczne badanych układów. Przeprowadzone badania dla organiczno-nieorganicznych układów

hybrydowych typu barwnik/sfunkcjonalizowana nanocząstka złota jako potencjalnych fotouczulaczy III generacji, zweryfikowały i dostarczyły ważnych informacji (dotyczących m.in. wydajności generowania tlenu singletowego i wygaszania fluorescencji oraz przekazywania energii pomiędzy nanocząstką a barwnikiem) istotnych z punktu widzenia możliwości ich zastosowania w PDT (lub diagnostyce fotodynamicznej (PDD)). Dla funkcjonalizowanych nanocząstek złota określono ich stabilność w czasie, oszacowano wydajność konwersji energii wzbudzenia na ciepło oraz oceniono ich przydatność w PTT. Przeanalizowano także, w jaki sposób lokalny wzrost temperatury spowodowany fotoaktywacją nanocząstek wpływa na właściwości i organizację modelowej błony biologicznej, co może mieć kluczowe znaczenie dla efektywności PTT oraz zrozumienia mechanizmu fotoindukowanego niszczenia komórek i/lub transportu substancji leczniczych przez błony.

Do badań wykorzystane zostały następujące techniki pomiarowe: stacjonarna spektroskopia absorpcyjna i emisyjna w obszarze UV-vis oraz czasowo-rozdzielna laserowo-indukowana spektroskopia optoakustyczna (LIOAS), transmisyjna mikroskopia elektronowa (TEM) i dynamiczne rozpraszanie światła (DLS). Wykorzystując technikę Langmuira, wyznaczono parametry termodynamiczne modelowych błon biologicznych, które zobrazowano za pomocą mikroskopii kąta Brewstera (BAM) i kamery termowizyjnej. Przeprowadzono również obliczenia w celu przeanalizowania mechanizmów procesu przekazywania energii stosując modele Försterowskiego rezonansowego przekazywania energii (FRET), nanocząstkowego powierzchniowego przekazywania energii (NSET) i zmodyfikowany model NSET. Eksperymenty wspomagane były także symulacjami komputerowymi właściwości optycznych nanocząstek z wykorzystaniem techniki całkowania skończonego (FIT).

Wyniki badań przedstawiono w czterech oryginalnych artykułach opublikowanych w czasopismach naukowych znajdujących się na liście *Journal Citation Reports* (JCR).

2. Forma rozprawy doktorskiej oraz wkład doktoranta

Rozprawę doktorską pt. *Optymalizacja procesu syntezy i funkcjonalizacji nanocząstek złota oraz określenie istotnych do zastosowań biomedycznych parametrów fotofizycznych nanocząstek i ich układów hybrydowych z wybranymi barwnikami* stanowią cztery oryginalne artykuły opublikowane w recenzowanych czasopismach naukowych indeksowanych na liście JCR*:

1. [Błaszkiwicz, JL 2017] P. Błaszkiwicz, M. Kotkowiak, A. Dudkowiak, *Fluorescence quenching and energy transfer in a system of hybrid laser dye and functionalized gold nanoparticles*, Journal of Luminescence 183 (2017), 303-310. (MNiSW 35, IF 2,732)
2. [Błaszkiwicz, JPCC 2020] P. Błaszkiwicz, M. Kotkowiak, E. Coy, A. Dudkowiak, *Tailoring fluorescence and singlet oxygen generation of a chlorophyll derivative and gold nanorods via a silica shell*, Journal of Physical Chemistry C 124(3) (2020), 2088-2095. (MEiN 140, IF 4,126)
3. [Błaszkiwicz, JPCC 2019] P. Błaszkiwicz, M. Kotkowiak, E. Coy, A. Dudkowiak, *Laser-induced optoacoustic spectroscopy studies of inorganic functionalized metallic nanorods*, Journal of Physical Chemistry C 123(44) (2019), 27181–27186. (MEiN 140, IF 4,189)
4. [Tim, JML 2022] B. Tim, P. Błaszkiwicz, M. Kotkowiak, *Altering model cell membranes by means of photoactivated organic functionalized gold nanorods*, Journal of Molecular Liquids 349 (2022), 118179-1-118179-7. (MEiN 100, IF 6,165)

*Liczba punktów przyznanych dla danego czasopisma przez Ministerstwo Nauki i Szkolnictwa Wyższego (MNiSW) lub Ministerstwo Edukacji i Nauki (MEiN) oraz współczynnik wpływu *Impact Factor* (IF) są zgodne z Systemem Informacji Naukowej Politechniki Poznańskiej (SIN PP).

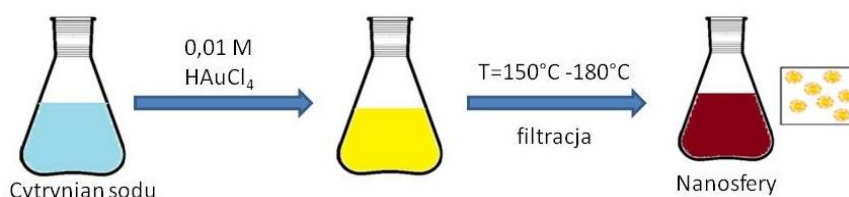
Zgodnie z załączonymi oświadczeniami współautorów, wkład doktorantki w powstanie publikacji był następujący:

1. [**Błaszkiwicz, JL 2017**] – doktorantka wykonała przegląd aktualnej literatury dotyczącej syntezy i funkcjonalizacji Au-NPs oraz brała udział w planowaniu badań. Przeprowadziła i zoptymalizowała syntezę oraz funkcjonalizację Au-NPs, przygotowała mieszaniny hybrydowe, a także scharakteryzowała badane układy wykorzystując metody spektroskopii absorpcyjnej i fluorescencyjnej. Uczestniczyła w analizie i dyskusji wyników pomiarowych oraz współredagowała tekst manuskryptu.
2. [**Błaszkiwicz, JPCC 2020**] – doktorantka brała udział w planowaniu badań, przeprowadziła syntezę oraz funkcjonalizację Au-NRs i przygotowała mieszaniny hybrydowe z fotouczulaczem II generacji. Określiła parametry spektralne oraz właściwości fotofizyczne Au-NRs i mieszanin hybrydowych. Przeprowadziła badania spektroskopowe, m.in. wykorzystując rozdzielną w czasie spektroskopię optoakustyczną. Brała udział w analizie i dyskusji wyników pomiarowych oraz współredagowała tekst manuskryptu.
3. [**Błaszkiwicz, JPCC 2019**] – doktorantka wykonała przegląd aktualnej literatury dotyczącej syntezy i funkcjonalizacji Au-NRs. Zaplanowała, zmodyfikowała oraz zoptymalizowała metodę syntezy i funkcjonalizacji Au-NRs. Przeprowadziła badania z wykorzystaniem stacjonarnych metod spektroskopowych. Doktorantka odpowiadała także za analizę i interpretację wyników oraz współredagowała tekst manuskryptu.
4. [**Tim, JML 2022**] – doktorantka zaplanowała, zmodyfikowała i przeprowadziła syntezę oraz funkcjonalizację Au-NRs, przygotowała roztwory wykorzystywane do wytworzenia warstw Langmuira. Uczestniczyła w analizie i dyskusji uzyskanych wyników oraz współredagowała tekst manuskryptu.

3. Badane materiały oraz zastosowane techniki pomiarowe

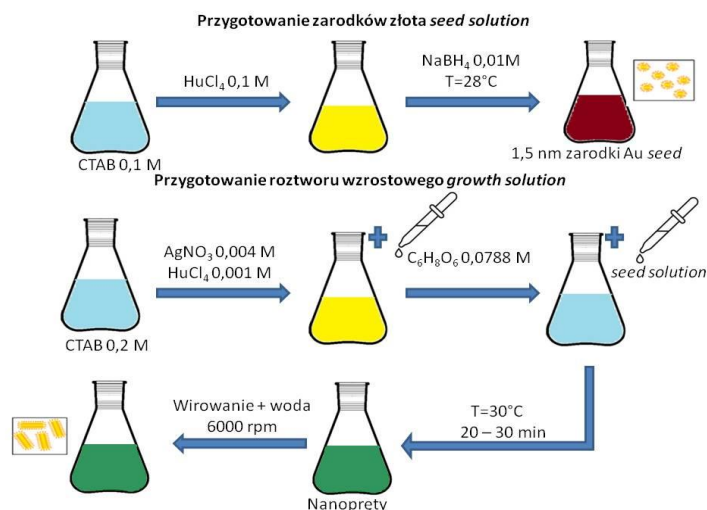
Przedmiotem opisanych badań w niniejszej rozprawie doktorskiej były sfunkcjonalizowane nanocząstki złota oraz układy hybrydowe typu barwnik/sfunkcjonalizowana nanocząstka. Do badań wybrano komercyjnie dostępne barwniki laserowe (C-481 – 7-N,N-dimetyloamino-4-trifluorometylo-1,2-benzopiran, C-510 – 2,3,5,6-1H,4H-tetrahydro-9-(3-pirydylo)chinolizino [9,9a,1-gh]kumaryna, DCM – 4-(dicyjanometyleno)-2-metylo-6-(4-dimetyloaminostyryl)-4H-piran) (Sigma Aldrich, Polska) oraz pochodną chlorofilu *a* – feoforbid *a* (Pheide) (Frontier Scientific, USA). Wygaszacz, 1,3-difenyloizobenzofuran (DPBF) (Sigma Aldrich, Polska) wykorzystano do wyznaczenia wydajności generowania tlenu singletowego, którą określono na podstawie kinetyk reakcji fotooksydacji. Fosfolipid – DPPC (Avanti Polar Lipids, Alabama) wybrano do wytworzenia modelowej błony biologicznej techniką Langmuira.

Au-NPs zostały otrzymane metodą *bottom-up* (rys. 1) w wyniku redukcji kwasu chlorozłotowego (III) (HAuCl_4) w obecności cytrynianu sodu ($\text{Na}_3\text{C}_6\text{H}_5\text{O}_7$) w rozpuszczalniku wodnym. Następnie został przeprowadzony proces ich funkcjonalizacji polimerem PEG-SH, o różnej masie cząsteczkowej ($M_w \approx 5000$ i $M_w \approx 10000$).



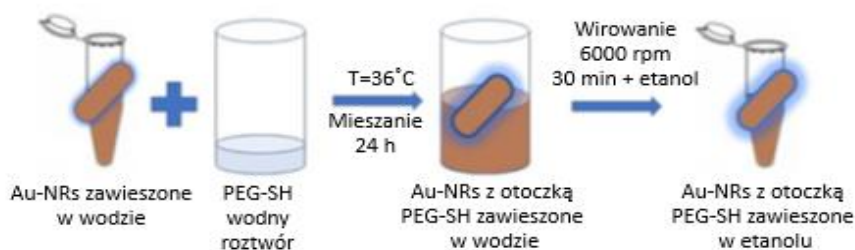
Rys. 1. Schemat syntezy kulistych nanocząstek złota.

Synteza Au-NRs była procesem dwuetapowym (rys. 2) z wykorzystaniem metody *seed-mediated growth*, podczas której ziarna złota koloidalnego są przyłączane do wcześniej otrzymanych kulistych rdzeni złota, wokół których tworzy się złota powłoka powodująca wzrost NRs. Au-NRs uzyskano wykorzystując, podobnie jak w przypadku Au-NPs, metodę *in situ bottom-up* oraz reakcję chemiczną polegającą na redukcji prekursora. Jako prekursor został użyty HAuCl_4 , a reduktorami były borowodorek sodu (NaBH_4) i kwas askorbinowy ($\text{C}_6\text{H}_8\text{O}_6$). W procesie syntezy wykorzystano sole srebra (AgNO_3), które pozwalają na uzyskanie odpowiedniego (pożądanego) stosunku długości do szerokości NRs.

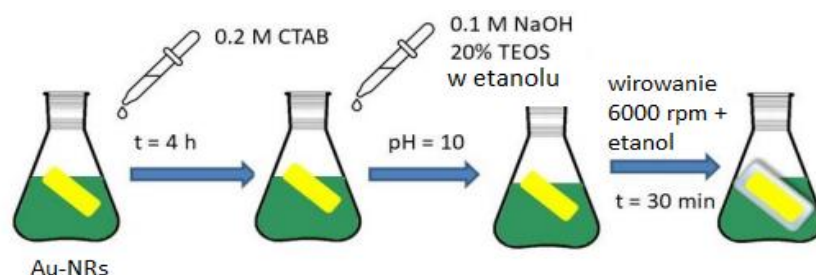


Rys. 2. Schemat syntezy prętopodobnych nanocząstek złota [Błaszkiwicz, JPCC 2019].

Funkcjonalizacja zmienia właściwości powierzchni nanocząstek w wyniku trwałego przyłączenia się molekuł określonych związków chemicznych. Na proces funkcyjalizacji nanocząstek ma wpływ rodzaj surfaktantu, natomiast kształt nanocząstek nie jest parametrem zmieniającym warunki reakcji. Organiczne otoczki polimerowe NPs i NRs otrzymano wykorzystując poli(tlenek etylenu) z grupą tiolową (PEG-SH) (rys. 3), w przypadku NRs o masie cząsteczkowej ($M_w \approx 2000$). Nieorganiczne powłoki krzemionkowe (SiO_2) o kontrolowanej grubości na powierzchni Au-NRs wytworzono, stosując ortokrzemian tetraetylu (TEOS) i wodorotlenek sodu (NaOH), przy wartości pH roztworu równej 10 (rys. 4).



Rys. 3. Schemat funkcyjalizacji nanoprętów złota z wytworzeniem otoczki PEG-SH.



Rys. 4. Schemat funkcyjalizacji nanoprętów złota z wytworzeniem otoczki SiO_2 [Błaszkiwicz, JPCC 2019].

Proces syntezy i funkcjonalizacji oraz badania spektroskopowe zostały przeprowadzone w laboratoriach Zakładu Fizyki Molekularnej na Wydziale Inżynierii Materiałowej i Fizyki Technicznej Politechniki Poznańskiej. Do badań wykorzystano: (i) spektroskopię absorpcyjną w obszarze UV-vis (scharakteryzowano właściwości spektralne sfunkcjonalizowanych nanocząstek i układów hybrydowych typu barwnik/sfunkcjonalizowana nanocząstka, w tym wyznaczono położenie pasm rezonansu plazmonowego nanocząstek i pasm absorpcji barwników, określono foto- i stabilności badanych układów oraz kinetyki fotooksydacji DPBF), (ii) spektroskopię emisyjną (określono wydajności wzmocnienia lub wygaszania emisji fluorescencji, wyznaczono czasy życia fluorescencji), (iii) rozdzielną w czasie spektroskopię optoakustyczną (LIOAS) (wyznaczono wydajności procesów niepromienistych, w tym generowania tlenu singletowego oraz oszacowano wydajności konwersji energii wzbudzenia na ciepło), (iv) technikę Langmuira (wyznaczono parametry termodynamiczne monowarstw jedno- i dwuskładnikowych oraz ich potencjał powierzchniowy), (v) mikroskopię kąta Brewstera (BAM) oraz kamerę termowizyjną (zobrazowano teksturę badanych monowarstw, rejestrowano rozkłady temperatury podczas naświetlania nanocząstek w warstwie). Wykonano również obliczenia wykorzystując modele FRET, NSET i zmodyfikowany NSET oraz symulacje komputerowe z wykorzystaniem techniki FIT.

Obrazy uzyskane za pomocą transmisyjnej mikroskopii elektronowej (TEM) pozwoliły na określenie wymiarów NPs oraz grubości powłok SiO₂ i zostały wykonane w Centrum NanoBiomedycznym Uniwersytetu im. Adama Mickiewicza w Poznaniu. Wielkość Au-NPs oraz grubość powłok PEG-SH zostały potwierdzone metodą dynamicznego rozpraszania światła (DLS), dostępną w Wielkopolskim Centrum Zaawansowanych Technologii w Poznaniu.

4. Krótki opis badań

Celem badań była optymalizacja procesu syntezy nanocząstek złota o różnym kształcie oraz ich funkcjonalizacji organiczną (PEG-SH) i nieorganiczną (SiO_2) otoczką, a także określenie parametrów spektralnych i fotofizycznych sfunkcjonalizowanych nanocząstek oraz układów hybrydowych utworzonych ze sfunkcjonalizowanych nanocząstek złota i wybranych barwników organicznych, istotnych dla potencjalnych zastosowań biomedycznych.

W pracy [Błaszkiwicz, JL 2017] przedstawiono procedurę syntezy kulistych nanocząstek złota (Au-NPs) o średnicy 15 nm, które sfunkcjonalizowano PEG-SH o różnych masach cząsteczkowych ($M_w \approx 5000$ i $M_w \approx 10000$). Zmodyfikowanie procesu funkcjonalizacji nanocząstek polimerem PEG-SH (rys. 3) polegało na wprowadzeniu zmiany w stosunkach molowych reagentów i wkraplaniu PEG-SH do roztworu nanocząstek, poddawanego działaniu ultradźwięków. Metodą dynamicznego rozpraszania światła potwierdzono grubość uzyskanej powłoki polimerowej (7 nm i 10 nm, odpowiednio, dla $M_w \approx 5000$ i $M_w \approx 10000$) na powierzchni Au-NPs. Wytworzona powłoka PEG-SH pozwoliła na kontrolowanie/oszacowanie odległości pomiędzy Au-NPs i barwnikami laserowymi, wybranymi do badań. Widmo ekstynkcji wykazało, że w etanolu Au-NP@PEG-SH były stabilne w czasie i nie agregowały (3 m-ce), a maksimum ich pasma ekstynkcji było zlokalizowane w obszarze 524 nm.

Następnie wytworzono mieszaniny hybrydowe złożone z Au-NP@PEG-SH i barwników organicznych, odpowiednio, kumaryny C-510, kumaryny C-481 lub pyranu (DCM). Mieszaniny hybrydowe wytwarzano utrzymując stałe stężenie barwnika (3×10^{-5} M) dla różnych stężeń Au-NPs@PEG-SH ((0; 0,8; 1,6; 2,4; 3,2; 4,0; 4,8; 5,6; 6,4; 7,2; 8) $\times 10^{-10}$ M). Barwniki dobrano w ten sposób, żeby absorbowały w obszarze pasma LSPR nanocząstek. Różniły się one wydajnością emisji fluorescencji oraz charakteryzowały się różną wartością całki przekrywania obliczoną na podstawie widm absorpcji akceptora i emisji donora.

Pokazano, że dla mieszaniny hybrydowej wraz ze wzrostem stężenia Au-NPs (wzrastała wartość ekstynkcji) malało natężenie fluorescencji barwników. Obserwowane zjawisko wygaszania fluorescencji badanych barwników przebiegało z różną kinetyką, o czym świadczą wartości stałej Sterna-Volmera ($2,08-5,25 K_{SV} \times 10^8 \text{ M}^{-1}$). Optymalna odległość, istotna dla procesu przekazywania energii, między donorem a akceptorem została wyznaczona wykorzystując różne teoretyczne modele matematyczne. Uzyskane

wyniki pokazały, że zarówno modele FRET i NSET (zaproponowany przez Perssona-Langa [37]) nie opisują poprawnie mechanizmu przekazywania energii dla układu barwnik/Au-NPs@PEG-SH. Okazało się, że zmodyfikowany model NSET przedstawiony przez Breshike-Riskowski-Strouse [38], uwzględniający zmianę zdolności absorpcyjnej zależną od wielkości nanocząstek, jest podejściem najlepiej opisującym proces przekazywania energii w badanych układach typu barwnik/Au-NPs@PEG-SH. Wyznaczone wartości wydajności wygaszania fluorescencji barwników były porównywalne do wydajności przekazywania energii, co oznacza, że powierzchnia powłoki polimerowej nanocząstek nie oddziaływała z barwnikami. Zwiększenie grubości otoczki z polimeru wpływało na efektywność dynamicznego superwygaszania emisji fluorescencji spowodowanej przenoszeniem energii pomiędzy barwnikami i nanocząstkami, niezależnie od rodzaju barwnika. Najwydajniejsze przekazywanie energii zaobserwowano dla układu hybrydowego charakteryzującego się najwyższą wartością całki przekrywania, niezależnie od wydajności fluorescencji barwnika, oznacza to, że obszar przekrywania się donora i akceptora jest najważniejszą zmienną do przewidywania przebiegu i wydajności tego procesu w układzie typu barwnik/Au-NPs@PEG-SH.

Wyniki badań pokazały, że całka przekrywania jest parametrem determinującym proces przeniesienia energii w badanych układach, a zastosowanie PEG-SH, który jest polimerem nietoksycznym i jednocześnie nieoddziałujący z barwnikami sprawia, że wydajności fluorescencji barwników laserowych zmieniają się proporcjonalnie do stężenia NPs, dlatego hybrydowy układ typu barwnik/Au-NPs@PEG-SH wydaje się obiecującym dla obrazowania i detekcji układów biologicznych.

Wyniki opisane w pracy [**Błaszkiwicz, JPCC 2020**] pokazują sposób otrzymywania Au-NRs podczas dwuetapowej reakcji syntezy. W procesie tym można uzyskać Au-NRs wykazujące batochromowe przesunięcia maksimum pasma LSPR, skorelowane ze wzbudzeniem drgań plazmonowych wzdłuż dłuższej osi nanoprętów, w zależności od ich wielkości (współczynnika kształtu). Podczas syntezy Au-NRs, dwuwarstwa CTAB zapobiega tworzeniu aglomeratów nanocząstek, a stężenie AgNO_3 wpływa na proces ich anizotropowego wzrostu oraz kontrolę stosunku długości do szerokości. Do dalszych badań wybrano Au-NRs, które wykazywały maksimum pasma ekstynkcji zlokalizowane w obszarze 660 nm, tj. w zakresie tzw. okna terapeutycznego i absorpcji pasma Q wyselekcjonowanego fotouczulacza.

Proces funkcjonalizacji Au-NRs i wytworzenie otoczki SiO₂ zostały przeprowadzone zgodnie z procedurą opisaną w pracy [Błaszkiwicz, JPCC 2019]. Na podstawie widm ekstynkcji stwierdzono, że w etanolu otrzymane Au-NRs@SiO₂ są stabilne w czasie i nie agregują (po 60 dniach). Kontrolowana grubość wytworzonej na powierzchni Au-NRs otoczki krzemionkowej (w zakresie od 6 do 14 nm) determinowała odległość między barwnikiem (donorem) a nanocząstką (akceptorem). Barwnikiem wybranym do utworzenia mieszaniny hybrydowej z Au-NRs@SiO₂ został fotouczulacz II generacji – pochodna chlorofilu *a* (Pheide), ze względu na znaczne przekrywanie się widma emisji fluorescencji Pheide z pasmem ekstynkcji Au-NRs, co stwarza warunki do efektywnego przenoszenia energii w badanym układzie.

Mieszaniny hybrydowe Pheide/Au-NRs@SiO₂ wytworzono zachowując ustalone stężenie barwnika ($1,65 \times 10^{-6}$ M) i zmieniając stężenie nanocząstek ((0; 1,33; 2,66; 4,00; 5,33; 6,66) $\times 10^{-11}$ M). Na podstawie przeprowadzonych badań, wyznaczono właściwości spektralne mieszanin hybrydowych i przeanalizowano proces przekazywania energii oraz jego wpływ na konkurencyjne procesy zachodzące z udziałem stanów singletowych i trypletowych (emisję fluorescencji i generowanie tlenu singletowego). Analiza procesu wygaszania fluorescencji wykazała liniową zależność Sterna-Volmera dla mieszanin hybrydowych Pheide/Au-NRs@SiO₂ o różnych grubościach otoczki krzemionkowej (6-14 nm), co sugeruje dynamiczny mechanizm wygaszania. Wartość stałej Sterna-Volmera malała wraz ze wzrostem grubości powłoki SiO₂ i osiągnęła najniższą wartość dla najgrubszej otoczki, niezależnie od zastosowanej długości fali wzbudzenia. W badanych układach hybrydowych zaobserwowano wygaszanie emisji fluorescencji Pheide wraz ze wzrostem stężenia Au-NRs, oznacza to, że efektywność procesów dezaktywacji w Pheide jest modyfikowana obecnością Au-NRs@SiO₂ i ich wzajemną odległością. Najważniejszym parametrem fotofizycznym, określającym właściwości fotouczulające i zdolność toksycznego działania Pheide/Au-NRs@SiO₂, jest wydajność generowania tlenu singletowego. Stosując dwie niezależne metody (LIOAS oraz spektrometryczną pozwalającą wyznaczyć kinetyki fotodegradacji DPBF), pokazano, że mieszaniny hybrydowe typu barwnik/Au-NRs@SiO₂ mogą efektywniej generować tlen singletowy niż same barwniki. Wydajność generowania tlenu singletowego mieszanin hybrydowych zależała od grubości powłoki SiO₂ i stężenia Au-NRs. Okazało się, że najwyższą wartość generowania tlenu singletowego zaobserwowano dla stężenia $1,33 \times 10^{-11}$ M Au-NRs i powłoki krzemionkowej o grubości 14 nm. Uzyskany współczynnik wzmocnienia wyniósł około 8-11%. Eksperymentalne wyniki zostały uzupełnione symulacjami

komputerowymi (FIT) wykorzystanymi do obliczenia wydajności rozpraszania Au-NRs (tj. frakcji światła rozproszonego na strukturach Au-NRs). Z przeprowadzonych obliczeń teoretycznych daleko zasięgowych właściwości Au-NRs wynika, że w mieszaninach hybrydowych prawdopodobne jest „pułapkowanie” przez barwniki dodatkowego światła rozproszonego przez NRs. Zasugerowano zatem, że daleko zasięgowe właściwości optyczne Au-NRs mogą wyjaśniać obserwowany efekt wzmocnienia wydajności generowania tlenu singletowego.

W pracy [Błaszkiwicz, JPCC 2019] opisano modyfikację i optymalizację dwuetapowej reakcji syntezy oraz procesu funkcjonalizacji Au-NRs. Podczas procesu syntezy, wprowadzono modyfikacje zaproponowane przez Nikoobakth’a i in. [39], m.in. chłodzono wodę w celu przygotowania NaBH_4 , przechowywano zarodki złota w temperaturze 28°C oraz określono odpowiednie stężenie AgNO_3 pozwalające na precyzyjne kontrolowanie rozmiaru NRs. Po procesie syntezy, produkt reakcji został odpowiednio sfracjonowany i oczyszczony poprzez wirowanie oraz usunięcie supernatantu. Badania mikroskopowe pozwoliły oszacować rozmiar NRs (długość $(53,2 \pm 1,8)$ nm, szerokość $(23,6 \pm 1,3)$ nm). Otrzymane Au-NRs charakteryzowały się maksimum pasma ekstynkcji przy 660 nm, tj. w zakresie tzw. okna terapeutycznego.

Wytworzenie powłoki krzemionkowej (SiO_2) na powierzchni Au-NRs przeprowadzono modyfikując i optymalizując metodę zaproponowaną przez grupę Liz-Marzán [40–42]. Podczas funkcjonalizacji wprowadzono pewne modyfikacje procesu, tj. po odwirowaniu i oczyszczeniu NRs, dodano ponownie surfaktant w odpowiednich stężeniach w celu kontrolowania procesu wzrostu krzemionki, monitorowano wartość pH w trakcie trwania całego procesu, zmieniono także rozpuszczalnik dla silanu, natomiast transfer Au-NRs do etanolu przeprowadzono po wcześniejszym frakcjonowaniu i oczyszczeniu poprzez wirowanie oraz usunięcie supernatantu. W efekcie zastosowanych modyfikacji, otrzymano otoczki o zdefiniowanych, kontrolowanych grubościach (6, 8, 12, 14 nm).

Nanocząstki metaliczne są zdolne do absorbowania energii i zamiany jej na ciepło, co ma ogromne znaczenie dla potencjalnego ich zastosowania w PTT. Badania przeprowadzone metodą LIOAS umożliwiły oszacowanie wydajności konwersji energii wzbudzenia na ciepło. Nie zarejestrowano istotnych różnic w widmach ekstynkcji Au-NRs@ SiO_2 , przed i po pomiarach LIOAS, co oznacza, że energia impulsu laserowego (rzędu μJ) przy długości fali 668 nm nie powodowała degradacji (zmiany kształtu) nanocząstek. Jako odnośnik kalorymetryczny zastosowano Ni-pochodną chlorofilu

absorbującą w zakresie pasma LSPR. Metodę LIOAS wykorzystano do określenia jaka część energii wzbudzenia została zamieniona na ciepło przez Au-NRs@SiO₂, w czasach krótszych niż czasowa zdolność rozdzielcza aparatury (tj. poniżej 200 ns). Sygnały LIOAS wykazywały liniową zależność od energii lasera i na ich podstawie oszacowano, że Au-NRs@SiO₂ zamieniają ok. 87-95% energii wzbudzenia na ciepło (dla grubości otoczki SiO₂ wynoszącej odpowiednio 6-14 nm). Wyniki eksperymentalne skorelowano z obliczeniami teoretycznymi odpowiednich właściwości optycznych Au-NRs@SiO₂ i uzyskano porównywalne wartości. W pracy, po raz pierwszy wykazano, że metodę LIOAS można wykorzystać do precyzyjnego oszacowania ilości energii zamienianej na ciepło przez nanocząstki sfunkcjonalizowane otoczką nieorganiczną o różnej grubości, zawieszane w rozpuszczalnikach organicznych. Pokazano, że metoda LIOAS oferuje możliwość wyznaczenia istotnego parametru dla potencjalnych zastosowań nanocząstek w PTT, ponadto, charakteryzuje się wysoką czułością i możliwością wybrania długości fali, co można wykorzystać przy wzbudzaniu dowolnego pasma LSPR.

Obiektem badań w pracy [Tim, JML 2022] były Au-NRs, wykazujące maksimum ekstynkcji zlokalizowane w obszarze 660 nm. Funkcjonalizację Au-NRs polimerem PEG-SH ($M_w \approx 2000$) przeprowadzono wykorzystując zmodyfikowaną metodę opisaną w [Błaszkiwicz, JL 2017]. PEG-SH tworzy organiczną otoczkę, jest nietoksyczny, bezpieczny dla organizmów żywych i często stosowany jako nośnik leków, w kosmetykach oraz jako składnik szczepionek. Do wytworzenia błony biologicznej wybrano fosfolipid DPPC, który zwykle używany jest do badań modelowych, tworzenia lipidów lub dwuwarstw. DPPC jest także wrażliwy na zmiany temperatury, dlatego istotne było sprawdzenie jak lokalne wzbudzenie światłem NRs, powodujące wzrost temperatury, wpłynie na formowanie warstwy, jej stabilność i organizację.

Na wannie Langmuira wytworzono monowarstwy jedno- (DPPC) lub dwuskładnikowe (DPPC z Au-NRs@PEG-SH), porównywano ich parametry termodynamiczne oraz określono oddziaływania lipidów z NRs, bez i podczas ich oświetlania. Po wzbudzeniu światłem, ze względu na zachodzący w Au-NRs efektywny proces konwersji energii na ciepło, obserwowano na obrazach termowizyjnych stopniowy wzrost temperatury monowarstwy, powodowany przez lokalny wzrost temperatury w otoczeniu Au-NRs. Monowarstwy oświetlano światłem o długości fali charakterystycznej dla pasma LSPR Au-NPs. Dla ciśnień powierzchniowych powyżej 8 mN/m, izoterma oraz potencjał powierzchniowy pokazały, że wzrost powierzchni zajmowanej przez molekuly DPPC nie był związany ze zmianą ułożenia fosfolipidów, lecz raczej

spowodowany zmianą wzajemnych odległości między nimi w wyniku oświetlenia błony. Po oświetleniu monowarstwa DPPC–Au-NRs@PEG-SH, przy ciśnieniu powierzchniowym porównywalnym z panującym w natywnej błonie komórkowej ($30 \text{ mN}\cdot\text{m}^{-1}$), była stabilniejsza i bardziej elastyczna, w porównaniu z nieoświetloną. Ponadto, modelowa błona usztywniała się po 40 min od osiągnięcia ciśnienia powierzchniowego $30 \text{ mN}\cdot\text{m}^{-1}$, co świadczy o stabilizacji w czasie oddziaływań pomiędzy molekułami DPPC. Obrazy BAM potwierdziły różnice w morfologii powierzchni dla warstwy Langmuira bez i po oświetleniu. Zaobserwowano, że Au-NRs@PEG-SH nie stabilizują monowarstwy w czasie, natomiast wydaje się, że wzrost temperatury warstwy po oświetleniu, ze względu na oddziaływania odpychające między molekułami DPPC, powoduje jej stabilizację. Przeprowadzone badania pokazały, że niewielka ilość Au-NRs@PEG-SH w warstwie oraz oświetlenie ich światłem o odpowiedniej długości fali, zmienia stabilność i wywołuje zmiany w upakowaniu oraz organizacji lipidów w modelowych błonach komórkowych. Wydaje się, że wywołane efektem fototermicznym zmiany organizacji lipidów mogą wpływać na przepuszczalność i/lub integralność błony, co wymaga dalszych badań w celu ustalenia warunków optymalnych do stosowania NRs w PTT.

5. Podsumowanie

Przeprowadzone badania, opisane w niniejszej rozprawie doktorskiej, miały na celu wytworzenie, sfunkcjonalizowanie i scharakteryzowanie nanocząstek złota o różnych kształtach oraz ich układów hybrydowych wytworzonych z nanocząstek i wybranych barwników, w tym wyznaczenie jakościowych i ilościowych parametrów fotofizycznych (m.in. stabilności w czasie, określenia ilości energii zamienianej na ciepło, wydajności fluorescencji, wydajności generowania tlenu singletowego). Pozwoliło to ocenić możliwości projektowania i wykorzystania badanych układów do selektywnego obrazowania lub uczulania struktur biologicznych, wykorzystując materiały o niskiej cytotoksyczności. Przeanalizowano również wpływ fotoaktywacji nanocząstek złota na modelowe błony biologiczne, biorąc pod uwagę ich potencjał aplikacyjny w fototermicznej terapii.

Najważniejsze uzyskane osiągnięcia to:

- opracowanie i zoptymalizowanie warunków syntezy nanocząstek złota o różnych geometriach,
- modyfikacja procesu funkcjonalizacji nanocząstek złota z wykorzystaniem PEG-SH oraz SiO₂,
- wykazanie, że powierzchnia warstwy polimerowej nanocząstek sferycznych nie oddziałuje z barwnikami, a zwiększenie grubości warstwy polimeru wpływa na efektywność dynamicznego superwygaszania fluorescencji,
- dopasowanie właściwego modelu teoretycznego do opisu procesu przekazywania energii pomiędzy nanocząstką sferyczną (akceptorem) a barwnikiem (donorem),
- pokazanie, że powłoka krzemionkowa wytworzona na powierzchni nanocząstek prętopodobnych wpływa zarówno na proces przekazywania energii między barwnikiem a nanocząstką oraz wydajność generowania tlenu singletowego,
- wskazanie, że w mieszaninach hybrydowych prawdopodobne jest „pułapkowanie” przez barwniki dodatkowego światła rozproszonego przez nanocząstki,
- wykorzystanie metody optoakustycznej do oszacowania wydajności konwersji energii wzbudzenia na ciepło przez nanocząstki oraz porównanie wyników eksperymentalnych z obliczonymi,

- wykazanie, że lokalny wzrost temperatury indukowany w wyniku oświetlenia nanocząstek wpływa na elastyczność, stabilność i organizację modelowej błony biologicznej.

Podsumowując (i) wytworzono układy charakteryzujące się wydajniejszym generowaniem tlenu singletowego oraz efektywną konwersją energii na ciepło, (ii) podjęto próbę wyjaśnienia mechanizmów promienistych i bezpromienistych procesów dezaktywacji energii oraz dopasowano teoretyczny model, pozwalający na opisanie procesów przekazywania energii w układach hybrydowych typu barwnik/nanocząstka złota, a także (iii) pokazano zmiany właściwości modelowej błony biologicznej pod wpływem lokalnie generowanego ciepła w wyniku fotoaktywowania nanocząstek.

Wyniki badań dostarczyły istotnych informacji o właściwościach fotofizycznych badanych, funkcjonalizowanych nanocząstek i ich układów hybrydowych oraz wskazały na potencjalną możliwość ich wykorzystania w biomedycznych zastosowaniach.

Literatura

- [1] E. Locatelli, I. Monaco, M. Franchini, RSC Advances applications in nanomedicine, RSC Adv. 5 (2015) 21681–21699.
- [2] X. Huang, M.A. El-Sayed, Gold nanoparticles: Optical properties and implementations in cancer diagnosis and photothermal therapy, J. Adv. Res. 1 (2010) 13–28.
- [3] M.R.K. Ali, Y. Wu, M.A. El-Sayed, Gold Nanoparticle-Assisted Plasmonic Photothermal Therapy Advances Towards Clinical Application, J. Phys. Chem. C. 123 (2019) 15375–15393.
- [4] B. Khlebtsov, E. Panfilova, V. Khanadeev, O. Bibikova, G. Terentyuk, A. Ivanov, et al., Nanocomposites containing silica-coated gold-silver nanocages and Yb-2,4-dimethoxyhematoporphyrin: Multifunctional capability of IR-luminescence detection, photosensitization, and photothermolysis, ACS Nano. 5 (2011) 7077–7089.
- [5] K. Kucharczyk, K. Kaczmarek, A. Jozefczak, M. Slachcinski, A. Mackiewicz, H. Dams-Kozłowska, Hyperthermia treatment of cancer cells by the application of targeted silk/iron oxide composite spheres, Mater. Sci. Eng. C. 120 (2021) 111654.
- [6] P. Błaszkiwicz, M. Kotkowiak, Gold-based nanoparticles systems in phototherapy - current strategies, Curr. Med. Chem. 25 (2018) 5914–5929.
- [7] J. Nam, S. Son, L.J. Ochyl, R. Kuai, A. Schwendeman, J.J. Moon, Chemophotothermal therapy combination elicits anti-tumor immunity against advanced metastatic cancer, Nat. Commun. 9 (2018) 1–13.
- [8] L. Bai, X. Liu, M. Li, K. Guo, M. Luoshan, Y. Zhu, et al., Plasmonic Enhancement of the Performance of Dye-sensitized Solar Cells by Incorporating Hierarchical TiO₂ Spheres Decorated with Au Nanoparticles, Electrochim. Acta. 190 (2016) 605–611.
- [9] I.H. El-Sayed, X. Huang, M.A. El-Sayed, Surface plasmon resonance scattering and absorption of anti-EGFR antibody conjugated gold nanoparticles in cancer diagnostics: Applications in oral cancer, Nano Lett. 5 (2005) 829–834.
- [10] J.L. Li, M. Gu, Gold-nanoparticle-enhanced cancer photothermal therapy, IEEE J. Sel. Top. Quantum Electron. 16 (2010) 989–996.
- [11] S. He, M.W.C. Kang, F.J. Khan, E.K.M. Tan, M.A. Reyes, J.C.Y. Kah, Optimizing gold nanostars as a colloid-based surface-enhanced Raman scattering (SERS) substrate, J. Opt. 17 (2015) 1–13.
- [12] C. Carrillo-Carrión, R. Martínez, M.F. Navarro Poupard, B. Pelaz, E. Polo, A. Arenas-Vivo, et al., Aqueous Stable Gold Nanostar/ZIF-8 Nanocomposites for Light-Triggered Release of Active Cargo Inside Living Cells, Angew. Chemie - Int. Ed. 58 (2019) 7078–7082.
- [13] C. Fernández-López, C. Mateo-Mateo, R.A. Álvarez-Puebla, J. Pérez-Juste, I. Pastoriza-Santos, L.M. Liz-Marzán, Highly controlled silica coating of PEG-capped metal nanoparticles and preparation of SERS-encoded particles, Langmuir. 25 (2009) 13894–13899.

- [14] B. Pelaz, V. Grazu, A. Ibarra, C. Magen, P. Del Pino, J.M. De La Fuente, Tailoring the synthesis and heating ability of gold nanoprisms for bioapplications, *Langmuir*. 28 (2012) 8965–8970.
- [15] A. Gole, C.J. Murphy, Seed-mediated synthesis of gold nanorods: role of the size and nature of the seed, *Chem. Mater.* 16 (2004) 3633–3640.
- [16] N.S. Abadeer, C.J. Murphy, Recent Progress in Cancer Thermal Therapy Using Gold Nanoparticles, *J. Phys. Chem. C*. 120 (2016) 4691–4716.
- [17] X. Huang, P.K. Jain, I.H. El-Sayed, M.A. El-Sayed, Plasmonic photothermal therapy (PPTT) using gold nanoparticles, *Lasers Med. Sci.* 23 (2008) 217–228.
- [18] D. Jaque, L. Martínez Maestro, B. del Rosal, P. Haro-Gonzalez, A. Benayas, J.L. Plaza, et al., Nanoparticles for photothermal therapies, *Nanoscale*. 6 (2014) 9494–9530.
- [19] Y. Tian, S. Luo, H. Yan, Z. Teng, Y. Pan, L. Zeng, et al., Gold nanostars functionalized with amine-terminated PEG for X-ray/CT imaging and photothermal therapy, *J. Mater. Chem. B*. 3 (2015) 4330–4337.
- [20] X. Ye, H. Shi, X. He, K. Wang, D. Li, P.Q. Qiu, Gold nanorod-seeded synthesis of Au@Ag/Au nanospheres with broad and intense near-infrared absorption for photothermal cancer therapy, *J. Mater. Chem. B*. 2 (2014) 3667–3673.
- [21] J. Li, B. Zhu, Z. Zhu, Y. Zhang, X. Yao, S. Tu, et al., Simple and rapid functionalization of gold nanorods with oligonucleotides using an mPEG-SH/Tween 20-assisted approach, *Langmuir*. 31 (2015) 7869–7876.
- [22] Y. Xu, R. He, D. Lin, M. Ji, J. Chen, Laser beam controlled drug release from Ce6–gold nanorod composites in living cells: a FLIM study, *Nanoscale*. 7 (2015) 2433–2441.
- [23] O. Planas, N. Macia, S. Nonell, B. Heyne, Distance-dependent plasmon-enhanced singlet oxygen production and emission for bacterial inactivation, *J. Am. Chem. Soc.* 138 (2016) 2762–2768.
- [24] N. Macia, R. Bresoli-Obach, S. Nonell, B. Heyne, Hybrid silver nanocubes for improved plasmon-enhanced singlet oxygen production and inactivation of bacteria, *J. Am. Chem. Soc.* 141 (2019) 684–692.
- [25] B. Wu, D. Liu, S. Mubeen, T.T. Chuong, M. Moskovits, G.D. Stucky, Anisotropic growth of TiO₂ onto gold nanorods for plasmon-enhanced hydrogen production from water reduction, *J. Am. Chem. Soc.* 138 (2016) 1114–1117.
- [26] N.S. Abadeer, M.R. Brennan, W.L. Wilson, C.J. Murphy, Distance and plasmon wavelength dependent fluorescence of molecules bound to silica-coated gold nanorods, *ACS Nano*. 8 (2014) 8392–8406.
- [27] S. Fang, C. Li, J. Lin, H. Zhu, D. Cui, Y. Xu, et al., Gold nanorods-based theranostics for simultaneous fluorescence/two-photon luminescence imaging and synergistic phototherapies, *J. Nanomater.* 4 (2016) 1–10.
- [28] X. Lin, Y.Y. Zuo, N. Gu, Shape affects the interactions of nanoparticles with pulmonary surfactant, *Sci. China Mater.* 58 (2015) 28–37.
- [29] A.A. Torrano, Â.S. Pereira, O.N. Oliveira, A. Barros-Timmons, Probing the

- interaction of oppositely charged gold nanoparticles with DPPG and DPPC Langmuir monolayers as cell membrane models, *Colloids Surfaces B Biointerfaces*. 108 (2013) 120–126.
- [30] T.J. Matshaya, A.E. Lanterna, A.M. Granados, R.W.M. Krause, B. Maggio, R. V. Vico, Distinctive interactions of oleic acid covered magnetic nanoparticles with saturated and unsaturated phospholipids in langmuir monolayers, *Langmuir*. 30 (2014) 5888–5896.
- [31] F. Schulz, W. Friedrich, K. Hoppe, T. Vossmeier, H. Weller, H. Lange, Effective PEGylation of gold nanorods, *Nanoscale*. 8 (2016) 7296–7308.
- [32] P. Pallavicini, E. Cabrini, G. Cavallaro, G. Chirico, M. Collini, L. D’Alfonso, et al., Gold nanostars coated with neutral and charged polyethylene glycols: A comparative study of in-vitro biocompatibility and of their interaction with SH-SY5Y neuroblastoma cells, *J. Inorg. Biochem.* 151 (2015) 123–131.
- [33] C. Wu, Q. Xu, Stable and functionable mesoporous silica-coated gold nanorods as sensitive localized surface plasmon resonance (LSPR) nanosensors, *Langmuir*. 25 (2009) 9441–9446.
- [34] A. Khanal, C. Ullum, C.W. Kimbrough, N.C. Garbett, J.A. Burlison, M.W. McNally, et al., Tumor targeted mesoporous silica-coated gold nanorods facilitate detection of pancreatic tumors using Multispectral optoacoustic tomography, *Nano Res.* 8 (2015) 3864–3877.
- [35] A.B. Ormond, H.S. Freeman, Dye sensitizers for photodynamic therapy, *Materials (Basel)*. 6 (2013) 817–840.
- [36] B. Zhang, L. Sun, Artificial photosynthesis: Opportunities and challenges of molecular catalysts, *Chem. Soc. Rev.* 48 (2019) 2216–2264.
- [37] B.N.J. Persson, N.D. Lang, Electron-hole-pair quenching of excited states near a metal, *Phys. Rev. B*. 26 (1982) 5409–5415.
- [38] C.J. Breshike, R.A. Riskowski, G.F. Strouse, Leaving Foerster resonance energy transfer behind: Nanometal surface energy transfer predicts the size-enhanced energy coupling between a metal nanoparticle and an emitting dipole, *J. Phys. Chem. C*. 117 (2013) 23942–23949.
- [39] B. Nikoobakht, A. El Sayed, Preparation and growth mechanism of gold nanorods (NRs) using seed-mediated growth method, *Chem. Mater.* 15 (2003) 1957–1962.
- [40] A. Guerrero-Martínez, J. Pérez-Juste, L.M. Liz-Marzán, Recent progress on silica coating of nanoparticles and related nanomaterials, *Adv. Mater.* 22 (2010) 1182–1195.
- [41] L.M. Liz-Marzán, M. Giersig, P. Mulvaney, Synthesis of nanosized gold-silica core-shell particles, *Langmuir*. 12 (1996) 4329–4335.
- [42] C. Hanske, M.N. Sanz-Ortiz, L.M. Liz-Marzán, Silica-coated plasmonic metal nanoparticles in action, *Adv. Mater.* 30 (2018) 1–28.

Dorobek naukowy doktorantki

Publikacje naukowe (IF – *Impact Factor*, pkt. MNiSW/MEiN – punkty na podstawie wykazu czasopism i wydawnictw zgodnie z bazą SIN PP):

1. **P. Błaszkiwicz**, M. Kotkowiak, A. Dudkowiak, *Fluorescence quenching and energy transfer in a system of hybrid laser dye and functionalized gold nanoparticles*, *Journal of Luminescence* 183 (2017), 303-310. (IF=2,732; pkt. MNiSW=35)
2. **P. Błaszkiwicz**, M. Kotkowiak, *Gold-based nanoparticles systems in phototherapy - current strategies*, *Current Medicinal Chemistry* 25(42) (2018) 5914-5929. (IF=3,894; pkt. MNiSW=40)
3. **P. Błaszkiwicz**, M. Kotkowiak, E. Coy, A. Dudkowiak, *Laser-induced optoacoustic spectroscopy studies of inorganic functionalized metallic nanorods*, *Journal of Physical Chemistry C* 123(44) (2019), 27181-27186. (IF=4,189; pkt. MEiN=140)
4. **P. Błaszkiwicz**, M. Kotkowiak, E. Coy, A. Dudkowiak, *Tailoring fluorescence and singlet oxygen generation of a chlorophyll derivative and gold nanorods via a silica shell*, *Journal of Physical Chemistry C* 124(3) (2020), 2088-2095. (IF=4,126; pkt. MEiN=140)
5. B. Tim, **P. Błaszkiwicz**, M. Kotkowiak, *Recent advances in metallic nanoparticle assemblies for surface-enhanced spectroscopy*, *International Journal of Molecular Sciences*, 2022, 23(1), 291-1-291-24. (IF=5,924; pkt. MEiN=140)
6. B. Tim, **P. Błaszkiwicz**, A.B. Nowicka, M. Kotkowiak, *Optimizing SERS performance through aggregation of gold nanorods in Langmuir-Blodgett films*, *Applied Surface Science*, 2022, 573, 151518-1-121218-22. (IF=6,707; pkt. MEiN=140)
7. B. Tim, **P. Błaszkiwicz**, M. Kotkowiak, *Altering model cell membranes by means of photoactivated organic functionalized gold nanorods*, *Journal of Molecular Liquids*, 2022, 349, 118179-1-118179-7. (IF=6,165; pkt. MEiN=100)
8. J. Kałużny, A. Świetlicka, Ł. Wojciechowski, S. Boncel, G. Kinal, T. Runka, M. Nowicki, O. Stepanenko, B. Gapiński, J. Leśniewicz, **P. Błaszkiwicz**, K. Kempa, *Machine Learning Approach for Application-Tailored Nanolubricants' Design*, *Nanomaterials*, 2022, 12(10), 1765-1-1765-17. (IF=5,076; pkt. MEiN=100)

Rozdziały w wydawnictwach pokonferencyjnych:

1. A. Wiciak, E. Nowak, **P. Błaszkiwicz**, M. Kotkowiak, *Bogactwo zaklęte w srebrze – przegląd po właściwościach, metodach syntezy i zastosowaniu nanocząstek srebra*, Badania i Rozwój Młodych Naukowców w Polsce, ISBN (978-83-65362-48-3) (2017), 144-150.
2. A. Wiciak, **P. Błaszkiwicz**, E. Nowak, M. Kotkowiak, *Złote nanocząstki metaliczne – otrzymywanie oraz zastosowanie*, ISBN (978-83-65362-48-3) (2017), 151-157.
3. A. Batura, **P. Błaszkiwicz**, M. Kotkowiak, *Bezpieczeństwo i zagrożenia dla organizmów żywych wynikające z zastosowania nanomateriałów*, Badania i Rozwój Młodych Naukowców w Polsce, ISBN (978-83-66139-18-3) (2019), 7-13.
4. A. Batura, **P. Błaszkiwicz**, M. Kotkowiak, *Synteza i funkcjonalizacja nanocząstek złota i srebra*, Badania i Rozwój Młodych Naukowców w Polsce, ISBN (978-83-66139-18-3) (2019), 14-20.
5. A. Batura, **P. Błaszkiwicz**, *Dobrodziejstwa nanobiotechnologii w świecie jutra*, Dokonania naukowe doktorantów VII edycja, ISBN (978-83-63058-89-0) (2019), 78-84.
6. **P. Błaszkiwicz**, M. Kotkowiak, *Diagnostyka i terapia fotodynamiczna "wczoraj i dziś"*, Dokonania naukowe doktorantów VII edycja, ISBN (978-83-63058-89-0) (2019), 141-147.
7. **P. Błaszkiwicz**, *Tlenek tytanu (IV) w akcji – przegląd właściwości, metod otrzymywania i zastosowań*, Badania i Rozwój Młodych Naukowców w Polsce, ISBN (978-83-66392-90-8) (2020), 15-20.
8. **P. Błaszkiwicz**, *Procesy samoorganizacji nanomateriałów*, Badania i Rozwój Młodych Naukowców w Polsce, ISBN (978-83-66392-90-8) (2020), 7-13.

Udział w projektach badawczych (tytuł i numer projektu, źródło finansowania, lata i miejsce realizacji):**Kierownik:**

1. *Oddziaływanie chemoterapeutyka z mezoporowatymi nanocząstkami złota*, 06/62/DSMK/6203, Ministerstwo Nauki i Szkolnictwa Wyższego, Wydział Fizyki Technicznej, Politechnika Poznańska, 18.04-30.11.2017, wysokość finansowania: 9.397 PLN.

2. *Wpływ sfunkcjonalizowanych nanocząstek metalicznych na właściwości fotofizyczne barwników chlorofilowych*, 06/62/DSMK/6206, Ministerstwo Nauki i Szkolnictwa Wyższego, Wydział Fizyki Technicznej, Politechnika Poznańska, 10.07-18.12.2018, wysokość finansowania: 11.115 PLN.
3. *Wpływ półprzewodnikowej powłoki z ditlenku tytanu (IV) wytworzonej na powierzchni nanocząstek złota na właściwości fotofizyczne mieszanin hybrydowych*, 06/62/SBAD/6207, Ministerstwo Nauki i Szkolnictwa Wyższego, Wydział Fizyki Technicznej, Politechnika Poznańska, 12.04-02.12.2019, wysokość finansowania: 4.945 PLN.
4. *Wydajność procesów dezaktywacji energii wzbudzenia w układzie barwnika kowalencyjnie przyłączonego do powierzchni nanocząstki metalicznej*, 0512/SBAD/6210, Ministerstwo Nauki i Szkolnictwa Wyższego, Wydział Inżynierii Materiałowej i Fizyki Technicznej, Politechnika Poznańska, 17.01-31.12.2020, wysokość finansowania: 10.925 PLN.
5. *W jaki sposób właściwości blisko i dalekozasięgowe nanocząstek złota przyczyniają się do zwiększenia wydajności generowania tlenu singletowego w systemach hybrydowych?* 2021/41/N/ST4/03017, PRELUDIUM, Narodowe Centrum Nauki, Wydział Inżynierii Materiałowej i Fizyki Technicznej, Politechnika Poznańska, 25.01.2022-24.01.2024, wysokość finansowania: 139.080 PLN.

Wykonawca:

1. *Warstwy Langmuira na granicy gal-powietrze*, 06/62/DSMK/0199, Ministerstwo Nauki i Szkolnictwa Wyższego, Wydział Fizyki Technicznej, Politechnika Poznańska, 18.03-30.11.2016, wysokość finansowania: 10.807 PLN, kierujący pracą – dr inż. Kamil Kędziński.
2. *Synteza, właściwości optyczne i strukturalne nanocząstek metalicznych i ich oddziaływanie z barwnikiem organicznym*, 06/62/DSMK/0198, Ministerstwo Nauki i Szkolnictwa Wyższego, Wydział Fizyki Technicznej, Politechnika Poznańska, 18.03-30.11.2016, wysokość finansowania: 10.661 PLN, kierujący pracą – dr inż. Michał Kotkowiak.
3. *Warstwy Langmuira-Schaefera nanorurek węglowych wzbogaconych sferycznymi nanocząstkami srebra*, 06/62/DSMK/6204, Ministerstwo Nauki i Szkolnictwa Wyższego, Wydział Fizyki Technicznej, Politechnika Poznańska,

- 18.04-30.11.2017, wysokość finansowania: 5.562 PLN, kierujący pracą – mgr inż. Karol Rytel.
4. *Hybrydowe nanostruktury tlenek/nanocząstka metaliczna jako podłoża do powierzchniowo wzmocnionych spektroskopii*, 06/62/DSMK/6205, Ministerstwo Nauki i Szkolnictwa Wyższego, Wydział Fizyki Technicznej, Politechnika Poznańska, 10.07-18.12.2018, wysokość finansowania: 11.874 PLN, kierujący pracą – dr inż. Michał Kotkowiak.
 5. *Analiza zjawisk fizycznych warunkujących zapłon paliw wzbogaconych w nanorurki węglowe*, 2017/27/B/ST8/01838, OPUS, Narodowe Centrum Nauki, Wydział Inżynierii Lądowej i Transportu, Politechnika Poznańska, 10.09.2018-10.09.2021, wysokość finansowania: 895.805 PLN, kierujący pracą – prof. dr Krzysztof Kempa.
 6. *Optymalizacja struktury nanoplatfomy do powierzchniowo wzmocnionej detekcji pochodnych chlorofilu z wykorzystaniem techniki Langmuira*, 2019/35/D/ST4/02037, SONATA, Narodowe Centrum Nauki, Wydział Inżynierii Materiałowej i Fizyki Technicznej, Politechnika Poznańska, 10.10.2020-10.10.2023, wysokość finansowania: 965.760 PLN, kierujący pracą – dr inż. Michał Kotkowiak.

Staż naukowe:

1. POLLENA, Ostrzeszów 08.2013-09.2013 (2 m-ce)
Kluczowe zagadnienia: produkcja kremu do twarzy z nanocząstkami srebra, testy kosmetyczne, chemia organiczna, kontrola jakości, testy biologiczne, posiewy bakteryjne, pomiary spektroskopowe i mikroskopowe, itp.
2. Laboratorium Testów Radiacyjnych, Wojewódzka Stacja Sanitarno-Epidemiologiczna, Poznań, 07.2014-08.2014 (2 m-ce)
Kluczowe zagadnienia: pomiary radioaktywności, obliczanie dawek, testy radiacyjne żywności, techniczne wizyty w szpitalach, itp.
3. Instytut Fizyki Molekularnej, Polska Akademia Nauk, Poznań, 07.2015-08.2015 (2 m-ce)
Kluczowe zagadnienia: nanotechnologia, nanomateriały, synteza, układy hybrydowe, barwniki organiczne, pomiary spektroskopowe, itp.
4. French National Institute for Nuclear Science and Technology, Saclay, Francja, 10.2015-11.2015 (2 m-ce).

Kluczowe zagadnienia: zastosowanie nanotechnologii w elektrowni jądrowej, nanoceramika, nanomateriały, radioaktywność, pomiary radiacyjne, przeliczanie dawek promieniowania, testy i symulacje w reaktorze badawczym, odpady reaktywne, energia jądrowa, techniczne wizyty w elektrowniach jądrowych i związanymi z nimi obiektami, staż sfinansowany przez Ministerstwo Nauki i Szkolnictwa Wyższego.

5. Komenda Wojewódzka Policji w Poznaniu, 10.2017-12.2017 (3 m-ce)

Kluczowe zagadnienia: związki organiczne pochodzenia naturalnego, pomiary spektroskopowe, przeliczanie stężeń, identyfikacja związków organicznych, itp.

6. Centrum Nauk Biologiczno-Chemicznych Uniwersytetu Warszawskiego, Warszawa, 10.2019-11.2019 (2 m-ce)

Kluczowe zagadnienia: synteza, funkcjonalizacja nanocząstek metalicznych, charakteryzacja nanocząstek, wytwarzanie układów hybrydowych, syntezy organiczne, wymiany ligandów, pomiary spektroskopowe i mikroskopowe, itp.

Nagrody i wyróżnienia:

Stypendia:

2015-2016 - Stypendium z dotacji projakościowej,

2017-2018 - Stypendium Rektora dla 30% najlepszych doktorantów,

2017-2018 - Stypendium z dotacji projakościowej,

2018-2019 - Stypendium Rektora dla 30% najlepszych doktorantów,

2019-2020 - Stypendium Rektora dla 30% najlepszych doktorantów,

2019-2020 - Stypendium z dotacji projakościowej,

2020-2021 - Stypendium Rektora dla 30% najlepszych doktorantów,

2020-2021 - Stypendium z dotacji projakościowej.

Nagrody:

III Nagroda Polskiego Towarzystwa Nukleonowego w konkursie na najlepsze prace doktorskie, magisterskie, inżynierskie i licencjackie związane tematycznie z atomistyką (wykorzystaniem zjawisk, procesów i technik jądrowych, ekonomią i odbiorem społecznym zastosowań energetyki jądrowej itp.). Temat pracy magisterskiej: *Materiały na pojemniki i osłony przed promieniowaniem jonizującym*. – promotor: dr inż. Wiesław Gorączko.

Szkolenia:

02.2012 - Skuteczne zarządzanie czasem, organizator: Era Inżyniera.

11.2015 - Certificate of the Training and Internship on Nuclear Energy, organizator: French National Institute for Nuclear Science and Technology, Francja.

Udział w konferencjach naukowych:**- wystąpienia prezentowane osobiście:**

- **wyklady**

12.06.2017 – na zaproszenie prof. Jacka Waluka, Seminar of Photochemistry and Spectroscopy, *Fabrication and characterization of new hybrid systems based on gold nanoparticles for diagnostic and therapeutic applications*, Instytut Chemii Fizycznej, Polska Akademia Nauk, Warszawa.

- **komunikaty ustne**

12.2015 - **P. Błaszkwicz**, First International Nuclear Conference, Poznań, *Building of high-level, long-life radioactive waste repository in France*.

09.2016 - **P. Błaszkwicz**, M. Kotkowiak, XX Ogólnopolska Konferencja Kryształy Molekularne 2016, Kazimierz Dolny, *Oddziaływanie nanocząstek metalicznych o różnym kształcie z barwnikami organicznymi*.

02.2017 - **P. Błaszkwicz**, M. Kotkowiak, V Ogólnokrajowa Konferencja, Młodzi Naukowcy w Polsce – Badania i Rozwój, Będlewo, *Nanocząstki metaliczne - otrzymywanie, funkcjonalizacja i zastosowanie*.

09.2017 - **P. Błaszkwicz**, M. Kotkowiak, E. Coy, A. Dudkowiak, Kryształki molekularne 2017, Warszawa, *Wpływ nanocząstek metalicznych na właściwości fotofizyczne barwników chlorofilowych*.

04.2018 - **P. Błaszkwicz**, M. Kotkowiak, A. Dudkowiak, Dokonania naukowe doktorantów 2018, Poznań, *Wpływ rodzaju powłoki na parametry fotofizyczne układów hybrydowych na bazie nanocząstek złota*.

12.2018 - **P. Błaszkwicz**, M. Kotkowiak, E. Coy, A. Dudkowiak, III Ogólnopolska Studencka Fizyczno-Optyczna Konferencja, Wrocław, *Wytworzenie i charakteryzacja nowych układów hybrydowych na bazie nanocząstek złota do celów diagnostycznych i terapeutycznych*.

03.2019 - **P. Błaszkwicz**, M. Kotkowiak, E. Coy, A. Dudkowiak, Dokonania naukowe doktorantów VII edycja, Poznań, *Ocena fotosensybilizującej*

efektywności pochodnych chlorofilu a w układach hybrydowych na bazie nanocząstek złota.

11.2019 - **P. Błaszkiwicz**, M. Kotkowiak, E. Coy, A. Dudkowiak, X Ogólnokrajowa konferencja naukowa, Młodzi naukowcy w Polsce - Badania i rozwój, Poznań, *Proces generowania tlenu singletowego i wygaszania fluorescencji w układach hybrydowych typu core-shell.*

- **plakaty**

06.2016 - **P. Błaszkiwicz**, M. Kotkowiak, A. Dudkowiak, NanoTech Poland International Conference & Exhibition, Poznań, *Fluorescence quenching and energy transfer in hybrid laser dye and gold nanoparticles system.*

06.2017 - **P. Błaszkiwicz**, M. Kotkowiak, E. Coy, A. Dudkowiak, InterNano Poland, Katowice, *Modulated sensitizing properties in photosensitizer containing gold nanorods.*

06.2017 - **P. Błaszkiwicz**, M. Kotkowiak, E. Coy, A. Dudkowiak, NanoTech Poland International Conference & Exhibition, Poznań, *Gold nanorods modulated fluorescence and singlet oxygen generation of chlorophyll derivatives.*

11.2017 - **P. Błaszkiwicz**, M. Kotkowiak, E. Coy, A. Dudkowiak, IWAN'13, Poznań, *Influence of metallic nanoparticles on photophysical properties of chlorophyll dyes.*

06.2018 - **P. Błaszkiwicz**, M. Kotkowiak, E. Coy, A. Dudkowiak, NanoTech Poland International Conference & Exhibition, Poznań, *Effect of the gold nanorods with different type of coating on photophysical properties of chlorophyll dyes.*

12.2018 - **P. Błaszkiwicz**, M. Kotkowiak, A. Dudkowiak, III Ogólnopolska Studencka Fizyczno-Optyczna Konferencja, Wrocław, *Proces wygaszania fluorescencji i przekazywania energii w układzie hybrydowym na bazie nanocząstek.*

03.2020 - **P. Błaszkiwicz**, M. Kotkowiak, E. Coy, A. Dudkowiak, Microsymposium on Soft and Plasmonic Nanomaterials, Warsaw, *Photophysical processes in core-shell hybrid systems.*

- wystąpienia prezentowane przez współautorów:

- **komunikaty ustne**

03.2019 - A. Batura, **P. Błaszkiwicz**, Dokonania naukowe doktorantów VII edycja, Poznań, *Synteza i fizyko-chemiczna charakteryzacja nanocząstek srebra*.

- **plakaty**

08.2017 - A. Wiciak, **P. Błaszkiwicz**, M. Kotkowiak, ICPS 2017, Turyn, Italy, *Functionalized gold nanorods at air-water interface*.

09.2017 - K. Rytel, M. Widelicka, P. Błaszkiwicz, B. Barszcz, Krysztalki molekularne 2017, Warszawa, *Warstwy Langmuira-Schaefera nanorurek węglowych wzbogacone sferycznymi nanocząstkami srebra*.

11.2018 - A. Batura, P. Błaszkiwicz, M. Kotkowiak, VIII Ogólnokrajowa konferencja naukowa, Młodzi naukowcy w Polsce - Badania i rozwój, Poznań, *Podejście bottom-up jako chemiczne metoda syntezy nanocząstek metalicznych*.

Załączniki

Oświadczenia współautorów o wkładzie w publikacje naukowe doktorantki

Poznań, dnia 27.07.2022

prof. dr hab. Alina Dudkowiak
Wydział Inżynierii Materiałowej
i Fizyki Technicznej
Politechnika Poznańska

Oświadczenie

Oświadczam, że w niniejszych publikacjach:

P. Błaszkiwicz, M. Kotkowiak, A. Dudkowiak,
Fluorescence quenching and energy transfer in a system of hybrid laser dye and functionalized gold nanoparticles,
Journal of Luminescence 183 (2017), 303-310

P. Błaszkiwicz, M. Kotkowiak, E. Coy, A. Dudkowiak,
Laser-induced optoacoustic spectroscopy studies of inorganic functionalized metallic nanorods,
Journal of Physical Chemistry C 123(44) (2019), 27181–27186

P. Błaszkiwicz, M. Kotkowiak, E. Coy, A. Dudkowiak,
Tailoring fluorescence and singlet oxygen generation of a chlorophyll derivative and gold nanorods via a silica shell,
Journal of Physical Chemistry C 124(3) (2020), 2088-2095

mój udział polegał na analizie i interpretacji wyników oraz ostatecznej redakcji artykułu.

Wyrażam zgodę na przedłożenie ww. prac przez mgr inż. Paulinę Błaszkiwicz jako część rozprawy doktorskiej w formie zbioru opublikowanych i powiązanych tematycznie artykułów naukowych.



(podpis współautora)

Poznań, dnia 27.07.2022

dr inż. Michał Kotkowiak
Wydział Inżynierii Materiałowej i Fizyki Technicznej
Politechnika Poznańska

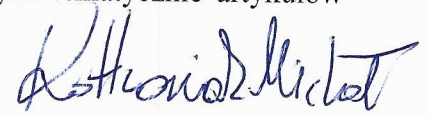
Oświadczenie

Oświadczam, że w niniejszych publikacjach:

1. P. Błaszkiwicz, M. Kotkowiak, A. Dudkowiak,
Fluorescence quenching and energy transfer in a system of hybrid laser dye and functionalized gold nanoparticles,
Journal of Luminescence 183 (2017), 303-310
2. B. Tim, P. Błaszkiwicz, M. Kotkowiak,
Altering model cell membranes by means of photoactivated organic functionalized gold nanorods,
Journal of Molecular Liquids 349 (2022), 118179-1-118179-7
3. P. Błaszkiwicz, M. Kotkowiak, E. Coy, A. Dudkowiak,
Laser-induced optoacoustic spectroscopy studies of inorganic functionalized metallic nanorods,
Journal of Physical Chemistry C 123 (44) (2019), 27181-27186
4. P. Błaszkiwicz, M. Kotkowiak, E. Coy, A. Dudkowiak,
Tailoring fluorescence and singlet oxygen generation of a chlorophyll derivative and gold nanorods via a silica shell,
Journal of Physical Chemistry C 124 (3) (2020), 2088-2095

Mój udział w publikacji (1-2) polegał na zaplanowaniu badań, analizie i interpretacji wyników oraz współredagowaniu artykułu, a w publikacji (3-4) polegał na wykonaniu pomiarów z zakresu czasowo-rozdzielczej laserowo indukowanej spektroskopii optoakustycznej (LIOAS) oraz symulacji komputerowych analizie i interpretacji wyników oraz współredagowaniu artykułu.

Wyrażam zgodę na przedłożenie ww. prac przez mgr inż. Paulinę Błaszkiwicz jako część rozprawy doktorskiej w formie zbioru opublikowanych i powiązanych tematycznie artykułów naukowych.



.....
(podpis współautora)

Poznań, dnia 27.07.2022

dr hab. inż. Emerson Coy, prof. UAM
Uniwersytet im. Adama Mickiewicza
Centrum NanoBioMedyczne
Adam Mickiewicz University
NanoBioMedical Centre

Oświadczenie

Oświadczam, że w niniejszej publikacji:

P. Błaszkwicz, M. Kotkowiak, E. Coy, A. Dudkowiak,
Tailoring fluorescence and singlet oxygen generation of a chlorophyll derivative and gold
nanorods via a silica shell,
Journal of Physical Chemistry C 124(3) (2020), 2088-2095

mój udział polegał na wykonaniu pomiarów TEM oraz ich analizie.

Wyrażam zgodę na przedłożenie ww. pracy przez mgr inż. Paulinę Błaszkwicz jako część
rozprawy doktorskiej w formie zbioru opublikowanych i powiązanych tematycznie artykułów
naukowych.

Declaration

I declare that in this publication:

P. Błaszkwicz, M. Kotkowiak, E. Coy, A. Dudkowiak,
Tailoring fluorescence and singlet oxygen generation of a chlorophyll derivative and gold
nanorods via a silica shell,
Journal of Physical Chemistry C 124(3) (2020), 2088-2095

my contribution consisted in making TEM measurements and their analysis.

I agree to submit the above work by Paulina Błaszkwicz, as a part of the Ph.D. dissertation in the
form of a collection of published and thematically related scientific articles.



(podpis współautora)
(co-author's signature)

Poznań, dnia 27.07.2022

dr hab. inż. Emerson Coy, prof. UAM
Uniwersytet im. Adama Mickiewicza
Centrum NanoBioMedyczne
Adam Mickiewicz University
NanoBioMedical Centre

Oświadczenie

Oświadczam, że w niniejszej publikacji:

P. Błaszkwicz, M. Kotkowiak, E. Coy, A. Dudkowiak,
Laser-induced optoacoustic spectroscopy studies of inorganic functionalized metallic nanorods,
Journal of Physical Chemistry C 123(44) (2019), 27181–27186

mój udział polegał na wykonaniu pomiarów TEM oraz ich analizie.

Wyrażam zgodę na przedłożenie ww. pracy przez mgr inż. Paulinę Błaszkwicz jako część rozprawy doktorskiej w formie zbioru opublikowanych i powiązanych tematycznie artykułów naukowych.

Declaration

I declare that in this publication:

P. Błaszkwicz, M. Kotkowiak, E. Coy, A. Dudkowiak,
Laser-induced optoacoustic spectroscopy studies of inorganic functionalized metallic nanorods,
Journal of Physical Chemistry C 123(44) (2019), 27181–27186

my contribution consisted in making TEM measurements and their analysis.

I agree to submit the above work by Paulina Błaszkwicz, as a part of the Ph.D. dissertation in the form of a collection of published and thematically related scientific articles.



(podpis współautora)
(co-author's signature)

Poznań, dnia 27.07.2022

mgr inż. Beata Tim
Wydział Inżynierii Materiałowej
i Fizyki Technicznej
Politechnika Poznańska

Oświadczenie

Oświadczam, że w niniejszej publikacji:

B. Tim, P. Błaszkiwicz, M. Kotkowiak,
Altering model cell membranes by means of photoactivated organic functionalized gold nanorods,
Journal of Molecular Liquids 349 (2022), 118179-1-118179-7

mój udział polegał na wykonaniu pomiarów z zakresu techniki Langmuira, mikroskopii kąta Brewstera (BAM), analizie i interpretacji wyników oraz współredagowaniu artykułu.

Wyrażam zgodę na przedłożenie ww. pracy przez mgr inż. Paulinę Błaszkiwicz jako część rozprawy doktorskiej w formie zbioru opublikowanych i powiązanych tematycznie artykułów naukowych.



(podpis współautora)

Przedruk publikacji [**Błaszkiwicz, JL 2017**]

P. Błaszkiwicz, M. Kotkowiak, A. Dudkowiak,

Fluorescence quenching and energy transfer in a system of hybrid laser dye and functionalized gold nanoparticles,

Journal of Luminescence 183 (2017), 303-310. (MNiSW 35, IF 2,732)



Fluorescence quenching and energy transfer in a system of hybrid laser dye and functionalized gold nanoparticles



Paulina Błaszkiwicz, Michał Kotkowiak, Alina Dudkowiak*

Faculty of Technical Physics, Poznan University of Technology, Piotrowo 3, 60-965 Poznan, Poland

ARTICLE INFO

Article history:

Received 19 July 2016

Received in revised form

21 September 2016

Accepted 10 November 2016

Available online 15 November 2016

Keywords:

Fluorescence quenching efficiency

Hybrid system

Nanoparticles surface energy transfer

Noble metal nanoparticles

Surface plasmon resonance

ABSTRACT

The photoinduced distance dependent molecular processes in a hybrid mixture of dyes and nanoparticles (NPs) were studied. Gold-NPs were functionalized with polyethylene glycol of different chain lengths in order to check their stability on storage in ethanol and to control the dye-NPs distance. The mixtures of NPs at concentrations from the range 10^{-9} – 10^{-10} M with three laser dyes (C-481, C-510 and DCM), characterized by different yields of fluorescence and fluorescence emissions in different regions of the surface plasmon resonance spectrum of gold-NPs, were studied. It is shown that the energy transfer between the dyes and gold-NPs functionalized with polymer chains can be well described by the size-dependent NSET model. The most effective energy transfer was observed for the dye with the highest spectral donor-acceptor overlap integral despite the difference in donor fluorescence yield, it means that the overlap integral is the most important variable to predict the course and efficiency of this process in the hybrid dye-NP systems. The polymer layer was found not to interact with the dye but its thickness influenced the effectiveness of super-quenching of dye fluorescence (the Stern-Volmer constant, K_{SV} , 10^8 M $^{-1}$) caused by energy transfer. The hybrid mixture of laser dyes and pegylated gold-NPs seems to be very attractive for imaging and detection of targets in biological systems.

© 2016 Elsevier B.V. All rights reserved.

1. Introduction

The continuous and dynamic development of nanotechnology allows the application of new, highly advanced materials in nanomedicine, nanobiology, bioimaging and optoelectronics [1]. Much interest has been focused on metal and semiconductor nanoparticles (NPs), which can act as attractive components of optical detection systems. Their tunable optoelectronic properties, shapes and sizes make these materials perfect for detection in nanoscale of analyte trace concentration [2–4]. Metal NPs have additionally been used in surface enhanced Raman spectroscopy [5] and surface enhanced fluorescence spectroscopy [6,7]. The interest in the application of NPs has expanded as their functionalization have turned out to be more productive [8].

The noble metals NPs (gold (Au) and silver (Ag)) have been under particularly intensive study due to their optical properties. They show a strong resonance in the visible range of the electromagnetic radiation, attributed to charge motions on the metal surface [1,9]. Plasmon oscillations interact with the frequencies of incident light (localized surface plasmon resonance – LSPR), which appears as a strong band in the UV–vis range [4,10,11]. NPs are

good scatterers and good absorbers of light and their resonant frequencies strongly depend on the composition, size, geometry, dielectric environment and separation distance.

When the dyes or dye marked receptors are present in the proximity of NPs or are conjugated with them, their fluorescence can be extinguished through energy or electron transfer [12–15]. Usually, two mechanisms are taken into account to explain the photoinduced energy transfer process: the Förster resonance energy transfer (FRET) and nanoparticle surface energy transfer (NSET). FRET generally is a common nonradiative process, through which an electronically excited donor forwards its excitation energy to an acceptor prompting a decrease in the fluorescence intensity and also in the lifetime of the donor [12,16]. Efficiency of this process requires that the energy gap between the ground state and excited energy level of donor and acceptor are well matched. This suggests that the fluorescence emission spectrum of donor must overlap the absorption spectrum of acceptor [13,16,17] and the optimal distance to transfer excitation energy of donor to acceptor should be preserved. In contrast, NSET does not require a resonant electronic transitions and when the emission spectrum of donor overlaps the plasmon band of NPs, the dipole vectors on the surface of the metal NPs can harvest the energy from the donor [18,19].

A few theoretical models have been developed to calculate the distance at which the probabilities of spontaneous emission of the

* Corresponding author.

E-mail address: alina.dudkowiak@put.poznan.pl (A. Dudkowiak).

dye and energy transfer between donor and acceptor are the same. The first model was introduced by Förster and explained the interactions between two oscillating zero point dipoles [20]. Further modifications include the Kuhn approach [21] in which energy is transferred from a dipole to a thin metal film. Later Chance et al. [22] have added a correction factor to the Kuhn's model (the so-called CPS-Kuhn model) to incorporate the dielectric functions of the metal. Gersten and Nitzan [23] have developed a model which explains the interaction between an oscillating dipole and a metal NPs in which the NPs is considered as a volume of dipoles each of which can couple to the donor. Later on Persson and Lang [24] have described the interaction between a dipole and an infinite metal surface.

Recently, much attention has been paid to fluorescence quenching in the hybrid systems composed of a dye and metal NPs in which the distance between interacting objects is not strictly controlled [7,9,16,25–28]. The system in which dye-NPs distance can be chemically controlled has been also analyzed both experimentally and theoretically [8,29–32]. For example, by smart design and DNA self-recognition, a set of core-shell Au-NPs and quantum dots have been obtained and the photoluminescence quenching, controlled by the DNA linker lengths, caused by nonradiative NSET has been observed [8]. Breshike et al. [33,34] have developed the size-dependent NSET model which accurately predicts experimental data for the systems made of the dye and Au-NPs of different diameters with the duplex DNA as a donor-acceptor spacer. The DNA origami structures were also used as a breadboard, in which both the dye and the NPs were positioned with nanometer precision [29]. They have been found to show a significant quenching of the fluorescence intensity and a reduction of the fluorescence lifetime of a dye when its distance to NPs was smaller than 15 nm, while for longer distances their interaction tends to disappear. The quenching study of four different dyes, which absorb light at different wavelengths, has been also performed using a rigid silica shell on Au-NPs surface as a spacer [30]. By a systematic variation of the silica shell thickness, a comprehensive experimental determination of the distance dependence from complete quenching to no coupling was carried out. Mandal et al. [31] have investigated the NPs embedded in micelles for controlled NSET by tuning the precise location of donor dyes. They have pointed out that neither FRET nor NSET is good enough for describing fluorescence quenching efficiency as a function of separation distance in their system. To study the NSET or FRET in the nanoscale, fluorescence quenching studies for hybrid mixtures composed of laser dyes and Au-NPs have been also performed for fluorescein, coumarin-153, rhodamine 6 G and N,N-bis(2,5-di-tert-butylphenyl)-3,4:9,10-perylenebis(dicarboximide) (DBPI) [7,19,27,28].

In this work, capped Au-NPs citrate was functionalized using polyethylene glycol (PEG) polymer with two different alkyl chain lengths. PEG is very useful in biomedical applications because it can reduce the non-specific binding of proteins as well as the cytotoxicity of pharmaceuticals [35]. The coating of NPs with PEG allows a control of their suspension and stability in organic solvent (i.e. ethanol (EtOH)) as well as a distance between energy donors (dye) and acceptors (NPs). Furthermore, Au-NPs were mixed separately with three different laser dyes characterized by different yields of fluorescence and localization of their fluorescence emission spectra in different spectral regions of the LSPR spectrum of Au-NPs. The effect of the overlapping of the donor fluorescence spectrum and the acceptor extinction spectrum was discussed in terms of the ability to efficiently quench dye fluorescence using both experimental and theoretical approaches. Interpretation of the experimental results was supported by calculation of the FRET or NSET model parameters for different donor-acceptor distances proposed in literature [24,33,36]. The results of the presented work demonstrate that the hybrid systems consisting of a laser dye and pegylated Au-NPs with well-defined donor-acceptor distance

could be used as labels or optical sensors for bionanotechnology applications.

2. Materials and methods

2.1. Chemicals

Tetrachloroauric acid ($\text{HAuCl}_4 \cdot \text{H}_2\text{O}$), sodium citrate ($\text{HO}(\text{COONa})(\text{CH}_2\text{COONa})_2 \cdot 2\text{H}_2\text{O}$), O-[2-(3-mercaptopropionylamino)ethyl]-O'-methylpolyethylene glycol (PEG-SH $M_w \approx 5000$, (PI)) and O-(2-mercaptoethyl)-O'-methylpolyethylene glycol (PEG-SH $M_w \approx 10000$, (PII)) were purchased from Sigma-Aldrich (USA). Laser dyes, coumarins such as 7-N,N-diethylamino-4-trifluoromethyl-1,2-benzopyrone (C-481) and 2,3,5,6-1 H,4H-Tetrahydro-9-(3-pyridyl)quinolizino[9,9a,1-gh]coumarin (C-510) were purchased from Exciton (USA), whereas the 4-(dicyanomethylene)-2-methyl-6-(4-dimethylaminostyryl)-4H-pyran (DCM) was from Sigma Aldrich (USA). EtOH 99.8% H_2O free was purchased from POCH S.A. (Poland).

2.2. Chemical synthesis of nanospheric Au particles, pegylation protocol and their characterization

All chemicals were dissolved in Mili-Q ultra-pure water in glass flasks treated with aqua regia prior to use. Citrate stabilized Au-NPs (~ 15 nm in diameter) were synthesized according to the procedure described elsewhere [37]. Au-NPs capping by PEG-SH was performed according to the procedure described earlier [6,37,38]. Pegylation process ensures good suspension and aggregation resistance of Au-NPs in organic solvents due to formation of ultrathin PEG-SH layer on the Au-NPs surface [6,38]. Particle size distributions were obtained by means of dynamic light scattering measurements (DLS) using Mastersizer 3000 (Malvern Instruments Ltd.) device.

2.3. Absorption and fluorescence studies

The hybrid dye-Au-NPs mixtures were prepared according to the following procedure. The volume of all mixtures was kept constant and equal to 1.5 mL. The concentrations of Au-NPs capped by PEG-SH were as follows (0, 0.8, 1.6, 2.4, 3.2, 4.0, 4.8, 5.6, 6.4, 7.2, 8.0) $\times 10^{-10}$ M (extinction coefficient $2.33 \times 10^8 \text{ M}^{-1} \text{ cm}^{-1}$ at 524 nm). The dye concentration was set at 3×10^{-5} M. The concentration ratio of the dye and Au-NPs was kept constant for all laser dyes to get comparable results. The absorption and fluorescence spectra were collected using a Varian Cary 4000 spectrometer and a Hitachi F4500 fluorometer, respectively. The quantum yield of fluorescence (ϕ_F) of laser dye-Au-NPs mixtures was calculated by the relative method according to [39]:

$$\phi_F = \phi_{\text{Ref}} \frac{F}{F_{\text{Ref}}} \frac{1 - 10^{-A_{\text{Ref}}}}{1 - 10^{-A}} \cdot 100\%, \quad (1)$$

where F and F_{Ref} are the areas under the fluorescence emission spectra of the mixture and the reference, respectively; A and A_{Ref} are the absorbance of the mixture and the references at the excitation wavelength. All measurements were performed at room temperature.

Fluorescence decay curves were obtained using EasyLife V™ (OBB Corp.) lifetime fluorometer with a 1.5 ns pulse of LED (405 nm) as an excitation source. Sample fluorescence responses were collected in the range of 425–800 nm. The amplitude averaged fluorescence lifetimes (τ) were estimated by fitting the decay curves using a deconvolution procedure implemented into DecayFit 1.4 software using bi-exponential decay profile.

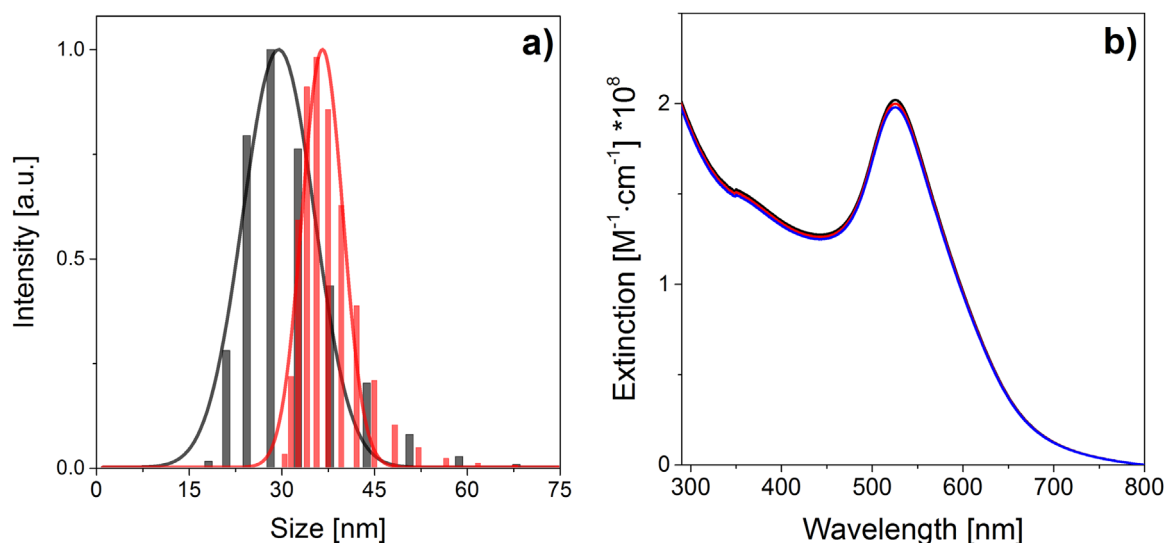


Fig. 1. (a) Size distribution of Au-NPs functionalized with PI (grey) and PII (red). Full width at half maximum ($\Delta\text{Size}_{1/2}$) (14 ± 1) nm and (7.8 ± 0.5) nm for PI and PII, respectively. Gaussian curves were used to fit DLS data with $R^2 \geq 0.94$; (b) the extinction spectra of Au-NPs coated with PI measured as a function of time stored (black, red, blue lines, 1–3 months, respectively).

3. Results and discussion

The particle size distribution of prepared 15 nm Au-NPs functionalized with PI and PII (Fig. 1a) was narrow and the polymer layer formed on the Au-NPs surface was around 7 nm thick for PI and around 10 nm thick for PII, as postulated earlier [38]. For both PI and PII functionalized Au-NPs in EtOH, the maximum of Au-NPs LSPR spectrum is observed at 520 nm and 524 nm (before and after pegylation, respectively) which suggests that the 4 nm shift is the effect of PEG attached to NPs through Au-SH chemical bonding. According to the earlier published results for pegylated 15 nm Au-NPs [6,9] the maximum appeared at 519 nm. Coating NPs with PEG-SH has been reported to shift the maximum of plasmon extinction band by about 2 nm due to a change in the dielectric constant at the NPs surface [6]. Additional red shift of the LSPR band can arise from changes in the refractive index of the solvents [37]. By measuring the extinction spectra for this sample it was checked that the LSPR maximum does not decrease and does not shift on storage in cool conditions (4 °C) (Fig. 1b). It means that in suspension of Au-NPs functionalized by PEG-SH of different chain lengths, the stability of these particles and their homogeneous dispersion are preserved in EtOH up to 3 months.

Fig. 2 presents the extinction spectrum of PI functionalized Au-NPs and the fluorescence spectra of C-481, C-510, DCM (excited at the maximum of the absorption spectrum of each dye (Table 1)). The C-510 fluorescence maximum in EtOH is localized at 493 nm, whereas the C-481 maximum is slightly bathochromically shifted to 503 nm, but the half width (FWHM) of fluorescence band of the latter is greater (Fig. 2). The maximum of the fluorescence spectrum of DCM observed at 611 nm is about 100 nm red shifted.

The absorption and fluorescence spectra of hybrid mixtures composed of C-481, C-510 and DCM with different contents of Au-NPs are presented in Fig. 3a–c. Increase in the fluorescence quenching is observed for all dyes with increasing Au-NPs concentration in the mixture. For the investigated dye-Au-NPs hybrid mixtures, it seems that even very low Au-NPs concentration is sufficient to reduce the initial fluorescence intensity. The emission quenching is probably due to non-radiative energy transfer between laser dyes and Au-NPs. To get the information about this process, the overlap integral $J(\lambda)$ (Table 1) between donor (dye) fluorescence spectrum and acceptor (NPs) LSPR spectrum was calculated as follows:

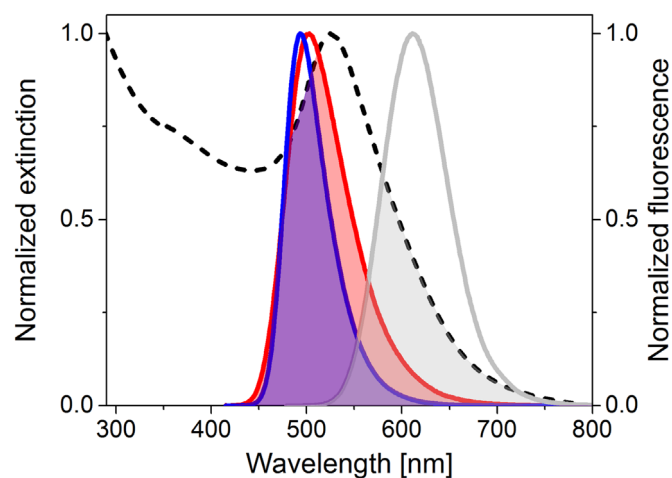


Fig. 2. Normalized extinction spectrum of polymer functionalized Au-NPs (dashed, black line) and fluorescence spectra of C-481 (red line), C-510 (blue line) and DCM (grey line) in EtOH. Additionally overlaps between donor and acceptor spectra are presented.

$$J(\lambda) = \int_0^\lambda F(\lambda)\epsilon(\lambda)\lambda^4 d\lambda \left(\int_0^\lambda F(\lambda) d\lambda \right)^{-1}, \quad (2)$$

where $F(\lambda)$ is normalized to the unit fluorescence spectrum of donor in the absence of acceptor and $\epsilon(\lambda)$ is the molar extinction coefficient (expressed in $M^{-1}cm^{-1}$) of acceptor. The highest $J(\lambda)$ value was observed for C-481 and the lowest for DCM (Table 1). The order of obtained $J(\lambda)$ values is comparable to that observed by others [36].

The fluorescence lifetimes (τ) of investigated dyes were estimated to be equal 0.71, 1.31 ns, respectively, for C-418 and DCM in EtOH [40,41] whereas 7.6 ns for C-510 in polystyrene [42]. The fluorescence decay studies as a function of NPs concentration were performed for C-510 as a representative (Fig. 3d) because of its long τ and high ϕ_F as well because of the limitations of the instrument used. In EtOH, the estimated τ -value was found to be equal (4.89 ± 0.06) ns for C-510 alone and decreased continuously with increasing NPs concentration in the samples, up to (3.67 ± 0.10) ns for the highest NPs concentration used.

It was shown that the fluorescence quenching takes a leading

Table 1
Spectral parameters of laser dyes in EtOH (λ_{abs} , λ_{flu} – maxima of absorption and fluorescence, respectively, ϕ_F – the quantum yields of fluorescence obtained using rhodamine 6 G as the reference sample ($\phi_{Ref}=94\%$) [32]), spectral overlap integral ($J(\lambda)$) between the donor (dye) and acceptor (Au-NPs), K_{SV} – the Stern-Volmer constant for hybrid mixture of dyes and Au-NPs functionalized with PI and PII, R_0 and d_0, D_0 – distance at which the probabilities of spontaneous emission and energy transfer are the same, respectively, for FRET and NSET models, calculated from Eqs. (4)–(6), respectively.

Sample	λ_{abs} [nm]	λ_{flu} [nm]	ϕ_F [%]	$J(\lambda) \times 10^{15}$ [$M^{-1} cm^{-1} nm^4$]	$K_{SV} \times 10^8$ [M^{-1}] PI/PII	FRET		
						R_0 [Å]	d_0 [Å]	D_0 [Å]
C-481	402	503	9	1.41	5.25/4.45	36	39	151
C-510	424	493	82	1.32	4.82/4.02	52	70	259
DCM	469	611	43	1.19	3.20/2.08	45	62	160

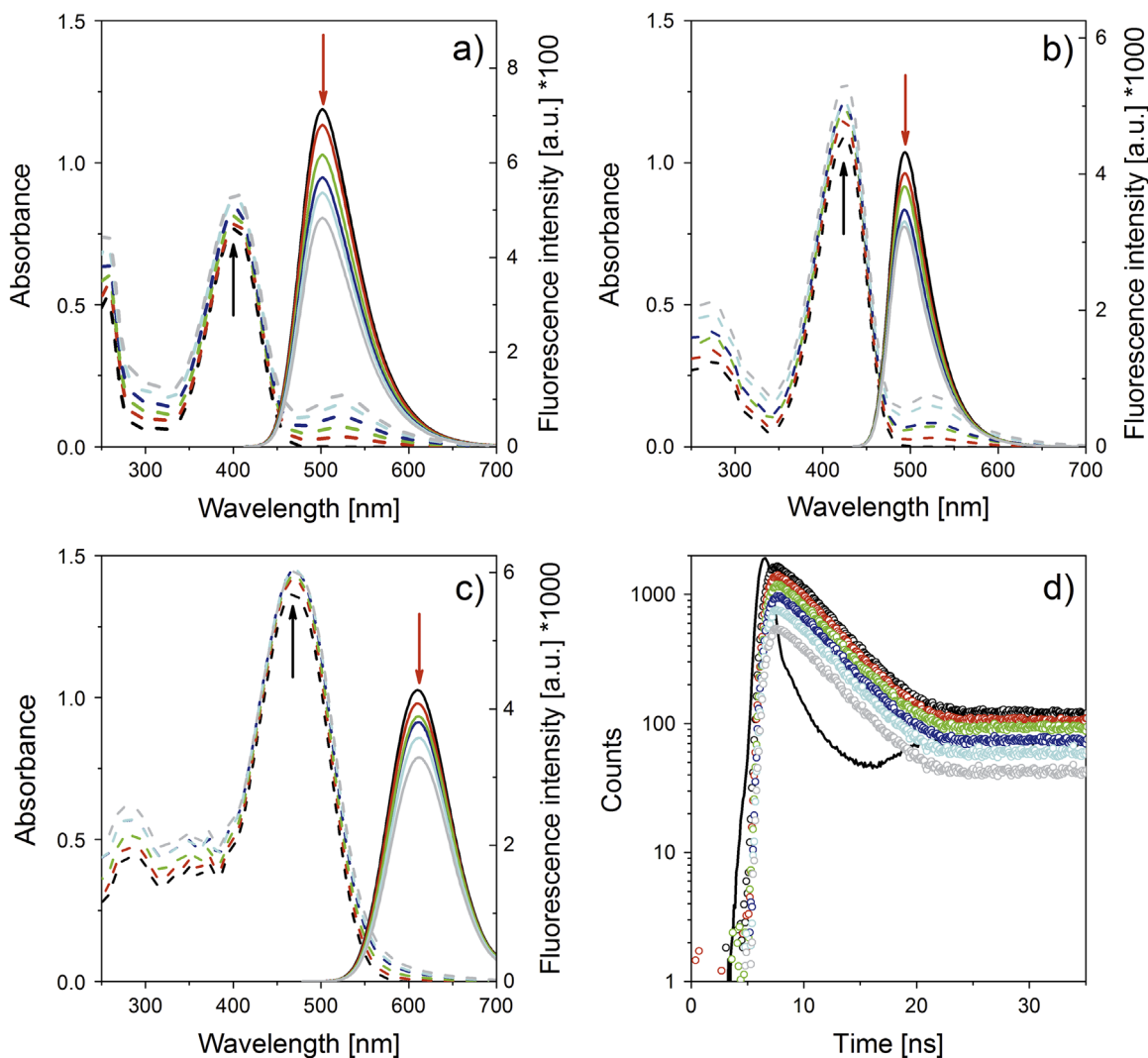


Fig. 3. Absorption (dashed lines), fluorescence spectra (solid lines) and decays (d) of hybrid mixtures composed of C-481 (a), C-510 (b,d), DCM (c) with different contents of Au-NPs functionalized with PI. Excitation wavelengths were located at dye absorption maximum (a–c) (Table 1) and at 405 nm (d). The concentrations of Au-NPs were varied (0, 1.6, 3.2, 4.8, 6.4, 8.0) $\times 10^{-10}$ M (from black to grey); the black line in (d) represents the instrument response function.

role, when NPs diameter is greater than 10 nm [27,43]. As a result of static quenching, a non-fluorescent complex in the ground state is formed as manifested by a new absorption band or changes in the emission spectrum of the donor. Such changes were not observed for the dyes-Au-NPs mixtures studied (Fig. 3a–c). It was checked that the absorption spectra of hybrid mixture components were additive. Because of possible diffusion interaction, the dynamic quenching of the fluorescence could be considered. If in a given system the process of dynamic quenching dominates, a

quantity that brings the information is the Stern-Volmer constant (K_{SV}) defined by the expression [43]:

$$\frac{F_0}{F} - 1 = \frac{\tau_0}{\tau} - 1 = K_{SV} [NPs], \quad (3)$$

where F_0 , τ_0 and F , τ are intensities at the maximum spectra or lifetimes of dye fluorescence in the absence and presence of a quencher (NPs), respectively, $[NPs]$ is the concentration of Au-NPs. Linear Stern-Volmer dependencies for all investigated dyes were

obtained (not shown) suggesting a single quenching mechanism. The K_{SV} values are gathered in Table 1 and they are lower for the systems with Au-NPs coated with PII than by PI. Linear Stern-Volmer dependencies for C-510 (not shown) were also obtained from lifetime measurements. The K_{SV} values were equal to $(4.91 \pm 0.10) \times 10^8 M^{-1}$ and $(4.12 \pm 0.10) \times 10^8 M^{-1}$ in hybrid mixture with NPs functionalized with PI or PII, respectively. These values are similar (comparable) to that estimated from fluorescence measurements (Table 1). It confirms that the dynamic quenching in the investigated systems is actually observed. The obtained K_{SV} values are of the order 10^8 and the quenching phenomenon is described and called the super- or hyper-quenching, as reported earlier for dye and plasmonic particles [1,27], in contrast to the quenching process of a small dye molecule.

It has been shown that to describe the energy transfer between the donors (dyes) and acceptors (NPs), the FRET or NSET model provides satisfactory correlation between experimental results and theory [14,26,27,33]. It is difficult to attribute the mechanism of the energy transfer process to either of the two. As it is not possible to measure directly the donor-acceptor distance, the energy transfer parameters were calculated using the experimental data and different models proposed in literature [14,33,36].

In the energy transfer theory, the Förster distance (R_0) at which the probabilities of spontaneous emission of the dye and energy transfer between donor and acceptor are the same, is given by [36]:

$$R_0 = 0.211 \left(\kappa^2 n^{-4} \phi_F J(\lambda) \right)^{1/6} [\text{Å}], \quad (4)$$

where κ^2 is a factor that describes the relative orientation of the transition dipoles of the donor and acceptor (for randomized situation it is assumed to be 2/3) and n is the refractive index of solution.

The donor-acceptor distance (D_0 or d_0) (equivalent to R_0) could be also calculated as proposed by Persson and Lang [24] or by Breshike et al. [33,34] for NSET. The distance d_0 can be found from the following equation:

$$d_0 = \left(0.225 \frac{c^3 \phi_F}{\omega_{dye}^2 \omega_F k_F} \right)^{1/4} [\text{Å}], \quad (5)$$

where c is the speed of light, ϕ_F , ω_{dye} are the fluorescence quantum yield and the frequency of the electronic transition of the dye, ω_F and k_F are the Fermi frequency and Fermi wavevector of the metal, respectively [14]. The alternative donor-acceptor distance (D_0) for NPs larger than 2 nm could be calculated using the modified model based on the CPS-Kuhn approach [22,33,34]. In this model the electronic properties of NPs are dependent on their size and the D_0 values could be then calculated as follows:

$$D_0 = \frac{\alpha \lambda}{n_m} (A \phi_F)^{1/4} \left(\frac{n_r}{2n_m} \left(1 + \frac{\epsilon_1^2}{|\epsilon_2|^2} \right) \right)^{1/4} [nm], \quad (6)$$

where λ is the emission wavelength maximum for the donor, A is the absorptivity of a thin film mirror, n_r , ϵ_2 and are the refractive index and the dielectric function of the metal, respectively, n_m and ϵ_1 are the index of reflection and real dielectric constant of the solvent (EtOH) and gold, respectively, α is the orientation of the donor to the metal plasmon vector and is influenced only by the averaged vector resulting $\left((9/2)^{1/4} / 4\pi \right)$.

For small spherical Au-NP, the absorptivity (A) could be described in a way similar to that of molecular absorption and calculated from the equation [33]:

$$A = 10^3 \ln(10) \left(\frac{\epsilon_z \left(2r \left(\frac{2r}{\delta_{skin}} \right) \right)}{N_A V} \right), \quad (7)$$

where ϵ_z is the extinction coefficient of the Au-NPs at the maximum emission wavelength of the donor, r is Au-NPs radius (expressed in cm), δ_{skin} is skin depth of Au, N_A is Avogadro's number, and V is the volume of the particle (expressed in cm^3). The size-dependent A -term and dielectric constant were estimated on the basis of literature [33,34,44].

The energy transfer efficiency (ϕ_{ET}) is defined by [43]:

$$\phi_{ET} = 1 - \frac{F}{F_0} = 1 - \frac{\tau}{\tau_0}, \quad (8)$$

and the formula describing ϕ_{ET} as a function of the distance between donor and acceptor (R) is given by [14]:

$$\phi_{ET} = \frac{1}{1 + \left(\frac{R}{R_0} \right)^n}, \quad (9)$$

where $n = 6$ for FRET or $n = 4$ for NSET. The donor-acceptor distances R_0 , D_0 or d_0 (Eqs. 4–6) for all mixtures of laser dyes and Au-NPs were used to calculate ϕ_{ET} and R (the distance between the dye and PI or PII functionalized Au-NPs) according to Eqs. (8) and (9), respectively (Table 2). For all pigments, the calculated R (D_0) are longer than $R(R_0)$ or $R(d_0)$. When the R_0 or d_0 distances for FRET or NSET models, respectively, are taken into account, it is clearly seen that the distance between the dye and the surface of Au-NPs is shorter (especially for C-481) than the thickness of the polymer layers separating both components. Due to the fact that small Au-NPs display a higher density of thiol ligand attachment which has been attributed to their high surface curvature, it seems that the dye is not able to penetrate the PEG layer of Au-NPs. The dependencies of ϕ_{ET} on R evaluated for FRET and NSET models are

Table 2

The donor-acceptor distances obtained using FRET (R_0 , Eq. (4)) and NSET (d_0, D_0 , Eqs. (4) and (5)) parameters for a hybrid mixture of a dye and Au-NPs in various concentrations.

[NPs] $\times 10^{-10}$ [M]	Polymer	C-481		C-510				DCM	
		$\phi_{ET} \pm 0.5$ [%]	R[Å] FRET (R_0)/NSET (d_0/D_0)	$\phi_{ET} \pm 0.5$ [%]	R[Å] FRET (R_0)	NSET (d_0/D_0)	$\phi_{ET} \pm 0.5$ [%]	R[Å] FRET (R_0)/NSET (d_0/D_0)	
1.6	PI	5	59/84/324	8	79/130/481	5	73/127/327		
	PII	5	59/82/319	3	92/166/615	3	80/144/372		
3.2	PI	13	49/62/241	13	72/114/421	8	69/116/299		
	PII	10	52/68/263	10	75/121/449	7	71/120/310		
4.8	PI	21	45/55/211	19	66/101/372	13	62/99/257		
	PII	18	46/57/220	14	70/110/406	8	68/113/293		
6.4	PI	24	43/52/200	23	63/94/348	18	59/91/234		
	PII	21	45/55/211	21	65/97/361	12	63/101/261		
8.0	PI	32	40/47/183	28	61/89/329	20	57/87/225		
	PII	27	42/50/193	25	63/93/343	15	61/96/247		

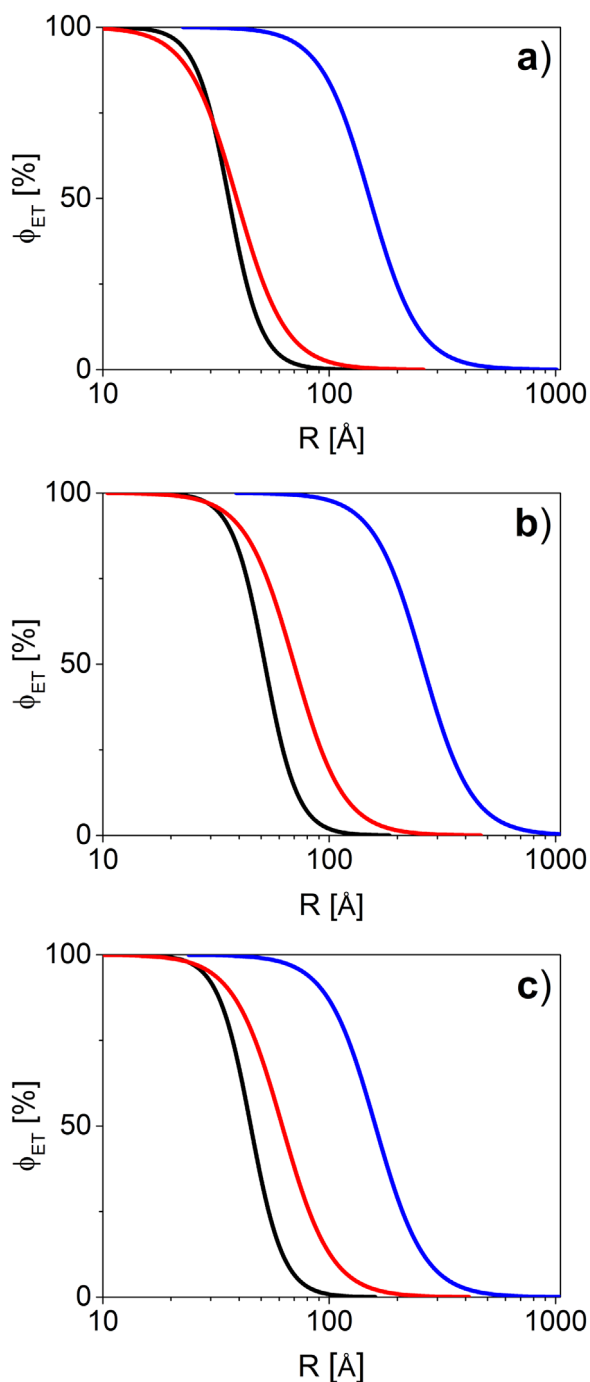


Fig. 4. Energy transfer efficiency (ϕ_{ET}) versus the distance (R) between the dye C-481 (a), C-510 (b) and DCM (c) and Au-NPs simulated for FRET (using R_0 , black line) or NSET (using D_0 or d_0 , red or blue line, respectively).

shown in Fig. 4. As follows from Table 2 and the simulation (Fig. 4), the energy transfer between the dye molecules and Au-NPs coated with 7 and 10 nm polymer layer could be well described by NSET mechanism using the D_0 distance. It confirms that only the size-dependent modification to the NSET theory predicts the interaction between the dye and NPs for distances greater than the thickness of the polymer coated NPs.

As follows from Table 2, the most effective energy transfer occurs for C-481, which is related to the highest spectral overlap, despite the lowest donor yield of fluorescence (Table 1). The dye C-510 characterized by significant yield of fluorescence shows a slightly lower efficiency of energy transfer than C-481, probably

due to a decrease (about 6%) in the spectral overlap. For the hybrid system with DCM whose maximum of absorption was red shifted with respect to LSPR maximum of Au-NPs and the spectral overlap was about 16% smaller and the yield of fluorescence about 5 times higher than those for C-481 (Table 1), the lowest quenching of fluorescence due to energy transfer process was observed. It was of about 36% and 44%, for Au-NPs coated with PI and PII, respectively, less effective for DCM than for C-481 (Table 2). In general, the spectral overlap integral ($J(\lambda)$) between the emission spectrum of the donor and the absorption spectrum of the acceptor, quantum fluorescence yield of the donor, donor-acceptor distance and relative orientation of the transition dipoles are mainly responsible for the FRET. In the hybrid systems when the acceptor (NPs) particles have spherical shape, the orientation of transition dipoles is irrelevant and the energy transfer occurs for any orientation. In the NSET approach irrespective of metal properties, the d_0 or D_0 values (Eqs. 5 and 6) depend on ϕ_F of the donor (similarly as in the FRET model), but also on the absorption or emission wavelength maxima of the donor (dye). In contrast to FRET, these approaches do not take into account the donor-acceptor spectral overlap. However, analysis of the results suggests that the spectral overlap integral is an important parameter influencing the effectiveness of the process, also for NSET because neither ϕ_F nor localization of the dye electronic transitions permits prediction of the course and efficiency of energy transfer in the hybrid dye-NP systems (e.g. for C-481 and C-510). In our experiment the concentrations of NPs were five orders of magnitude lower than that of the dyes and the distance between donor and acceptor did exceed 100 Å suited for FRET (the average dye-NP distance calculated independently from the maximum Au-NPs concentrations used was about 23 nm). Additionally the calculation for NSET approximating the metal as a 2D surface also did not give satisfying results (R in Table 2 is shorter than the thickness of the polymer layer). Therefore it seems that the modified NSET theory by Breshike et al. [33,34] is the best approach to describe the long-range energy transfer process in the investigated dye-NP systems.

The dependencies of ϕ_{ET} and ϕ_F on concentration of Au-NPs for C-481, C-510 and DCM are shown in Fig. 5. The yields were calculated according to Eqs. (3), (8) and (1), respectively, on the basis of the steady state fluorescence studies and lifetime analysis. For all dyes and both polymers attached to Au-NPs, the linear dependencies on the fluorescence quenching on NPs concentration were observed, therefore it was possible to calculate the NPs concentration at which the probabilities of both deactivation processes will be the same. In the investigated hybrid systems the concentration of Au-NPs should be $(12.8, 14.2$ and $18.8) \times 10^{-10}$ M for PI and $(14.4, 16.7$ and $27.1) \times 10^{-10}$ M for PII, respectively, for C-481, C-510 and DCM.

For both PEG-SH layers and the highest concentration of Au-NPs used (Table 2 and Fig. 5), the yield of fluorescence quenching was comparable to the yield of energy transfer (and it was equal 27–32% for C-481, 25–28% for C-510 and 15–20% for DCM). It suggests that the dyes do not interact with the polymer layers, therefore the modification of Au-NPs surface has no influence on the deactivation paths of dye (i.e. no radiationless processes other than energy transfer takes place). The increase in the polymer layer thickness by 3 nm, changes only the K_{SV} value (Table 1) and for all dyes it leads to a decrease in the fluorescence quenching effectiveness (and energy transfer between donor and acceptor) by about 3–5% for the highest Au-NPs concentration used (Table 2).

4. Conclusions

To sum up, it was found that in the hybrid systems of a laser dye and NPs, the transfer energy between the laser dye molecules

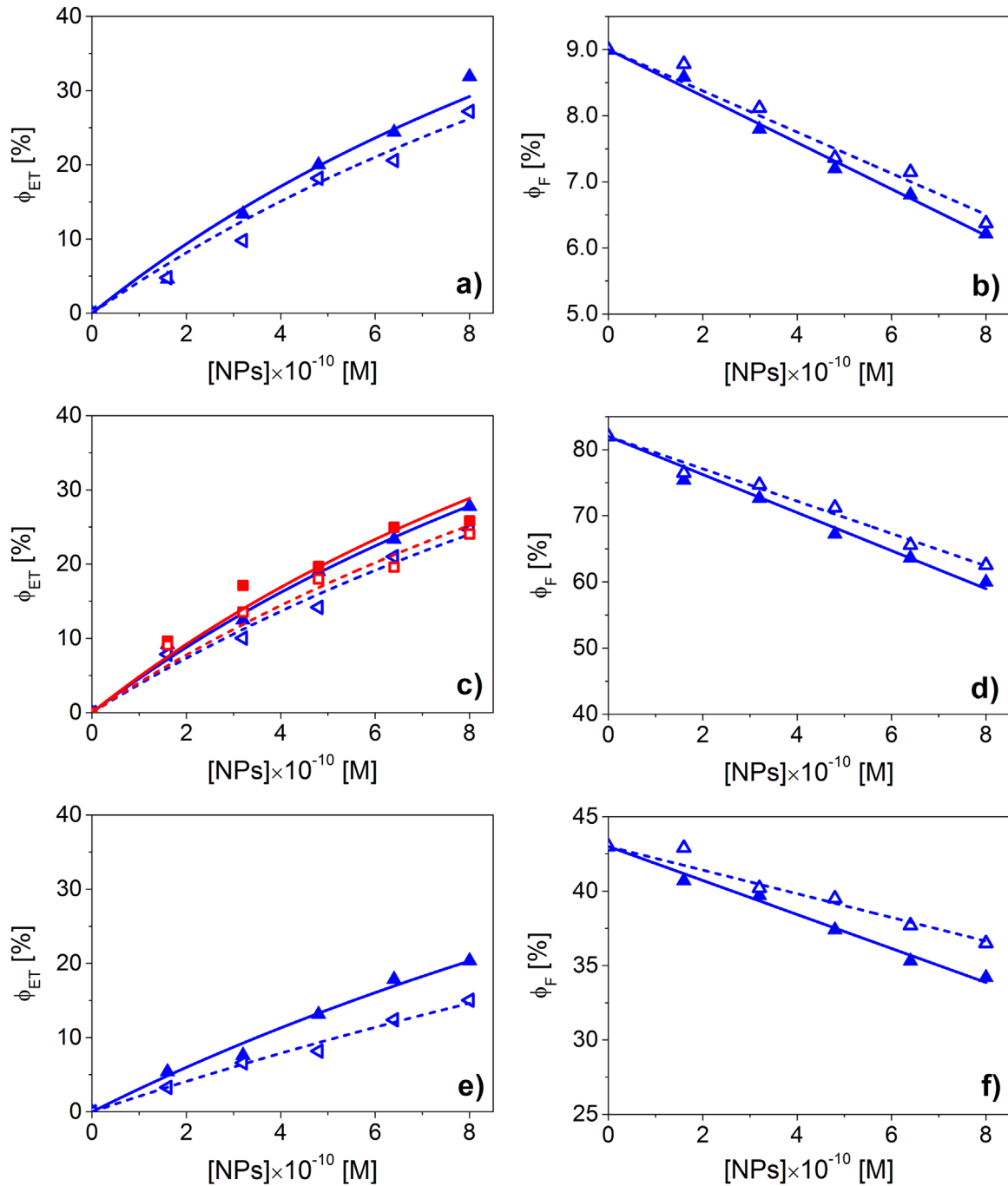


Fig. 5. The energy transfer efficiency (ϕ_{ET}) (a, c, e) and quantum yield of fluorescence (ϕ_{F}) (b, d, f) versus various concentrations of Au-NPs functionalized with PI (closed triangles, solid lines) or PII (opened triangles, dashed lines) for C-481 (a-b), C-510 (c-d) and DCM (e-f) based on steady state fluorescence studies. The red line and points in (c) follows from lifetime analysis. The data of $\phi_{\text{ET}}=f([\text{NPs}])$ were fitted using Eqs. (3) and (8), $R^2 \geq 0.97$.

and 15 nm Au-NPs coated with polymer chain of different lengths could be well described by the NSET mechanism using the estimated D_0 distance as proposed by Breshike et al. [33,34]. It seems that the FRET theory describing the interaction between point dipoles at limited distances is not able to reflect the nonradiative energy transfer in hybrid systems consisting of dyes and a few nm-sized NPs, because the assumption that NPs can behave as point dipoles is too rough. The infinite metal surface proposed in the Persson-Lang approach of the NSET theory also does not describe the real situation of spherical NPs whose absorptivity varies with the size as shown by the Breshike-Riskowski-Strouse NSET theory development [33,34]. Their modified NSET theory is the best approach to describe the long-range energy transfer process in the

investigated dye-NP systems.

The yield of fluorescence quenching was comparable to the yield of energy transfer, which suggests that the Au-NPs polymer surfaces do not interact specifically with the dyes, thus modifying the deactivation processes of their excited electronic states. The increase in the thickness of the polymer layer influenced the effectiveness of dynamic super-quenching of fluorescence caused by energy transfer between the dyes and Au-NPs to the same degree for all dyes. The most effective energy transfer was observed for the dye with the highest spectral donor-acceptor overlap integral, despite the difference in donor fluorescence yield, it means that the overlap integral is the most important variable to predict the course and efficiency of this process in hybrid dye-NP systems. The

results suggest that it should be worthwhile to consider a further development of NSET theory taking into account the spectral donor-acceptor overlap integral analogous to the FRET.

The Au-NPs functionalization with PI or PII prevents their aggregation and helps maintain their stability and homogenous dispersion in EtOH on storage. It has been reported [6] that Au-NPs coated with PEG were not toxic to murine colon carcinoma cell line (CT-26), which opens a possibility to apply hybrid dye-Au-NPs systems as labels or optical sensor. Because for all laser dyes and polymer lengths, the dye yield of fluorescence was proportional to pegylated Au-NPs concentration, it seems that these dye-NPs hybrid mixture could be very attractive for nanobiotechnology for imaging or detection of many targets in biological systems.

Acknowledgements

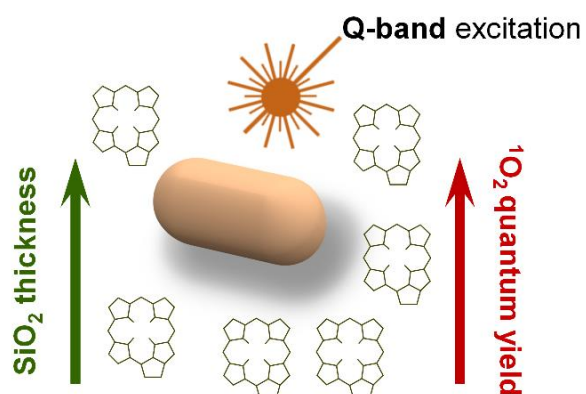
This work was supported by the Ministry of Science & Higher Education in Poland in 2016 year under Project No 06/62/DSMK/0198.

References

- [1] D. Ghosh, N. Chattopadhyay, Gold and silver nanoparticles based super-quenching of fluorescence: a review, *J. Lumin.* 160 (2015) 223–232.
- [2] X. Huang, M.A. El-Sayed, Plasmonic photo-thermal therapy (PPTT), *Alexandria J. Med.* 47 (2011) 1–9.
- [3] Y. Qi, F.R. Xiu, Sensitive and rapid chemiluminescence detection of propranolol based on effect of surface charge of gold nanoparticles, *J. Lumin.* 171 (2016) 238–245.
- [4] D. Jaque, L. Martínez Maestro, B. del Rosal, P. Haro-Gonzalez, A. Benayas, J. L. Plaza, E. Martín Rodríguez, J. García Solé, Nanoparticles for photothermal therapies, *Nanoscale* 6 (2014) 9494–9530.
- [5] S. Murphy, L. Huang, P.V. Kamat, Charge-transfer complexation and excited-state interactions in porphyrin-silver nanoparticle hybrid structures, *J. Phys. Chem. C* 115 (2011) 22761–22769.
- [6] K. Rahme, L. Chen, R.G. Hobbs, M.A. Morris, C. O'Driscoll, J.D. Holmes, PEGylated gold nanoparticles: polymer quantification as a function of PEG lengths and nanoparticle dimensions, *RSC Adv.* 3 (2013) 6085–6094.
- [7] S.A. El-Daly, M.M. Rahman, K.A. Alamry, A.M. Asiri, Fluorescence quenching of perylene DBPI dye by colloidal low-dimensional gold nanoparticles, *J. Fluoresc.* 25 (2015) 973–978.
- [8] D. Sun, Y. Tian, Y. Zhang, Z. Xu, M.Y. Sfeir, M. Cotlet, O. Gang, Light-harvesting nanoparticle core-shell clusters with controllable optical output, *ACS Nano* 9 (2015) 5657–5665.
- [9] M. Kotkowiak, A. Dudkowiak, Multiwavelength excitation of photosensitizers interacting with gold nanoparticles and its impact on optical properties of their hybrid mixtures, *Phys. Chem. Chem. Phys.* 17 (2015) 27366–27372.
- [10] A. Partanen, M.O.A. Erola, J. Mutanen, H. Lajunen, S. Suvanto, M. Kuittinen, T. T. Pakkanen, Enhancing effects of gold nanorods on luminescence of dyes, *J. Lumin.* 157 (2015) 126–130.
- [11] Y.A. Attia, D. Buceta, F.G. Requejo, L.J. Giovanetti, M.A. López-Quintela, Photostability of gold nanoparticles with different shapes: the role of Ag clusters, *Nanoscale* 7 (2015) 11273–11279.
- [12] M. Swierczewska, S. Lee, X. Chen, The design and application of fluorophore-gold nanoparticle activatable probes, *Phys. Chem. Chem. Phys.* 13 (2011) 9929–9941.
- [13] X. Ke, D. Wang, C. Chen, A. Yang, Y. Han, L. Ren, D. Li, H. Wang, Co-enhancement of fluorescence and singlet oxygen generation by silica-coated gold nanorods core-shell nanoparticle, *Nanoscale Res. Lett.* 9 (2014) 666–678.
- [14] C.S. Yun, A. Javier, T. Jennings, M. Fisher, S. Hira, S. Peterson, B. Hopkins, N. O. Reich, G.F. Strouse, Nanometal surface energy transfer in optical rulers, breaking the FRET barrier, *J. Am. Chem. Soc.* 127 (2005) 3115–3119.
- [15] J. Chao, Y. Lin, H. Liu, L. Wang, C. Fan, DNA-based plasmonic nanostructures, *Mater. Today* 18 (2015) 326–335.
- [16] V.V. Mokashi, A.H. Gore, V. Sudarsan, M.C. Rath, S.H. Han, S.R. Patil, G. B. Kolekar, Evaluation of interparticle interaction between colloidal Ag nanoparticles coated with trisodium citrate and safranin by using FRET: Spectroscopic and mechanistic approach, *J. Photoch. Photobiol. B* 113 (2012) 63–69.
- [17] J. Zhang, C. Li, X. Zhang, S. Huo, S. Jin, F.F. An, X. Wang, X. Xue, C.I. Okeke, G. Duan, F. Guo, X. Zhang, J. Hao, P.C. Wang, J. Zhang, X.J. Liang, In vivo tumor-targeted dual-modal fluorescence/CT imaging using a nanoprobe co-loaded with an aggregation-induced emission dye and gold nanoparticles, *Biomaterials* 42 (2015) 103–111.
- [18] M.R. Hormozi-Nezhad, H. Bagheri, A. Bohloul, N. Taheri, H. Robatjazi, Highly sensitive turn-on fluorescent detection of captopril based on energy transfer between fluorescein isothiocyanate and gold nanoparticles, *J. Lumin.* 134 (2013) 874–879.
- [19] J. John, L. Thomas, A. Kurian, S.D. George, Modulating fluorescence quantum yield of highly concentrated fluorescein using differently shaped green synthesized gold nanoparticles, *J. Lumin.* 172 (2016) 39–46.
- [20] L. Stryer, R.P. Haugland, Energy transfer: a spectroscopic ruler, *Proc. Natl. Acad. Sci.* 58 (1967) 719–725.
- [21] H. Kuhn, Classical aspects of energy transfer in molecular systems, *J. Chem. Phys.* 53 (1970) 101–108.
- [22] R.R. Chance, A. Prock, R. Silbey, Comments on the classical theory of energy transfer, *J. Chem. Phys.* 62 (1975) 2245–2253.
- [23] J. Gersten, A. Nitzan, Spectroscopic properties of molecules interacting with small dielectric particles, *J. Chem. Phys.* 75 (1981) 1139–1152.
- [24] B.N.J. Persson, N.D. Lang, Electron-hole-pair quenching of excited states near a metal, *Phys. Rev. B* 26 (1982) 5409–5415.
- [25] R.E. Armstrong, R.A. Riskowski, G.F. Strouse, Nanometal surface energy transfer optical ruler for measuring a human telomere structure, *Photochem. Photobiol.* 91 (2015) 732–738.
- [26] J. John, L. Thomas, N.A. George, A. Kurian, S.D. George, Tailoring of optical properties of fluorescein using green synthesized gold nanoparticles, *Phys. Chem. Chem. Phys.* 17 (2015) 15813–15821.
- [27] D. Ghosh, A. Girigoswami, N. Chattopadhyay, Superquenching of coumarin 153 by gold nanoparticles, *J. Photoch. Photobiol. A* 242 (2012) 44–50.
- [28] B.R. Kumar, N.S. Basheer, A. Kurian, S.D. George, Study of concentration-dependent quantum yield of rhodamine 6G by gold nanoparticles using thermal-lens technique, *Appl. Phys. B* 115 (2014) 335–342.
- [29] G.P. Acuna, M. Bucher, I.H. Stein, C. Steinhauer, A. Kuzyk, P. Holzmeister, R. Schreiber, A. Moroz, F.D. Stefani, T. Liedl, F.C. Simmel, P. Tinnefeld, Distance dependence of single-fluorophore quenching by gold nanoparticles studied on DNA origami, *ACS Nano* 6 (2012) 3189–3195.
- [30] P. Reineck, D. Gómez, S. Hock Ng, M. Karg, T. Bell, P. Mulvaney, U. Bach, Distance and wavelength dependent quenching of molecular fluorescence by Au@SiO₂ core-shell nanoparticles, *ACS Nano* 7 (2013) 6636–6648.
- [31] S. Mandal, C. Ghatak, V.G. Rao, S. Ghosh, N. Sarkar, Pluronic micellar aggregates loaded with gold nanoparticles (Au NPs) and fluorescent dyes: a study of controlled nanometal surface energy transfer, *J. Phys. Chem. C* 116 (2012) 5585–5597.
- [32] Y.F. Huang, K.H. Ma, K. Bin Kang, M. Zhao, Z.L. Zhang, Y.X. Liu, T. Wen, Q. Wang, W.Y. Qiu, D. Qiu, Core-shell plasmonic nanostructures to fine-tune long Au nanoparticle-fluorophore distance and radiative dynamics, *Colloid. Surf. A* 421 (2013) 101–108.
- [33] C.J. Breshike, R.A. Riskowski, G.F. Strouse, Leaving Foerster resonance energy transfer behind: nanometal surface energy transfer predicts the size-enhanced energy coupling between a metal nanoparticle and an emitting dipole, *J. Phys. Chem. C* 117 (2013) 23942–23949.
- [34] C.J. Breshike, Electromagnetic Interactions Between Metal Nanoparticles and Fluorescent Dipoles, Florida State University, 2013.
- [35] J.V. Jokerst, T. Lobovkina, R.N. Zare, S.S. Gambhir, Nanoparticle PEGylation for imaging and therapy, *Nanomedicine* 6 (2011) 7150728.
- [36] M.A. Habeeb Muhammed, A.K. Shaw, S.K. Pal, T. Pradeep, Quantum clusters of gold exhibiting FRET, *J. Phys. Chem. C* 112 (2008) 14324–14330.
- [37] C. Fernández-López, C. Mateo-Mateo, R.A. Álvarez-Puebla, J. Pérez-Juste, I. Pastoriza-Santos, L.M. Liz-Marzán, Highly controlled silica coating of PEG-capped metal nanoparticles and preparation of SERS-encoded particles, *Langmuir* 25 (2009) 13894–13899.
- [38] R.G. Shimmin, A.B. Schoch, P.V. Braun, Polymer size and concentration effects on the size of gold nanoparticles capped by polymeric thiols, *Langmuir* 20 (2004) 5613–5620.
- [39] J.R. Lakowicz, Principles of fluorescence spectroscopy, Springer, 2006.
- [40] S. Nad, M. Kumbhakar, H. Pal, Photophysical properties of coumarin-152 and coumarin-481 dyes: unusual behavior in nonpolar and in higher polarity solvents, *J. Phys. Chem. A* 107 (2003) 4808–4816.
- [41] J.M. Drake, M.L. Lesiecki, D.M. Camaioni, Photophysics and cis-trans isomerization of DCM, *Chem. Phys. Lett.* 113 (1985) 530–534.
- [42] A. Pla-Dalmau, G.W. Foster, G. Zhang, Coumarins as wavelength shifters in polystyrene, *Nucl. Instrum. Methods A* 361 (1995) 192–196.
- [43] B.I. Ipe, K.G. Thomas, S. Barazzouk, S. Hotchandani, P.V. Kamat, Photoinduced charge separation in a fluorophore-gold nanoassembly, *J. Phys. Chem. B* 106 (2002) 18–21.
- [44] P.G. Etchegoin, E.C. Le Ru, M. Meyer, An analytic model for the optical properties of gold, *J. Chem. Phys.* 125 (2006) 164705–164708.

Przedruk publikacji [**Błaszkiwicz, JPCC 2020**]

P. Błaszkiwicz, M. Kotkowiak, E. Coy, A. Dudkowiak,
Tailoring fluorescence and singlet oxygen generation of a chlorophyll derivative and gold nanorods via a silica shell,
Journal of Physical Chemistry C 124(3) (2020), 2088-2095. (MEiN 140, IF 4,126)



Tailoring Fluorescence and Singlet Oxygen Generation of a Chlorophyll Derivative and Gold Nanorods via a Silica Shell

Paulina Błaszczewicz, Michał Kotkowiak, Emerson Coy, and Alina Dudkowiak*

Cite This: *J. Phys. Chem. C* 2020, 124, 2088–2095

Read Online

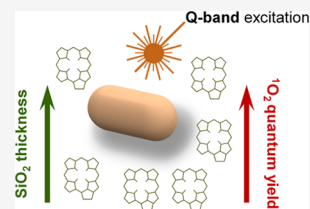
ACCESS |

Metrics & More

Article Recommendations

Supporting Information

ABSTRACT: Gold nanorods deserve special attention as they exhibit tunable longitudinal localized surface plasmon resonances (LSPRs). In our study, gold nanorods of the aspect ratio of 2.25 (maximum of LSPR band at 660 nm) and of controllable SiO₂ thickness in the range of 6–14 nm were mixed with pheophorbide (chlorophyll derivative) in order to create a hybrid system. Energy transfer and singlet oxygen generation were studied for different SiO₂ thicknesses of the nanorod shell. The spectral properties of the hybrid mixture were characterized, and the overlapping of the pheophorbide fluorescence and the longitudinal LSPR band of nanorods on the fluorescence emission, energy transfer, and generation of singlet oxygen were studied. Two independent approaches were used to determine the quantum yield and enhanced factor of singlet oxygen generation. For a certain thickness of the SiO₂ shell and for certain concentrations of gold nanorods, the effect of the plasmon-enhanced singlet oxygen production was observed. Moreover, the enhanced of singlet oxygen yield enhancement was correlated with the far-field optical properties of the gold nanorods. The results obtained indicate the significance of further studies of dye-photosensitizers in hybrid mixtures, taking into account the spectral overlap between dye emission and longitudinal LSPR bands as well as the character of coatings (type and thickness) and scattering yields of gold nanorods.



1. INTRODUCTION

Metallic nanoparticles (NPs) show the localized surface plasmon resonance (LSPR) in the UV–vis range; therefore an intense color of their colloidal solution can be observed. The optical, electronic, and catalytic properties of NPs and their applications strongly depend on their shape and size.¹ Ideal probes for biological applications are gold nanorods (Au-NRs) with interesting optical properties and their known biological neutrality.² Because of their shape, Au-NRs show the transverse and longitudinal LSPR bands. These NPs are characterized by a higher cross-sectional area for light absorption than the other NPs; their absorption (assigned to the longitudinal LSPR band) can be easily tuned from UV to near infrared and they can be produced on a large scale, while maintaining control of the particle size.^{3,4} The high efficiency and reliability of the Au-NR synthesis and possibility of their functionalization as well as a broad range of tunable LSPR band make them very attractive from the applications point of view.^{5,6} The gold NPs (nanospheres, Au-NRs, nanocubes, nanoshells, nanostars, etc.)^{7,8} are investigated in terms of applications in the diagnostics or photothermal and photodynamic therapy (PDT).⁹ PDT is a noninvasive complementary strategy for the treatment of cancer. Through the association of dye-photosensitizer (PS), light and tissue oxygen, the singlet oxygen (¹O₂) can be generated, in order to target neighboring pathological cells and tissues. Formation of new dye-NP hybrid systems requires determination of their spectral parameters and understanding of the photophysical processes occurring at the molecular level. Modification of NP size or shape and functionalization of their surface (by different

types of coatings of different thicknesses) have a significant impact on the photophysical parameters, describing the radiative and nonradiative processes of deactivation in the investigated systems. One strategy is to coat the NPs with a tunable thickness layer, in order to keep the distance and control the interaction between the dye and the NPs. Functionalization of the NP surface gives also the possibility to significantly improve the photophysical parameters of dye-NP hybrid systems toward diagnostic or therapeutic applications.^{10–12} Modification of the size of the NRs can change the position of the longitudinal LSPR extinction band. These modifications allow the formation of a system in which dye absorption or emission band will be overlapped with the LSPR band, which ensures favorable conditions for the interaction between the dye and NRs. Additionally, the coating of NRs permits maintenance and control of the distance between the interacting components. Silicon dioxide (SiO₂) has been widely used as a shell material for NPs.^{13–16} Nevertheless, the question remained if the ability of generating ¹O₂ by NRs coated with SiO₂ (NRs@SiO₂) and sensitized by a selected dye can be modulated (quenched, enhanced) or retained by the SiO₂ shell. So far, the ability to generate ¹O₂ has been investigated for PS bound to the functionalized

Received: August 28, 2019

Revised: December 13, 2019

Published: December 31, 2019

spherical Ag-NPs¹⁷ and Au-NRs.¹⁸ The interaction of the dye with plasmonic Au-NPs@SiO₂ is a complicated process; so it can lead to the enhancement or quenching of deactivation processes involving excited singlet and triplet states of PS. Therefore, the aim of our present studies is to check the influence of the thickness of the SiO₂ shell of Au-NRs on the optical properties of the chlorophyll derivative [pheophorbide *a* (Pheide)] and deactivation processes in physical, hybrid mixtures of the dye and Au-NRs@SiO₂. The optimal conditions for energy transfer in the investigated Pheide and the Au-NRs@SiO₂ system that would increase the ¹O₂ generation were identified. The influence of the thickness of the SiO₂ layer coating Au-NRs on the dye fluorescence quenching and singlet oxygen production was observed.

2. MATERIALS AND METHODS

2.1. Chemicals. Tetrachloroauric acid (HAuCl₄·xH₂O) (99.99%) from Alfa Aesar, cetyltrimethylammonium bromide (CTAB) (99.00%), sodium borohydride (NaBH₄) (98.00%), silver nitrate (AgNO₃) (99.99%), ascorbic acid (99.00%), sodium hydroxide (99.99%), tetraethylorthosilicate (TEOS) (99.99%), and 1,3-diphenylisobenzofuran (DPBF) were purchased from Sigma-Aldrich. Ethanol (EtOH) 99.80% H₂O free was purchased from POCH S.A. (Poland). Pheophorbide *a* (Pheide) (>95.00%) was commercially purchased from Frontier Scientific, Inc. (USA).

2.2. Chemical Synthesis of Gold Nanorods and Silica-Coated Gold Nanorods with Different Shell Thicknesses. Au-NRs were prepared following the procedure described by Nikoobakht et al.¹⁹ with suitable modifications (see Supporting Information). SiO₂ coating was prepared using the modified Stöber method²⁰ proposed by Liz-Marzán group^{14,15,21} with slight modifications.

2.3. Microscopic and Spectroscopic Measurements. The morphology and size dispersion of Au-NRs@SiO₂ were characterized by transmission electron microscopy (HR-TEM) using a JEOL ARM-200F instrument (200 kV) and JEOL 1400 (120 kV). Au-NRs@SiO₂ was drop-casted on Cu grids and placed on a vacuum desiccator overnight.

In hybrid mixtures with Pheide, the concentrations of Au-NRs@SiO₂ were as follows (0, 1.33, 2.66, 4.00, 5.33, 6.66) × 10⁻¹¹ M (extinction coefficient 3.11 × 10⁹ M⁻¹ cm⁻¹),²² whereas Pheide concentration was set at 1.65 × 10⁻⁶ M. To evaluate the quantity of Pheide adsorbed on the Au-NRs@SiO₂ surface, hybrid mixtures with different Au-NRs@SiO₂ (14 nm) concentrations were centrifuged at 6000 rpm for 15 min. The supernatant absorption spectra were measured, and the concentrations of the dye in the pellet were calculated. The estimated amount of the dye adsorbed on the Au-NR surface (*C*) versus the Au-NR concentration in the mixture shows linear decreasing dependence (not shown). It is surprising that by increasing the Au-NRs@SiO₂ concentration more unadsorbed (free dye) is detected in the supernatant. Similar dependences have been observed for the dyes chemically bonded to the NP surface.^{17,23} The *C* values change in the range of 53–20%. This means that at least 53% of the dye is loaded on the Au-NRs@SiO₂ surface for the lowest (1.33 × 10⁻¹¹ M) and about 20% for the highest (6.66 × 10⁻¹¹ M) Au-NR concentration in the hybrid mixture.

Absorption spectra were measured using a Varian Cary 4000 spectrometer. The fluorescence spectra were collected using a Hitachi F4500 fluorometer. All samples were stirred before and after each spectrum collection. The quantum yield of

fluorescence (ϕ_F) of Pheide in hybrid mixtures was calculated by the comparative method according to eq 1

$$\phi_F = \phi_{\text{Ref}} \frac{F_S}{F_{\text{Ref}}} \frac{1 - 10^{-A_{\text{Ref}}}}{1 - 10^{-A}} \frac{n^2}{n_{\text{Ref}}^2} \quad (1)$$

where F_S and F_{Ref} are the areas under the fluorescence emission spectra of samples and the reference, respectively; A and A_{Ref} are the absorbance of the investigated sample and the references at the excitation wavelength; and n and n_{Ref} are the refractive indices of EtOH. The reference was the Pheide dye ($\phi_{\text{Ref}} = 28\%$) dissolved in EtOH.²⁴ The process of fluorescence quenching of Pheide versus Au-NRs@SiO₂ concentration ($[\text{Au} - \text{NRs}]$) can be described by the Stern–Volmer constant (K_{SV}) defined by the expression

$$\frac{F_0}{F} - 1 = K_{\text{SV}}[\text{Au} - \text{NRs}] \quad (2)$$

where F_0 and F are the intensities at the maximum spectra of Pheide fluorescence in the absence and presence of a quencher (Au-NRs@SiO₂), respectively. Energy transfer efficiency (ϕ_{ET}) can be estimated from the following formula

$$\phi_{\text{ET}} = 1 - \frac{F}{F_0} \quad (3)$$

The dependence between ϕ_{ET} and $[\text{Au} - \text{NRs}]$ can be derived from eqs 2 and 3, as shown below

$$\phi_{\text{ET}} = \frac{K_{\text{SV}}[\text{Au} - \text{NRs}]}{K_{\text{SV}}[\text{Au} - \text{NRs}] + 1} \quad (4)$$

As Au-NRs show the extinction bands (Figure 1) at the 510 and 667 nm wavelengths, used for Pheide excitation, the inner

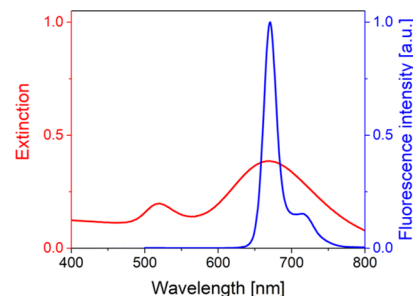


Figure 1. Extinction spectrum of Au-NRs coated with 6 nm SiO₂ (red line, concentration 1.30 × 10⁻¹⁰ M) and fluorescence emission spectra of Pheide (blue line).

filter effect (IFE) should be taken into account.¹² The fluorescence intensities were corrected according to the equation shown below^{12,25}

$$I_{\text{corr}} = I_0 \times \text{antilog} \left(\frac{\text{OD}_{\text{ex}} + \text{OD}_{\text{em}}}{2} \right) \quad (5)$$

where I_{corr} and I are the corrected and measured fluorescence intensities at the maximum emission spectra of Pheide; OD_{ex} and OD_{em} are the optical density values for Pheide and Au-NRs@SiO₂ solution at the excitation and the emission wavelengths, respectively.

The efficiency of singlet oxygen (ϕ_{Δ}) can be evaluated by using the photometric method based on absorbance of DPBF widely used as ¹O₂ trap. ¹O₂ was detected via the photo-degradation of DPBF which readily undergoes a 1,4-cyclo-

addition in reaction with $^1\text{O}_2$ to form endoperoxides which irreversibly yield 1,2-dibenzoylbenzene.^{18,26} To estimate ϕ_Δ , Pheide dissolved in EtOH was used as the reference.²⁴ The mixtures of the investigated (or reference) sample were irradiated with monochromatic light by a 1200 W (Oriel 66070) lamp and a Carl Zeiss SPM2 monochromator with 10 nm half-width of the band. The irradiation wavelength (668 nm) was adjusted at the maximum of Q_y absorption band of Pheide. The DPBF concentration was kept constant at the level of $\sim 0.75 \times 10^{-5}$ M. The reaction of DPBF with $^1\text{O}_2$ after irradiation was monitored by absorbance at 411 nm using a StellarNet Inc. Black-Comet-HR and DH-2000BAL Ocean Optics light source and two Ocean Optics high quality optical fibers were used to collect absorption spectra. The value of ϕ_Δ was determined according to the equation

$$\phi_\Delta = \phi_\Delta^R \frac{k_S}{k_R} \frac{1 - 10^{-A_R(0)}}{1 - 10^{-A_S(0)}} \quad (6)$$

where ϕ_Δ^R is the $^1\text{O}_2$ generation efficiency of the reference; $A_R(0)$ and $A_S(0)$ are the absorbances of the investigated sample and the reference, respectively, for time 0; and k_S and k_R are the slopes of the linear character of the semilogarithmic dependencies describing the photobleaching rate of DPBF in the presence of the investigated and reference samples, respectively. Moreover, the laser-induced optoacoustic spectroscopy (LIOAS)²⁷ was used to determine ϕ_Δ of the investigated samples. The LIOAS setup has been described in detail elsewhere.²⁷ LIOAS is a relative method which employs a photocalorimetric reference. To maintain mechanical properties of the medium, a mixture of Ni-substituted pheophytin *a* (Ni-Phea)²⁸ and Au-NRs@SiO₂ (in appropriate concentrations) was used as a reference sample. Ni-Phea was used at a concentration from the range of 10^{-6} M. The wavelength for dye-Au-NRs mixtures excitation was set to 668 nm (the Q_y band of Pheide). According to the approach proposed by Marti and co-workers,²⁹ the first maximum of the LIOAS signal (H_{\max}) is described by the equation

$$H_{\max} = C\alpha E_{\text{las}}(1 - 10^{-A}) \quad (7)$$

where A is the absorbance of the reference or investigated sample, E_{las} is the energy of the incident light; C is a coefficient related to the geometry of the experiment, and α is a fraction of excitation energy converted promptly into heat (below 0.2 μs in EtOH). The comparative LIOAS measurements were made for reference and the investigated samples to eliminate C and estimate α of the investigated sample. The values of α can be used then to evaluate ϕ_Δ for Pheide in a mixture with Au-NRs@SiO₂, from the following relation

$$\phi_\Delta = \frac{E_{\text{las}}(1 - \alpha) - E_S\phi_F}{E_\Delta} \quad (8)$$

where E_S is the energy of the S_1 state of Pheide (in $\text{kJ}\cdot\text{mol}^{-1}$), E_Δ is the energy of the S_1 state of molecular oxygen ($E_\Delta = 94 \text{ kJ}\cdot\text{mol}^{-1}$), and E_{las} is the light energy at excitation wavelength.

2.4. Computational Simulations. The finite integration technique was used to calculate the scattering yields (ϕ_{sc}) of Au-NRs@SiO₂. The details and methodology of simulation are given in our previous work.^{30–32} Taking into account the dimensions of Au-NRs@SiO₂ from the analysis of TEM images, the optical extinction and radar cross sections (i.e., ECS, RCS respectively) were calculated. ϕ_{sc} was determined by

the relative contribution of RCS to ECS. In this context, ϕ_{sc} for Au-NRs@SiO₂ can be defined as³³

$$\phi_{\text{sc}} = \frac{\sum_{\varphi=0^\circ}^{90^\circ} \int_{\lambda_1}^{\lambda_2} \text{RCS}(\lambda) d\lambda}{\sum_{\varphi=0^\circ}^{90^\circ} \int_{\lambda_1}^{\lambda_2} \text{ECS}(\lambda) d\lambda} \quad (9)$$

where λ_1 and λ_2 were 400 and 800 nm, respectively. The RCS and ECS spectra were obtained for different angles between the longitudinal axis of Au-NRs and the electric vector of the electromagnetic wave $\varphi \in 0-90^\circ$ and were then averaged according to formula 9 to obtain the mean value of ϕ_{sc} .

3. RESULTS AND DISCUSSION

Incomplete understanding of the Au-NR synthesis process makes the tuning of reaction conditions to obtain reproducible results much time-consuming. Hence, to precisely control the Au-NR size, the seed-mediated processes of their growth have to be developed. The Au-NR synthesis was carried out in homogenous solution with the use of relatively cheap substrates. It was checked that during the synthesis, high temperatures are not required; therefore the temperature was fixed in the range of 25–30 °C. In such conditions, the aspect ratio of the resulting Au-NRs was not limited. Incubation of gold seed solution was the most important step, it should be noted that they need to be stored at 28 °C until further use. CTAB-coated Au-NRs were prepared using the well-known seed-mediated growth procedure.^{19,34} The gold seeds were added to a growth solution containing CTAB, $\text{HAuCl}_4 \cdot x\text{H}_2\text{O}$, AgNO_3 , and ascorbic acid. A CTAB bilayer on the surface of Au-NRs protects against their conglomeration, and the addition of AgNO_3 to the growth solution encourages anisotropic growth and control of the aspect ratio. This enables tuning of the position of longitudinal LSPR maxima in different spectral ranges to obtain the desired spectral overlap between Au-NRs and chosen dye-PS. Au-NRs are characterized by two LSPR bands: transverse band observed at 520–530 nm and the longitudinal band whose location depends on the length of the longitudinal axis of Au-NRs. There is a direct relationship between the position of longitudinal LSPR maximum and the aspect ratio of Au-NRs. The reaction temperature (28 °C) and a suitable CTAB concentration are crucial for fabrication of stable and homogenous Au-NRs of a desired aspect ratio. The Au-NRs of different aspect ratios 2.0; 2.1; 2.4; 2.9; 3.4; and 4.3 were prepared, and their UV–vis absorption spectra are shown in Figure S1 (see Supporting Information). For our investigation, the Au-NRs of the aspect ratios 2.25 ± 0.23 [length (53.2 ± 1.8) nm and width (23.6 ± 1.3) nm] and maximum longitudinal LSPR in the region of approx. 660 nm were chosen. Simplification and optimization of the synthesis of Au-NRs and appropriate modification were based on the procedure proposed by Nikoobakht and Sayed.¹⁹ Earlier,^{34,35} it has been proposed to control the aspect ratio of Au-NRs by, for example, temperature (up to 55 °C), the amount of metal present, the ratio of metal seed to metal salt, and concentration of the precursor, salts, and surfactants. The synthesis with proposed modification (low, stable temperature, suitable CTAB and AgNO_3 concentration, etc.) permits obtaining reproducible results and is easy to perform in the basic chemical laboratory condition.

The next important step was coating of Au-NRs with the SiO₂ layer of controlled thickness. The functionalization of Au-NRs with SiO₂ (Au-NPs@SiO₂) was made according to the

scheme in Figure S2 (see Supporting Information) based on the Stöber method^{14,15,20,21} with our slight modifications. The Stöber's method can be optimized and adapted using different approaches. For instance, we used the method based a one-step reaction using CTAB templates, as proposed by Gorelikov and Matsuura.³⁶ Au-NRs before functionalization were centrifuged in order to wash out the excess of the CTAB surfactant. When significant excess of CTAB is present, empty CTAB micelles would be also templates for the SiO₂ layer formation on Au-NRs. Wrongly chosen CTAB concentration may change the structure of the layer, and as a result, heterogeneous SiO₂ coatings are formed. The CTAB concentration after centrifugation was below 1 mM, which corresponds to the critical CTAB micelle concentration. Free SiO₂ particles, which did not coat Au-NRs, were also removed during the centrifugation of CTAB excess. The concentration of the CTAB surfactant is an important factor and must be controlled during the whole functionalization process performed with the use of TEOS solution.^{37,38} The hydrolysis and condensation of TEOS to form SiO₂ can be catalyzed by a change in pH. The appropriate pH for SiO₂ growth is 10. Above pH 10.8, the SiO₂ shell showed inferior quality, whereas below pH 9, the shell was not formed. Through careful control of reaction parameters, it was possible to achieve highly reproducible and robust SiO₂ coatings. According to our results, by changing the concentration of the CTAB surfactant in solution, it was possible to control the thickness of coating. Functionalized Au-NRs with a coating of defined SiO₂ thicknesses 6.0 ± 0.9 , 8.0 ± 1.0 , 12.0 ± 1.7 , and 14.0 ± 2.4 nm were obtained. They were characterized by spectroscopic (Figure S3, see Supporting Information) and microscopic methods (TEM), as shown in Figure S4. The spectra of Au-NRs@SiO₂ in the UV–vis range, taken at various time intervals (Figure S3, see Supporting Information), evidence their stability in the organic solvent (EtOH) over 2 months. The positions of LSPR maxima of Au-NRs@SiO₂ were confirmed by theoretical calculations.

The procedure used by us for functionalization of Au-NRs with a controlled thickness provides results of high accuracy and reproducibility. It shows that adjustment of optimal pH and control of CTAB concentration are important for successful synthesis.

To observe the energy transfer process between the dye and Au-NRs@SiO₂ or investigate the plasmon-enhanced singlet oxygen generation, hybrid mixtures with the well-defined SiO₂ coating of Au-NRs and chlorophyll derivative (Pheide) were prepared. The system should fulfill a certain condition: that is, the longitudinal extinction band of the prepared Au-NRs has to overlap the fluorescence spectrum of the dye (Figure 1). The maximum of Pheide fluorescence is located at 667 nm; therefore the Au-NRs of the aspect ratio of 2.25 ± 0.23 (maximum extinction at 660 nm) was used.

The absorption spectra of the prepared mixtures with a constant Pheide concentration and variable concentrations of Au-NRs@SiO₂ are shown in Figure 2. The increase in absorbance results from the increase in the concentration of Au-NRs@SiO₂ in each subsequent hybrid Pheide-Au-NRs@SiO₂ mixture. The additivity of the Pheide and Au-NRs spectra was also checked, and the calculated and measured spectra of investigated hybrid mixture were compared (not shown). The experimental and calculated spectra match very well, suggesting that Pheide is simply adsorbed on the surface of SiO₂-coated Au-NRs. This means that Au-NRs@SiO₂ and

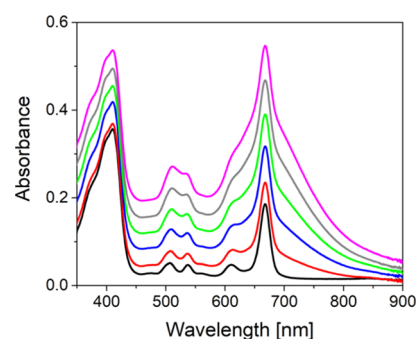


Figure 2. Absorption spectra of hybrid mixtures at the constant Pheide concentration (1.65×10^{-6} M) and different concentrations of Au-NRs for 6 nm SiO₂ thickness (0, 1.33, 2.66, 4.00, 5.33, 6.66) $\times 10^{-11}$ M from black to magenta line, respectively).

Pheide do not create a new complex upon mixing, which could affect the interaction of the dye with the plasmonic nanostructure. Absorption spectra of the investigated systems showed three distinct bands at 410, 510, and 667 nm corresponding to the Soret band of Pheide and to the Q_y Pheide bands overlapping the transversal and longitudinal LSPR bands of Au-NRs@SiO₂. As follows from the analysis of positions of the Soret and Q_y band of Pheide, the dye appears in the monomeric form. It is very important because the aggregation of the dye affects the ability to emit fluorescence and/or generate ¹O₂.

Fluorescence spectra of Pheide in a mixture with different Au-NRs@SiO₂ concentrations (Figure S5, see Supporting Information) show that its emission is quenched. Figure 3a,b presents ϕ_{ET} (eq 3) and ϕ_F (eq 1), respectively, for different Au-NRs concentrations and SiO₂ thicknesses. The K_{SV} values (obtained from the fits presented in Figure 3a) versus SiO₂ thickness are shown in Figure 3c for excitation wavelengths chosen on the basis of the absorption spectra. Linear Stern–Volmer dependencies (eq 2) plotted for the hybrid mixtures with different thicknesses of the SiO₂ layer suggest that in the investigated system, a single quenching mechanism is observed (Figure 3c). In each hybrid system with a different SiO₂ shell thickness (6–14 nm), a decrease in the Pheide fluorescence emission was observed along with increasing Au-NRs@SiO₂ concentration. This means that the efficiencies of deactivation processes which take place with the participation of singlet and/or triplet states of Pheide are modified by the presence and amounts of Au-NRs@SiO₂. In the physical mixture of the dye and NPs (in this case NRs), the dynamic quenching of fluorescence could be considered as reported in our previous study for spherical NPs.³⁹ As shown in Figure 3c, the value of K_{SV} decreases with the increasing thickness of the SiO₂ shell. The lowest value of K_{SV} is observed for the thickest shell, irrespectively of the excitation wavelength used. The value of K_{SV} ($4.3\text{--}2.4 \times 10^9$ M⁻¹) and similar slopes of linear dependencies also suggest that the dynamic quenching takes place and the distance between the dye and plasmonic NPs caused by the SiO₂ shell has some influence on the yield of this process. Taking into account the fact that the Au-NRs absorb light at the excitation wavelengths (at 510 and 667 nm), the IFE should be considered so the fluorescence data were corrected according to eq 5. Figure 3c showed that Stern–Volmer constant (K_{SV}) values are independent of the excitation wavelengths used but decrease with the SiO₂ thickness. The mean values of K_{SV} were $(4.34 \pm 0.15) \times$

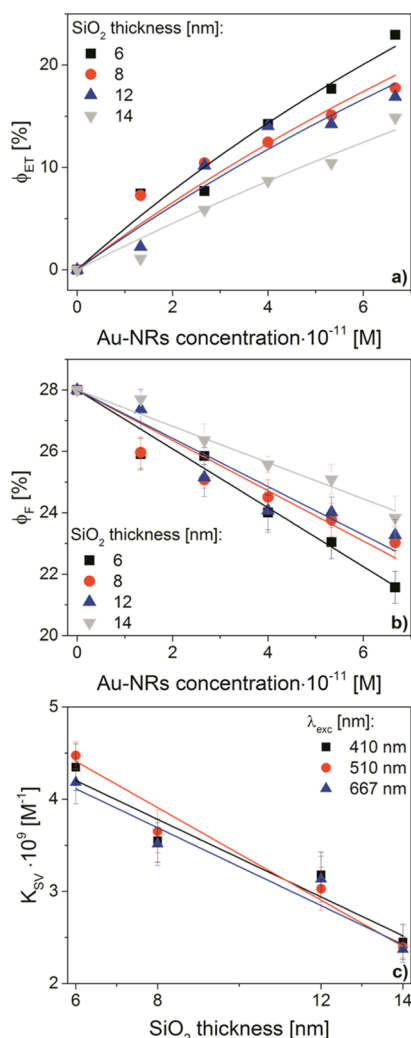


Figure 3. Energy transfer efficiency (ϕ_{ET}) (a) and fluorescence quantum yield (ϕ_F) (b) vs Au-NR concentration for different SiO₂ thicknesses (excitation at 667 nm), Stern–Volmer constant versus SiO₂ thickness for Pheide Au-NR mixtures for different excitation wavelengths (c). Taking into account the IFE, the presented photophysical parameters were obtained after correction (according to eq 5).

10^9 , $(3.57 \pm 0.07) \times 10^9$, $(3.11 \pm 0.07) \times 10^9$, and $(2.41 \pm 0.04) \times 10^9$ M⁻¹ for 6, 8, 12, and 14 nm thickness of SiO₂, respectively. In our previous studies²⁴ for spherical Au-NPs coated by polyethylene glycol, the K_{SV} values were about 1 order of magnitude lower, whereas Behera and Ram⁴⁰ have described the dynamic quenching process for spherical Au-NPs functionalized with polyvinylpyrrolidone characterized with a K_{SV} value of 2.23×10^6 M⁻¹.

The most important photophysical parameter, determining the photosensitizing properties and ability to affect the biological material, is the efficiency of singlet oxygen generation. For the system of dye-PS, the adequate triplet energy and the yield of triplet–triplet energy transfer between the dye and molecular oxygen determine the singlet oxygen generation. For this reason, the naturally occurring chlorophyll derivative (Pheide) was used. NPs by themselves are not able to generate ¹O₂ but the presence of a dye in the vicinity of NPs can cause plasmon-enhanced singlet oxygen generation. Thinking about the application of such a system to disturb

the pathological cells, it needs to be composed of the materials nontoxic for healthy cells. Our hybrid mixtures were based on such materials, that is, nanogold, SiO₂, and natural organic dyes. The influence of Au-NRs@SiO₂ on the value of ϕ_{Δ} of Pheide is illustrated in Figure 4. Two independent approaches

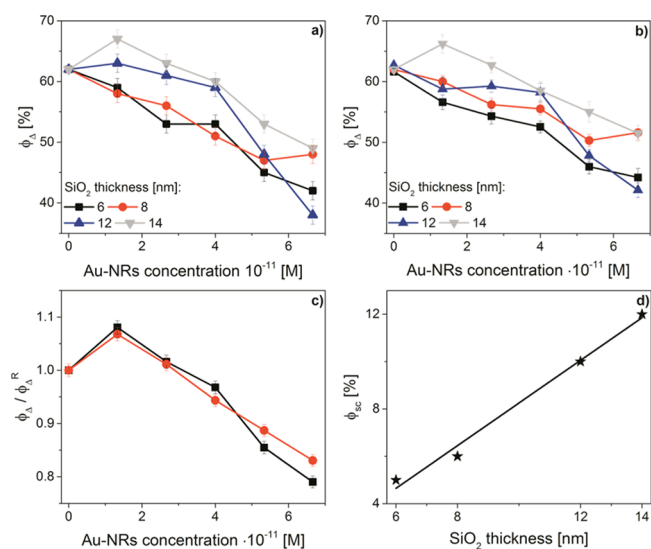


Figure 4. Singlet oxygen quantum yields (ϕ_{Δ}) for hybrid mixtures of Pheide and Au-NRs@SiO₂ (black, red, blue, and grey line: 6, 8, 12, and 14 nm of SiO₂, respectively) obtained using LIOAS (a) and photodegradation studies of DPBF (b), the enhancement factor of ϕ_{Δ} generation based on the results presented in (a,b) panel (black and red line, respectively) for 14 nm SiO₂ thickness (c), and the scattering yields of Au-NRs (ϕ_{sc}) vs SiO₂ thickness (d).

were used (and compared) to determine ϕ_{Δ} , that is, LIOAS (Figure 4a) and the photometric method based on photodegradation of DPBF (Figure 4b). Exemplary spectra and results used for the calculations of ϕ_{Δ} are presented in Figures S6 and S7 (see Supporting Information).

As it follows from Figure 4a,b, the enhancement of ϕ_{Δ} depends on the thickness of the SiO₂ shell and concentration of Au-NRs@SiO₂. The highest ϕ_{Δ} was observed for a low concentration of Au-NPs@SiO₂ (1.33×10^{-11} M) and a distance to the dye molecule of above 12 nm (defined by SiO₂ shell thickness). On the basis of the results from Figure 4a,b, the enhancement factor of ϕ_{Δ} generation was estimated for Au-NRs with SiO₂ coating thickness of 14 nm. The enhancement factor was calculated by dividing ϕ_{Δ} obtained for each hybrid mixture by ϕ_{Δ} determined for the dye (Figure 4c). The plot of the enhancement factor versus Au-NR concentration obtained by applying the two methods was similar. For the dyes covalently bound to Ag-NPs,^{17,33} the observed efficiency of ¹O₂ generation was the highest when the distance between the dye and the plasmonic structure was about 10–20 nm, depending on the shape of NPs. It seems that the distance of dye and plasmonic NPs even in the physical mixture confirmed that for the shell higher than 12 nm the increase in oxygen generation could be observed. The enhancement factor obtained by us is about 9% and is lower than that reported for spherical Ag-NPs.^{17,33} There are two reasons for this effect. At first it should be mentioned¹⁷ that the shape of NPs and the type of metal used have been shown to affect the effectiveness ϕ_{Δ} . As reported earlier,²³ the dye attached to nanocubes is more efficient in singlet oxygen

generation than that attached to nanospheres. On the other hand, the Ag-NPs have shown more than twice higher enhancement effect than Au-NPs.³³ It has been explained in terms of the far-field contribution to the plasmon-enhance mechanism and evidences the superiority of Ag as the plasmonic core in NPs. The second reason is that we used indirect and independent techniques to estimate ϕ_{Δ} : monitoring of the loss of absorbance of the $^1\text{O}_2$ trap (DPBF) and detection of heat generated by the investigated system (in time longer than 0.2 μs) related to processes other than the fast depopulation of dye singlet states. It is possible that using indirect methods we have obtained underestimated values of the enhancement factor (even 3-times according to the literature^{17,23,33}). The highest ϕ_{Δ} enhancement for 14 nm SiO_2 layer of Au-NRs could be also correlated with the value of ϕ_{sc} (Figure 4d). The ϕ_{sc} quantifies the fraction of light removed from the incident electromagnetic field that is re-emitted as scattered light by LSPR. Theoretically calculated RCS and ECS spectra of Au-NRs coated with 14 nm SiO_2 are shown in Figure S8 (see Supporting Information). For 6, 8, 12, and 14 nm SiO_2 -coated Au-NRs, the obtained ϕ_{sc} values are 5, 6, 10, and 12%. It seems, as proposed earlier,³³ that depending on the distances from the metal surface, the dye absorption could be enhanced due to the fact that the plasmonic structure can act as a secondary light source. This means that the far-field effect can increase the level of light trapping in the whole sample.

Recent studies⁴¹ have shown that Rayleigh scattering can lead to an increase in the optical path in solution, resulting in the increase in the ϕ_{Δ} not linked to the plasmonic effect. Bregnhøj et al.⁴¹ have also pointed out the importance of considering the influence of the scattering medium on optical measurement results. The authors claim that they have observed NP-mediated effect on the probability of the optical transition excited directly at 765 nm and explained it in terms of a NP-dependent change in the path length of light propagation through the sample. They investigated NPs with the ϕ_{sc} in the range of 5.5–88%. The ϕ_{sc} of the Au-NRs we used was from the range of 8–11% (Figure 4d) and the ϕ_{Δ} decreased with increasing concentration of Au-NRs (Figure 4c). In our samples, the singlet oxygen generation is followed by energy transfer between the donor (Pheide) and the acceptor (Au-NRs@ SiO_2). The advantage of methods used by us to determine ϕ_{Δ} is that they are relative and are based on independent approaches (detection of heat and photo-degradation of singlet oxygen quencher), and they give similar results. The results were carefully analyzed and to avoid Rayleigh scattering influence on LIOAS experiments, a mixture of dye-reference (Ni-substituted pheophytin *a*) and Au-NRs@ SiO_2 (in appropriate concentrations) was used as a reference sample. A similar experiment was performed using only dye as a reference sample. Therefore, we were able to compare ϕ_{Δ} values from two independent experiments and see if there is any difference in the enhancement of ϕ_{Δ} not linked to the plasmonic effect. Both used approaches need references, and the techniques are independent. As shown, in the investigated system, ϕ_{sc} is in the range of 8–11% and the increase in the scattering properties of the medium did not cause an increase in ϕ_{Δ} . The dye adsorption (*C*) decreases linearly with an increasing content of Au-NPs@ SiO_2 and *C* is correlated with the dependence of ϕ_{Δ} on Au-NR concentration. Decrease in *C* (with increasing concentration of Au-NRs) caused a decrease in ϕ_{Δ} . It suggested that the amount of the dye adsorbed at the

Au-NRs surface determine the values of ϕ_{Δ} as a result of the plasmonic interaction. The best condition for enhancement of ϕ_{Δ} was observed for 14 nm layer of silica (the highest one), 1.33×10^{-11} M Au-NPs@ SiO_2 concentration (the lowest one) and for about 53% of Pheide loading on the Au-NR surface. It seems that many variables and effects influence the process of enhancement singlet oxygen generation in hybrid dye-plasmonic nanostructure mixture.

4. CONCLUSIONS

The aim of the study was to modify the methods for the synthesis and functionalization of Au-NRs so that they would provide the possibility of synthesizing Au-NRs@ SiO_2 of reproducible properties realizable in any standard chemical laboratory. The prepared Au-NRs@ SiO_2 of well-defined SiO_2 coating thickness and showing properly localized LSPR band of Au-NRs@ SiO_2 , overlapping with the Q band of the chlorophyll derivative (Pheide) would permit investigation of distance-dependent deactivation processes in a gold nanostructure–natural dye hybrid mixture.

In hybrid mixtures of not chemically bound and interacting components (Pheide and Au-NRs coated with SiO_2 of different thickness), the deactivation processes were studied. It was found that even in such physical mixtures not only the presence of metal NPs but also the distance between the plasmonic structure and the dye (defined by the thickness of silica) influence the yields of nonradiative and radiative depopulation of singlet and/or triplet states of Pheide whose emission band overlapped the LSPR band of NRs. The yield of plasmon-enhanced singlet oxygen generation in the hybrid mixtures depends on the thickness of the coating layer, the concentration of metal nanostructures, and their scattering yields. Fluorescence quenching studies showed also that the thickness of SiO_2 layer coating of Au-NRs influences the Stern–Volmer constant. Another advantage of using NRs is also the possibility to tune their longitudinal LSPR to obtain the overlap with the fluorescence bands with any PSs, especially those that absorb light in the therapeutic window (above 650 nm). The size of NPs is also important to be easily incorporated into the biological system without disordering the biological membrane of healthy cells. Au-NRs with an LSPR band shown in Figure S1 (see Supporting Information) have the long axis from the range 630–740 nm. Their size is similar or smaller than that of NPs used to inactivate different bacteria culture.¹⁷ The results suggest a potential of hybrid mixtures of Pheide and Au-NRs@ SiO_2 , based on only nontoxic materials, for phototherapeutic applications.

■ ASSOCIATED CONTENT

Supporting Information

The Supporting Information is available free of charge at <https://pubs.acs.org/doi/10.1021/acs.jpcc.9b08204>.

Chemical synthesis of gold nanorods; characterization of gold nanorods; spectroscopic studies of hybrid systems; and theoretical cross section spectra of gold nanorods (PDF)

■ AUTHOR INFORMATION

Corresponding Author

Alina Dudkowiak – Poznan University of Technology, Poznan, Poland; orcid.org/0000-0001-5487-4051; Email: alina.dudkowiak@put.poznan.pl

Other Authors

Paulina Blaszkiewicz – Poznan University of Technology, Poznan, Poland; orcid.org/0000-0002-2355-8889

Michał Kotkowiak – Poznan University of Technology, Poznan, Poland; orcid.org/0000-0001-6611-0366

Emerson Coy – Adam Mickiewicz University, Poznan, Poland; orcid.org/0000-0002-4149-9720

Complete contact information is available at:
<https://pubs.acs.org/10.1021/acs.jpcc.9b08204>

Notes

The authors declare no competing financial interest.

ACKNOWLEDGMENTS

This work was supported by the Polish Ministry of Science and Higher Education. E.C. acknowledges the partial support provided by the project H2020-MSCA-RISE-2017 (project number: 778157). We would also like to thank Prof. Leszek Fiedor from the Faculty of Biochemistry, Biophysics, and Biotechnology at the Jagiellonian University in Poland for kindly providing the Ni²⁺ complex with pheophytin a.

REFERENCES

- (1) Qi, Y.; Xiu, F.-R. Sensitive and Rapid Chemiluminescence Detection of Propranolol Based on Effect of Surface Charge of Gold Nanoparticles. *J. Lumin.* **2016**, *171*, 238–245.
- (2) Kuo, W.-S.; Chang, C.-N.; Chang, Y.-T.; Yang, M.-H.; Chien, Y.-H.; Chen, S.-J.; Yeh, C.-S. Gold Nanorods in Photodynamic Therapy, as Hyperthermia Agents, and in Near-Infrared Optical Imaging. *Angew. Chem., Int. Ed.* **2010**, *49*, 2711–2715.
- (3) Wang, X.-W.; Gao, W.; Fan, H.; Ding, D.; Lai, X.-F.; Zou, Y.-X.; Chen, L.; Chen, Z.; Tan, W. Simultaneous Tracking of Drug Molecules and Carriers Using Aptamer-Functionalized Fluorescent Superstable Gold Nanorod–Carbon Nanocapsules during Thermo-Chemotherapy. *Nanoscale* **2016**, *8*, 7942–7948.
- (4) Fang, S.; Li, C.; Lin, J.; Zhu, H.; Cui, D.; Xu, Y.; Li, Z. Gold Nanorods-Based Theranostics for Simultaneous Fluorescence/Two-Photon Luminescence Imaging and Synergistic Phototherapies. *J. Nanomater.* **2016**, *2016*, 1–10.
- (5) El-Sayed, I. H.; Huang, X.; El-Sayed, M. A. Surface Plasmon Resonance Scattering and Absorption of Anti-EGFR Antibody Conjugated Gold Nanoparticles in Cancer Diagnostics: Applications in Oral Cancer. *Nano Lett.* **2005**, *5*, 829–834.
- (6) He, S.; Kang, M. W. C.; Khan, F. J.; Tan, E. K. M.; Reyes, M. A.; Kah, J. C. Y. Optimizing Gold Nanostars as a Colloid-Based Surface-Enhanced Raman Scattering (SERS) Substrate. *J. Opt.* **2015**, *17*, 114013.
- (7) Gamaleia, N. F.; Shton, I. O. Gold Mining for PDT: Great Expectations from Tiny Nanoparticles. *Photodiagn. Photodyn. Ther.* **2015**, *12*, 221–231.
- (8) Blaszkiewicz, P.; Kotkowiak, M. Gold-Based Nanoparticles Systems in Phototherapy - Current Strategies. *Curr. Med. Chem.* **2019**, *25*, 5914–5929.
- (9) Wang, L.; Meng, D.; Hao, Y.; Zhao, Y.; Li, D.; Zhang, B.; Zhang, Y.; Zhang, Z. Gold Nanostars Mediated Combined Photothermal and Photodynamic Therapy and X-Ray Imaging for Cancer Theranostic Applications. *J. Biomater. Appl.* **2015**, *30*, 547–557.
- (10) Harmsen, S.; Huang, R.; Wall, M. A.; Karabeber, H.; Samii, J. M.; Spaliviero, M.; White, J. R.; Monette, S.; O'Connor, R.; Pitter, K. L.; et al. Surface-Enhanced Resonance Raman Scattering Nanostars for High-Precision Cancer Imaging. *Sci. Transl. Med.* **2015**, *7*, 271ra7.
- (11) Turcheniuk, K.; Turcheniuk, V.; Hage, C.-H.; Dumych, T.; Bilyy, R.; Bouckaert, J.; Héliot, L.; Zaitsev, V.; Boukherroub, R.; Szunerits, S. Highly Effective Photodynamic Inactivation of E. Coli Using Gold Nanorods/SiO₂ Core–Shell Nanostructures with Embedded Verteporfin. *Chem. Commun.* **2015**, *51*, 16365–16368.
- (12) Abadeer, N. S.; Brennan, M. R.; Wilson, W. L.; Murphy, C. J. Distance and Plasmon Wavelength Dependent Fluorescence of Molecules Bound to Silica-Coated Gold Nanorods. *ACS Nano* **2014**, *8*, 8392–8406.
- (13) Ung, T.; Liz-Marzán, L. M.; Mulvaney, P. Optical Properties of Thin Films of Au@SiO₂ Particles. *J. Phys. Chem. B* **2001**, *105*, 3441–3452.
- (14) Liz-Marzán, L. M.; Giersig, M.; Mulvaney, P. Synthesis of Nanosized Gold-Silica Core-Shell Particles. *Langmuir* **1996**, *12*, 4329–4335.
- (15) Guerrero-Martínez, A.; Pérez-Juste, J.; Liz-Marzán, L. M. Recent Progress on Silica Coating of Nanoparticles and Related Nanomaterials. *Adv. Mater.* **2010**, *22*, 1182–1195.
- (16) Kertmen, A.; Torruella, P.; Coy, E.; Yate, L.; Nowaczyk, G.; Gapiński, J.; Vogt, C.; Toprak, M.; Estradé, S.; Peiró, F.; et al. Acetate-Induced Disassembly of Spherical Iron Oxide Nanoparticle Clusters into Monodispersed Core-Shell Structures upon Nanoemulsion Fusion. *Langmuir* **2017**, *33*, 10351–10365.
- (17) Planas, O.; Macia, N.; Agut, M.; Nonell, S. Distance-Dependent Plasmon-Enhanced Singlet Oxygen Production and Emission for Bacterial Inactivation. *J. Am. Chem. Soc.* **2016**, *138*, 2762–2768.
- (18) Ke, X.; Wang, D.; Chen, C.; Yang, A.; Han, Y.; Ren, L.; Li, D.; Wang, H. Co-Enhancement of Fluorescence and Singlet Oxygen Generation by Silica-Coated Gold Nanorods Core-Shell Nanoparticle. *Nanoscale Res. Lett.* **2014**, *9*, 666.
- (19) Nikoobakht, B.; Sayed, A. El. Preparation and Growth Mechanism of Gold Nanorods (NRs) Using Seed-Mediated Growth Method. *Chem. Mater.* **2003**, *15*, 1957–1962.
- (20) Stöber, W.; Fink, A. Controlled Growth of Monodisperse Silica Spheres in the Micron Size Range. *J. Colloid Interface Sci.* **1968**, *26*, 62–69.
- (21) Hanske, C.; Sanz-Ortiz, M. N.; Liz-Marzán, L. M. Silica-Coated Plasmonic Metal Nanoparticles in Action. *Adv. Mater.* **2018**, *30*, 1707003.
- (22) Orendorff, C. J.; Murphy, C. J. Quantitation of Metal Content in the Silver-Assisted Growth of Gold Nanorods. *J. Mater. Chem. B* **2006**, *110*, 3990–3994.
- (23) Macia, N.; Bresoli-Obach, R.; Nonell, S.; Heyne, B. Hybrid Silver Nanocubes for Improved Plasmon-Enhanced Singlet Oxygen Production and Inactivation of Bacteria. *J. Am. Chem. Soc.* **2019**, *141*, 684–692.
- (24) Kotkowiak, M.; Dudkowiak, A. Multiwavelength Excitation of Photosensitizers Interacting with Gold Nanoparticles and Its Impact on Optical Properties of Their Hybrid Mixtures. *Phys. Chem. Chem. Phys.* **2015**, *17*, 27366–27372.
- (25) Lakowicz, J. R. *Principles of Fluorescence Spectroscopy*; Lakowicz, J. R., Ed.; Springer, 2006.
- (26) Chadwick, S. J.; Salah, D.; Livesey, P. M.; Brust, M.; Volk, M. Singlet Oxygen Generation by Laser Irradiation of Gold Nanoparticles. *J. Phys. Chem. C* **2016**, *120*, 10647–10657.
- (27) Kotkowiak, M.; Dudkowiak, A.; Fiedor, L. Intrinsic Photoprotective Mechanisms in Chlorophylls. *Angew. Chem., Int. Ed.* **2017**, *56*, 10457–10461.
- (28) Pilch, M.; Dudkowiak, A.; Jurzyk, B.; Łukasiewicz, J.; Susz, A.; Stochel, G.; Fiedor, L. Molecular Symmetry Determines the Mechanism of a Very Efficient Ultrafast Excitation-to-Heat Conversion in Ni-Substituted Chlorophylls. *Biochim. Biophys. Acta - Bioenerg.* **2013**, *1827*, 30–37.
- (29) Martí, C.; Nonell, S.; Nicolau, M.; Torres, T. Photophysical Properties of Neutral and Cationic Tetrapyrrolineporphyrazines. *Photochem. Photobiol.* **2000**, *71*, 53–59.
- (30) Kotkowiak, M.; Grześkiewicz, B.; Robak, E.; Wolarz, E. Interaction between Nanoprisms with Different Coupling Strength. *J. Phys. Chem. C* **2015**, *119*, 6195–6203.
- (31) Grześkiewicz, B.; Ptaszyński, K.; Kotkowiak, M. Near and Far-Field Properties of Nanoprisms with Rounded Edges. *Plasmonics* **2014**, *9*, 607–614.

- (32) Błaszkiwicz, P.; Kotkowiak, M.; Coy, E.; Dudkowiak, A. Laser-Induced Optoacoustic Spectroscopy Studies of Inorganic Functionalized Metallic Nanorods. *J. Phys. Chem. C* **2019**, *123*, 27181–27186.
- (33) Macia, N.; Kabanov, V.; Côté-Cyr, M.; Heyne, B. Roles of Near and Far Fields in Plasmon-Enhanced Singlet Oxygen Production. *J. Phys. Chem. Lett.* **2019**, *10*, 3654–3660.
- (34) Murphy, C. J.; Jana, N. R. Controlling the Aspect Ratio of Inorganic Nanorods and Nanowires. *Adv. Mater.* **2002**, *14*, 80–82.
- (35) Becker, R.; Liedberg, B.; Käll, P.-O. CTAB Promoted Synthesis of Au Nanorods - Temperature Effects and Stability Considerations. *J. Colloid Interface Sci.* **2010**, *343*, 25–30.
- (36) Gorelikov, I.; Matsuura, N. Single-Step Coating of Mesoporous Silica on Cetyltrimethyl Ammonium Bromide-Capped Nanoparticles. *Nano Lett.* **2008**, *8*, 369–373.
- (37) Zhao, J.; Xu, P.; Li, Y.; Wu, J.; Xue, J.; Zhu, Q.; Lu, X.; Ni, W. Direct Coating of Mesoporous Titania on CTAB-Capped Gold Nanorods. *Nanoscale* **2016**, *8*, 5417–5421.
- (38) Li, J.; Zhu, B.; Zhu, Z.; Zhang, Y.; Yao, X.; Tu, S.; Liu, R.; Jia, S.; Yang, C. J. Simple and Rapid Functionalization of Gold Nanorods with Oligonucleotides Using an MPEG-SH/Tween 20-Assisted Approach. *Langmuir* **2015**, *31*, 7869–7876.
- (39) Błaszkiwicz, P.; Kotkowiak, M.; Dudkowiak, A. Fluorescence Quenching and Energy Transfer in a System of Hybrid Laser Dye and Functionalized Gold Nanoparticles. *J. Lumin.* **2017**, *183*, 303–310.
- (40) Behera, M.; Ram, S. Intense Quenching of Fluorescence Intensity of Poly(Vinyl Pyrrolidone) Molecules in Presence of Gold Nanoparticles. *Appl. Nanosci.* **2013**, *3*, 543–548.
- (41) Bregnhøj, M.; Rodal-Cedeira, S.; Pastoriza-Santos, I.; Ogilby, P. R. Light Scattering versus Plasmon Effects: Optical Transitions in Molecular Oxygen near a Metal Nanoparticle. *J. Phys. Chem. C* **2018**, *122*, 15625–15634.

Supplementary Information

for

Tailoring Fluorescence and Singlet Oxygen Generation of a Chlorophyll Derivative and Gold Nanorods via a Silica Shell

Paulina Błaszkiwicz[†], Michał Kotkowiak[†], Emerson Coy[‡], Alina Dudkowiak^{†}*

[†]Faculty of Technical Physics, Poznan University of Technology, Piotrowo 3, 60-965 Poznan, Poland

[‡]NanoBioMedical Centre, Adam Mickiewicz University, Wszechnicy Piastowskiej 3, 61-614 Poznan, Poland

To whom correspondence should be addressed:

*e-mail: alina.dudkowiak@put.poznan.pl

1.1. Chemical synthesis of gold nanorods

All chemicals were dissolved in Mili-Q ultra-pure water in glass flasks treated with *aqua regia* prior to use. The synthesis of Au-NRs was performed by *in situ bottom-up* methods, which involved the reduction of HAuCl_4 with NaBH_4 . The synthesis of Au-NRs is a two-step process. Synthesis of gold nanorods was carried out according to the *seed-mediated growth* method proposed by Nikoobakht et al.¹ with our modifications. Details of the synthesis are presented in our previous paper.² For seed preparation, 5 mL of a 0.5 mM HAuCl_4 solution was added to 5 mL of 0.2 M CTAB solution. Then, 0.6 mL freshly prepared and cooled reducing agent (NaBH_4) was added under vigorous stirring at a constant temperature and humidity. The solution changes color from yellow to brownish-yellow. Seed solution of spherical gold NPs was stored at 28°C, which prevented the crystallization of CTAB surfactant. Subsequently 12 μL of seeds solution was added to the growth solution containing CTAB (0.2 M), HAuCl_4 (0.001 M), AgNO_3 (0.004 M) and ascorbic acid (0.078 M). After stirring, the growth solution has changed color, which indicated the formation of Au-NRs. Addition of increased volume of AgNO_3 caused a shift of the position of the longitudinal band assigned to Au-NRs (Fig. S1).

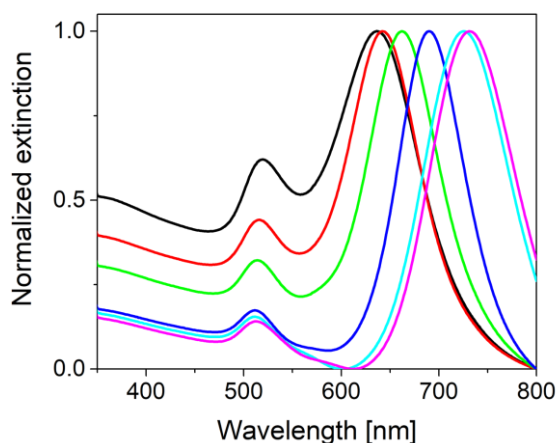


Figure S1. Extinction spectra of Au-NRs with different localized surface plasmon resonance (black, red, green, dark blue, blue, pink lines for 0.05, 0.075, 0.1, 0.15, 0.2, 0.25 mL of AgNO_3 per concentration (0.004 M), respectively).

1.2. Functionalization of gold nanorods

Functionalization was carried out using the CTAB template. More details about functionalization are given presented in our previous work.² After Au-NRs purification CTAB (0.2 M) was added in different volumes (0.4, 0.6, 1.2 and 1.2 mL) and stirred for 4 hours to equilibrate CTAB on the surface of Au-NRs. The SiO_2 layer thickness was controlled by a desired concentration of CTAB. The right pH (10) was fixed by addition of NaOH (0.1 M). After 1 hour, TEOS was added in dropwise injections at 30 min intervals (90 μL 20% in EtOH). The mixture was left undisturbed overnight at 25°C. Finally, the solution was centrifuged twice at 6000 rpm for 30 min. and Au-Ns@ SiO_2 was transferred to EtOH.

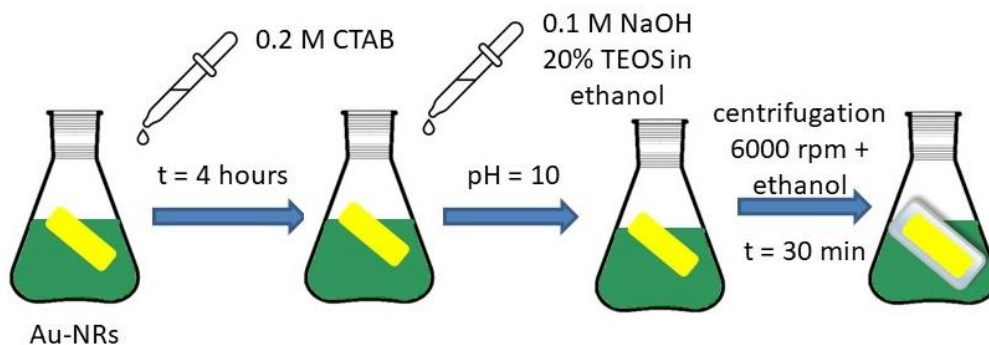


Figure S2. Scheme of functionalization of Au-NRs with SiO₂ (Au-NRs@SiO₂).

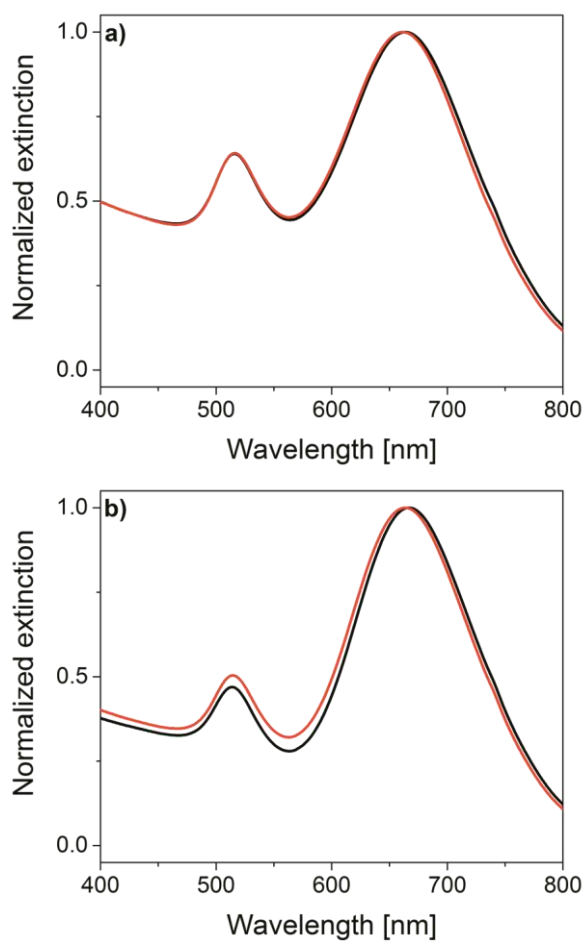


Figure S3. Stability of functionalized Au-NRs (AuNRs@SiO₂) in ethanol, exemplary curves for 6 nm (a) and 12 nm (b) SiO₂ thicknesses (black and red line, after synthesis and 2 months later, respectively).

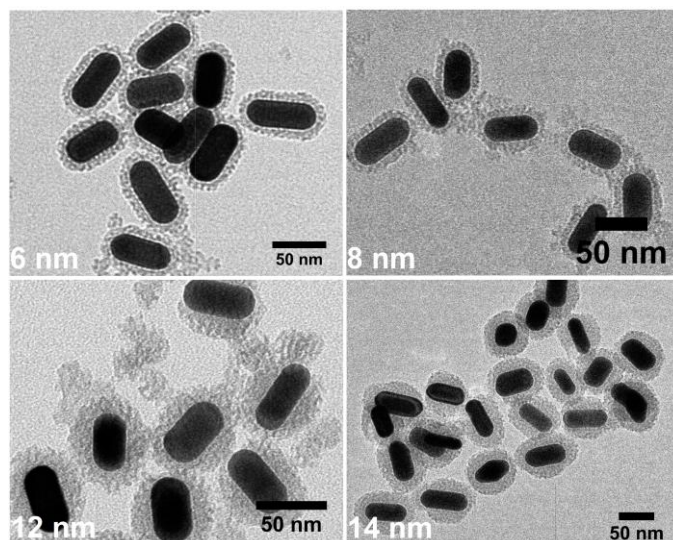


Figure S4. TEM images of SiO₂ coating on the surface of Au-NRs (in each panel SiO₂ thickness was indicated). Reprinted with permission from ref². Copyright 2019 American Chemical Society.

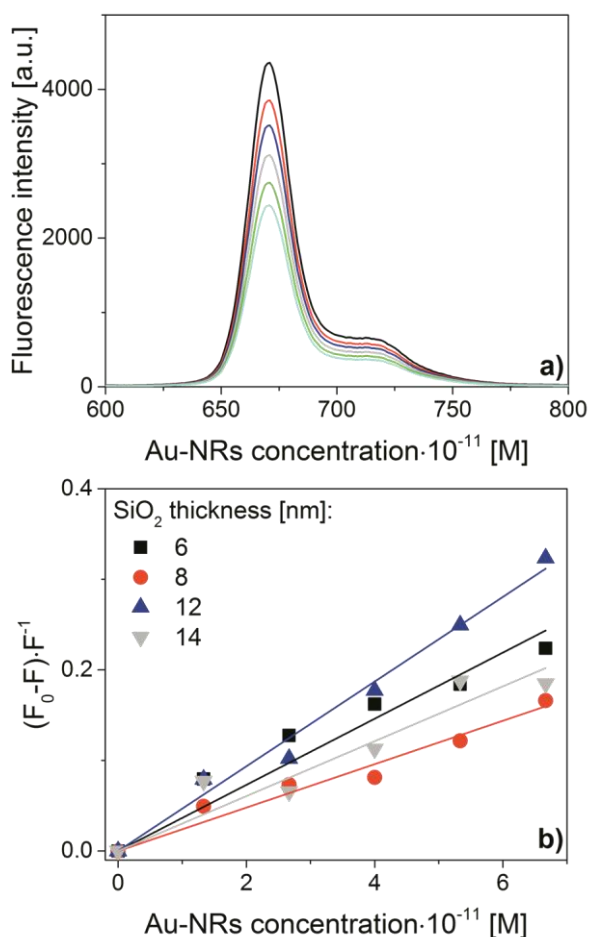


Figure S5. Fluorescence spectra of Pheide mixed with 6 nm Au-NRs@SiO₂ for different concentrations of Au-NRs@SiO₂ (a) and Stern-Volmer plots for Pheide mixed with Au-NRs@SiO₂ for different SiO₂ thicknesses, $R^2 > 0.95$. The excitation wavelengths was 510 nm.

The data presented in panel (a) were raw, while in panel (b) were recalculated taking into account the IFE.

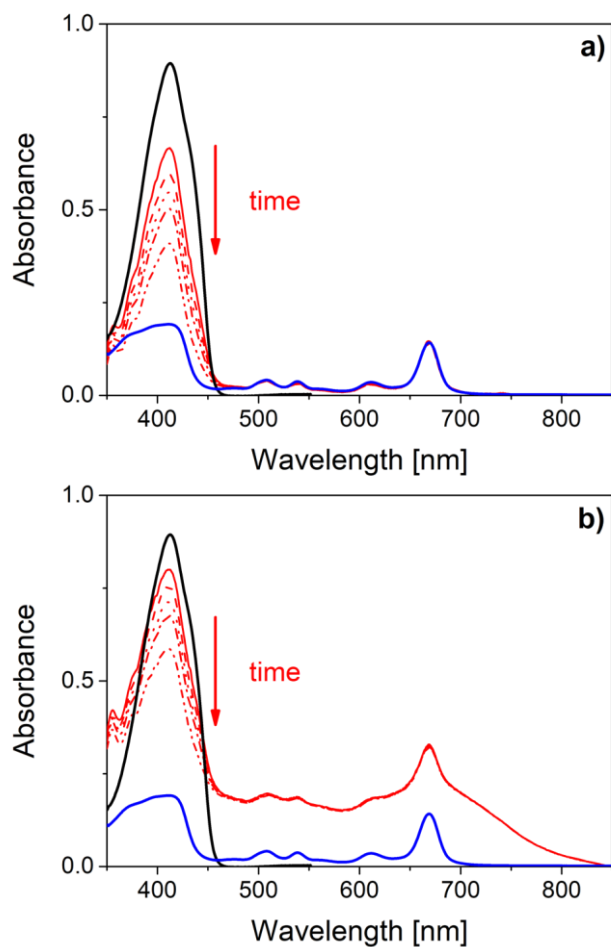


Figure S6. Absorption spectra of DPBF (black line), Pheide (blue line) and for their mixtures without (a) and with (b) Au-NRs@SiO₂ with 14 nm SiO₂ (red) recorded at different irradiated time (red lines).

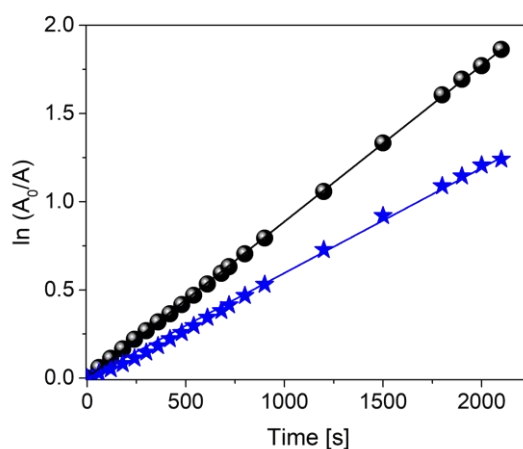


Figure S7. Kinetic curves of DPBF absorption decay upon oxidation by singlet oxygen generated during irradiation of Pheide (black) and Pheide with its mixture with Au-NRs@SiO₂ with 14 nm SiO₂ thickness (blue).

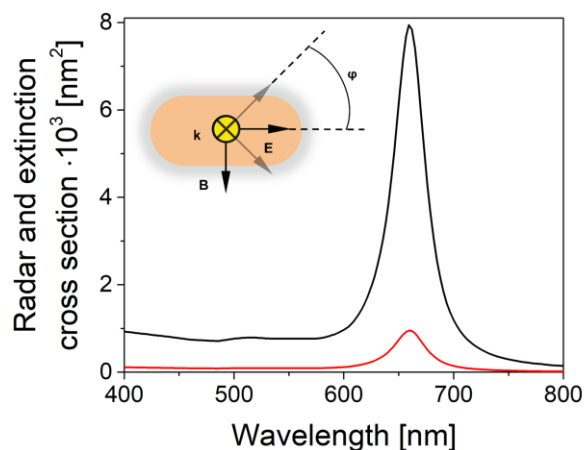


Figure S8. Theoretically calculated cross-section spectra of Au-NRs@SiO₂ coated with 14 nm SiO₂ (radar and optical extinction, black and red line, respectively) with the top view of excitation geometry shown in inset (the angle (φ) between the longitudinal axis of Au-NRs and the electric vector of the electromagnetic wave was fixed at 45°).

References

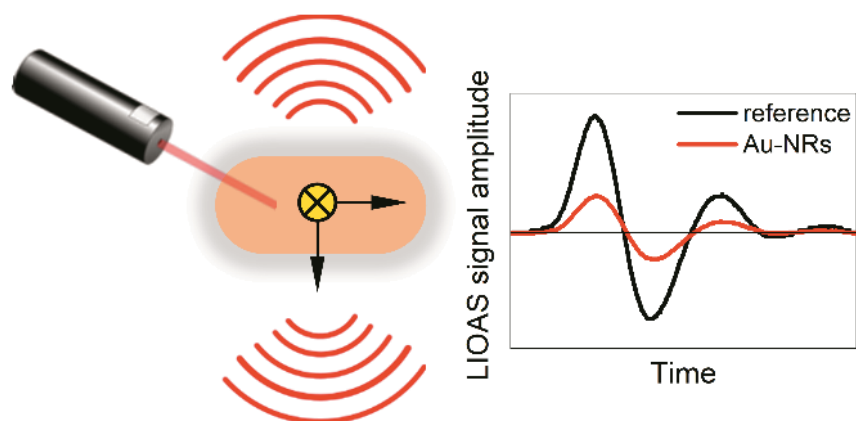
- (1) Nikoobakht, B.; Sayed, A. El. Preparation and Growth Mechanism of Gold Nanorods (NRs) Using Seed-Mediated Growth Method. *Chem. Mater.* **2003**, *15* (10), 1957–1962.
- (2) Błaszkiwicz, P.; Kotkowiak, M.; Coy, E.; Dudkowiak, A. Laser-Induced Optoacoustic Spectroscopy Studies of Inorganic Functionalized Metallic Nanorods. *J. Phys. Chem. C* **2019**, *123* (44), 27181–27186.

Przedruk publikacji [**Błaszkiwicz, JPCC 2019**]

P. Błaszkiwicz, M. Kotkowiak, E. Coy, A. Dudkowiak,

Laser-induced optoacoustic spectroscopy studies of inorganic functionalized metallic nanorods,

Journal of Physical Chemistry C 123(44) (2019), 27181–27186. (MEiN 140, IF 4,189)



Laser-Induced Optoacoustic Spectroscopy Studies of Inorganic Functionalized Metallic Nanorods

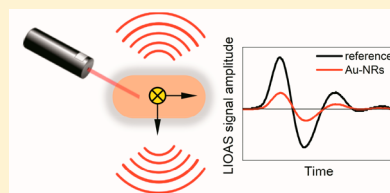
Paulina Błaszczewicz,[†] Michał Kotkowiak,^{*,†} Emerson Coy,[‡] and Alina Dudkowiak[†]

[†]Faculty of Technical Physics, Poznan University of Technology, Piotrowo 3, 60-965 Poznan, Poland

[‡]NanoBioMedical Centre, Adam Mickiewicz University, Wszechnicy Piastowskiej 3, 61-614 Poznan, Poland

S Supporting Information

ABSTRACT: Plasmonic nanoparticles can be used in photothermal therapy thanks to their ability to generate local heat. The light-to-heat conversion efficiency is crucial for therapeutic and diagnostic applications. The photothermal properties of gold nanorods functionalized with silica layers of controllable thickness were characterized using both theoretical and experimental approaches. The time-resolved laser-induced optoacoustic spectroscopy (LIOAS) was used to determine the amount of absorbed energy that changed promptly into heat. The heat generation efficiencies were simulated by the means of finite integration technique. The obtained parameters were correlated with silica thickness. Experimental results are consistent with theoretical predictions; thus, LIOAS is a unique reliable method for studying photothermal effect in gold nanoparticles.



1. INTRODUCTION

Nanotechnology has become a hot subject of interest worldwide. Most of the current research has been concerned with metal nanoparticles (NPs), which have been applied in many areas including electronics, photonics, biochemistry, imaging, and photomedicine.¹ The synthesis of gold NPs of well-defined morphology (shape and size) is a key aspect of fabrication of functional materials on the nanoscale.² A characteristic property of the colloidal solution of gold NPs is the intense color related to their localized surface plasmon resonance (LSPR). Gold nanorods (Au-NRs) show interesting optical properties which, coupled with their known biological inertness, make them ideal probes for biological applications. Au-NRs are characterized by the cross-sectional area for light absorption higher than those of other NPs; besides, it is easy to control their absorption of near-infrared radiation and to produce them on a large scale while maintaining particle size control.^{3,4} Depending on the synthesis conditions, NPs of different shapes and plasmon resonance spectral localizations can be obtained. Furthermore, a very attractive possibility from the applications point of view is efficient and reliable synthesis of NPs showing LSPR in different spectral ranges, from visible to infrared.^{5,6} Au-NRs are capable of highly efficient transformation of the absorbed energy into heat; thus, they are promising agents for application in photothermal therapy (PTT).^{7,8} Unlike photodynamic therapy, PTT does not require the presence of oxygen. PTT is a noninvasive method, which uses low-energy radiation in the infrared range of electromagnetic spectrum for the destruction of various pathological cells, including cancer.⁹ Depending on the cancer type, NPs with different shapes and optical properties are applied. The electromagnetic radiation, absorbed by the NPs localized in the pathological cells, is converted into heat, which increases the local temperature and causes protein denatura-

tion in cells, leading to their death. Gold NPs also efficiently absorb light from the visible spectral range, which allows their application as contrast materials in PTT.¹⁰ One of the problems related to the use of NPs in PTT is their aggregation in an aqueous environment, which decreases the light-to-heat conversion efficiency.¹¹ Thus, many encapsulation systems, such as polymers, human serum albumin, DNA, or mesoporous silica (SiO₂), have been designed and proposed to avoid NPs self-aggregation.¹² Moreover, suitable functionalization of the NPs used in the PTT also allows solving other issues, for example, increase in accumulation of NPs in the liver, the kidney, and spleen to be rapidly released from the organism as well as preserve the stability of the penetration efficiency at temperatures higher than human physiological temperature (application of a laser light and hyperthermia effect increase the temperature of NPs, which can change their properties).¹³ The changes in the Au-NRs shape can be inhibited by covering their surface, for example, by PEG polymer or an inorganic coating such as SiO₂ or TiO₂.^{14,15} The SiO₂ coating of Au-NRs can preserve their unique optical properties and improve colloidal and thermal stability in organic solvents.^{16,17} This type of coating also allows transportation of NPs into the pathological cells by the process of endocytosis.¹⁸ It is also important that the SiO₂ is nontoxic for living organisms and degrades in the human body to silica acid which is easily eliminated from the human organism.^{16,19} Coating of Au-NRs with SiO₂ shell improves also their stability and prevents aggregation in alcoholic/water solutions. To control the thickness of the SiO₂ coating and the reproducibility of its formation, it is necessary to develop and optimize a suitable procedure based on the Stöber method.²⁰

Received: October 7, 2019

Published: October 11, 2019

Moreover, laser-induced temperature increase is observed in SiO₂ coated Au-NRs system. This property of photothermal conversion could be used for noninvasive killing of cancer cells in vivo.²¹

Photothermal properties of metallic NPs can be determined by the quantification analysis of the generated heat. Both theoretical^{22–25} and experimental^{26–28} approaches to quantify plasmonic heating effect have appeared in the literature. However, not many reports have focused on the integration of these approaches,²⁹ which would help to predict the therapeutic and diagnostic outcome. Therefore, we have undertaken a study of the influence of SiO₂ shell thickness on the photothermal properties of Au-NRs using experimental and theoretical simulation methods. Moreover, we have shown for the first time the usefulness of time-resolved laser-induced optoacoustic spectroscopy (LIOAS) to quantify plasmonic heating effect in core–shell Au-NRs.

2. EXPERIMENTAL SECTION

2.1. Synthesis of Gold Nanorods. The details concerning the synthesis of Au-NRs were presented in the [Supporting Information](#).

2.2. Microscopic and Spectroscopic Techniques. The morphology of Au-NRs and their size distribution were characterized by transmission electron microscopy (HR-TEM) using a JEOL ARM-200F instrument (200 kV) and JEOL 1400 (120 kV). Particles were drop-casted on Cu grids and placed on a vacuum desiccator overnight. UV–vis absorption spectra were measured using a Varian Cary 4000 spectrometer. The LIOAS setup has been described in detail elsewhere.^{30,31} The excitation wavelength for LIOAS studies was set to the longitudinal localized surface plasmon resonance band of Au-NRs (approximately 660 nm). The temperature of the samples during LIOAS measurement was kept constant at (20.00 ± 0.01) °C. Ni-substituted pheophytin *a* (Ni-Phea)³² was used as photocalorimetric reference; see UV–vis absorption spectrum shown in [Figure S1](#). Ni-Phea was used at concentrations from the range of 1 × 10^{−6} M. According to the approach proposed by Marti and co-workers,³³ the first maximum of the LIOAS signal (H_{\max}) is described by the equation

$$H_{\max} = C\alpha E_{\text{las}}(1 - 10^{-A}) \quad (1)$$

where A is the absorbance of the reference or investigated Au-NRs, E_{las} is the energy of the incidence light, C is the coefficient related to the geometry of the experiment, and α is the fraction of excitation energy converted promptly into heat (in the time shorter than the time resolution of the apparatus). To eliminate C and estimate α , the comparative LIOAS measurements were made for reference. Ni-Phea is known to release all the absorbed energy as heat in times shorter than the time resolution of the apparatus ($\alpha_{\text{R}} = 1$). Because α_{R} and the absorbance of the sample and the reference are known (A_{S} and A_{R} , respectively), the absorbed energy promptly changed into heat by sample (α_{S}) can be expressed as

$$\alpha_{\text{S}} = \alpha_{\text{R}} \frac{H_{\max}^{\text{S}} E_{\text{las}}^{\text{R}} (1 - 10^{-A_{\text{R}}})}{H_{\max}^{\text{R}} E_{\text{las}}^{\text{S}} (1 - 10^{-A_{\text{S}}})} \quad (2)$$

In LIOAS experiment, α_{S} is estimated for an effective acoustic transit time defined as $\tau_{\text{a}}' = 2R/v_{\text{a}}$ where $2R$ is the beam diameter (the pinhole used was 1 mm) and v_{a} is the sound velocity in the solvent (τ_{a}' is 1.0 μs for ethanol (EtOH)).

The Au-NRs were dissolved in EtOH and their volume was kept constant and equal to 1.5 mL during LIOAS measurements. The concentration of Au-NRs capped by SiO₂ was 6.66 × 10^{−11} M (extinction coefficient 3.11 × 10⁹ M^{−1} cm^{−1} was taken from previous studies for bare Au-NRs³⁴). In the LIOAS experiment extinction coefficient of Au-NRs is not used in determination of α ; thus, we used a literature value for the extinction coefficient of bare Au-NRs.

2.3. Computational Simulations. Numerical simulations were performed by employing the finite integration technique (FIT) implemented into the CST Microwave Studio software. All the simulations presented in this paper used a frequency domain solver with a tetrahedral mesh. The tetrahedral grid provides flexibility in approximating arbitrary (rounded) geometries.³⁵ The details concerning this method are described elsewhere.^{36,37} We used a tetrahedral mesh of about 60 000 cells. The grid step varied from 0.5 nm inside the Au-NRs to 10 nm in the free space. The bulk dielectric permittivities ϵ used in the calculations were obtained from the experiment.³⁸ In this study the optical extinction, radar, and absorption cross sections (i.e., ECS, RCS, and ACS, respectively) of SiO₂-functionalized Au-NRs were calculated. Taking into account the analysis of TEM images, the mean length of the Au-NRs was fixed at (53.2 ± 1.8) nm, while the mean diameter at was (23.6 ± 1.3) nm. Light-to-heat conversion efficiency was determined by the relative contribution of ACS to ECS. In this context, the mean heating efficiency (ϕ_{heat} , defined as the fraction of extinction energy that is transformed into heat), for the Au-NRs, can be defined as^{39,40}

$$\phi_{\text{heat}} = \frac{\sum_{\varphi=0^{\circ}}^{90^{\circ}} \int_{\lambda_1}^{\lambda_2} \text{ACS}(\lambda) d\lambda}{\sum_{\varphi=0^{\circ}}^{90^{\circ}} \int_{\lambda_1}^{\lambda_2} \text{ECS}(\lambda) d\lambda} \quad (3)$$

where λ_1 and λ_2 were 400 and 800 nm, respectively. The ACS and ECS spectra were obtained for different angles between longitudinal axis of Au-NRs and electric vector of the electromagnetic wave $\varphi \in \langle 0^{\circ}-90^{\circ} \rangle$ and were then averaged according to [formula \(3\)](#) to obtain the mean value of ϕ_{heat} .

3. RESULTS AND DISCUSSION

The functionalized Au-NRs (with the longitudinal LSPR band in the spectral range at approximately 660 nm) with a defined SiO₂ shell thickness (6, 8, 12, and 14 nm) were characterized by spectroscopic and microscopic methods. TEM images of NRs coated with SiO₂ are shown in [Figure 1a](#). During the whole SiO₂ coating formation, the concentration of cetyltrimethylammonium bromide (CTAB) surfactant was controlled and tetraethyl orthosilicate (TEOS) was used as a precursor of silica for NPs functionalization.^{41–43} According to our results, the thickness of the coating can be changed by varying the concentration of the CTAB surfactant in solution. The hydrolysis and condensation of TEOS during the formation of SiO₂ can be catalyzed by a change in pH. We have also found that the pH of 10 is optimal for SiO₂ growth, which was confirmed by TEM images. At higher pH values in solutions, the SiO₂ shells are of poorer quality, while below pH 9, the SiO₂ coating does not form (TEM images are shown in the [Supporting Information](#)). CTAB micelles serve as template for SiO₂ deposition through the hydrolysis, whereas TEOS is the SiO₂ precursor. Through careful control of the reaction parameters, we were able to achieve highly reproducible and

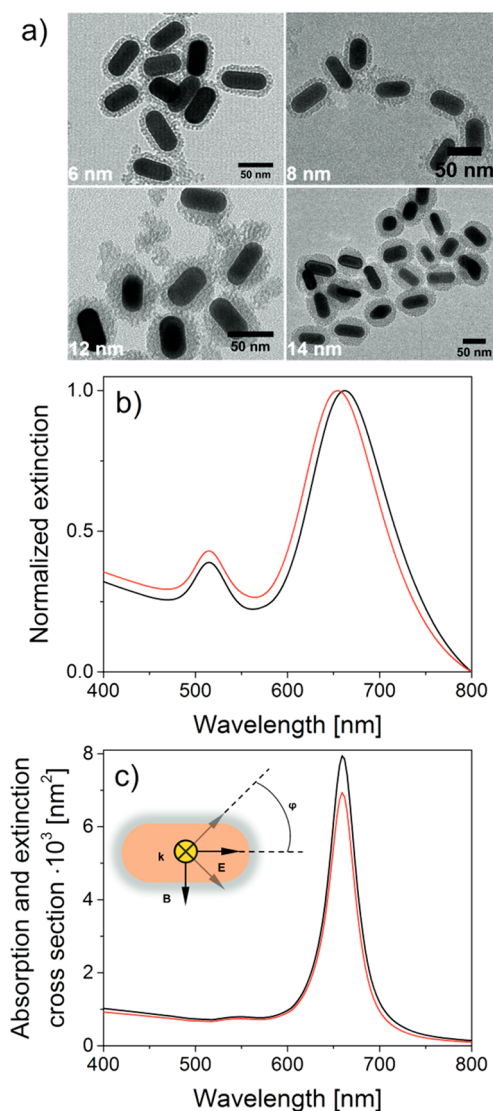


Figure 1. TEM images of SiO₂ coating on the surface of gold nanorods (Au-NRs) (in each panel SiO₂ thickness was indicated) (a), stability in ethanol of Au-NRs coated with 14 nm SiO₂ (after synthesis and 3 months later, black and red line, respectively) (b), and theoretically calculated cross-sections spectra of Au-NRs (absorption and optical extinction, red and black line, respectively) with the top view of excitation geometry shown in the inset (the angle (φ) between longitudinal axis of Au-NRs and electric vector of the electromagnetic wave was fixed at 45°) (c).

robust SiO₂ coatings. The Au-NRs of the same aspect ratio were coated with SiO₂. The shell thicknesses were 6.0 ± 0.9 , 8.0 ± 1.0 , 12.0 ± 1.7 , and 14.0 ± 2.4 nm, respectively. As an organic solvent in the investigation, EtOH was used because it could be biocompatible at low concentration. Moreover, for LIOAS studies both the reference and the sample studied should be well soluble in the same organic solvent. The functionalized Au-NRs were found to be stable in EtOH for over 3 months as confirmed by the exemplary UV-vis spectra of Au-NRs with 14 nm of SiO₂, taken at various time intervals (Figure 1b). Moreover, we have not observed significant differences between the UV-vis spectra of Au-NRs coated with SiO₂ of different thicknesses. Similar behavior of Au-NRs in EtOH has been recently reported by Abadeer et al.¹⁶ As follows from the results of conducted experiments, the suitable

procedure of functionalization with SiO₂ not only stabilizes the NRs by steric repulsion and trapping of seeds but also allows control of their continued growth as well as stability in organic solvents. It seems that the high electron affinity of gold is responsible for strong Au-CTAB interaction on the NRs surface to give rise to their homogeneity of size and shape. The synthesis and functionalization results were reproducible as evidenced by the analysis of the LSPR band parameters (position and full width at half-maximum of the longitudinal band) and TEM images of Au-NRs coated with SiO₂.

Optical ECS and ACS spectra of Au-NRs are shown in Figure 1c. The ACS and ECS spectra were obtained for the angle (φ) between the longitudinal axis of Au-NRs and the electric vector of the electromagnetic wave equal to 45°. Because of the asymmetry of Au-NRs compared to the spherical NPs, the proper orientation of the wave vector is crucial and should be taken into account. The mean size, used to calculate the optical properties of Au-NRs, was estimated from TEM images. The experimental and theoretical positions of longitudinal and transverse LSPR bands were similar. However, the longitudinal band was much wider than the theoretically predicted one (compare Figure 1b with Figure 1c). The reason is that, in the experimental extinction spectra, additional LSPR bands could appear because of the presence of side products such as spheres or cubes;⁴⁴ however, the TEM analysis did not show a considerable amount of these “impurities”. Qin et al.²⁹ reported on polydispersity and its impact on the optical properties of nonshell Au-NRs, by varying Au-NRs length and diameter. These authors found that the deviation of NRs size and shape from the nominal value significantly influences the cross sections spectra of Au-NRs. In the core-shell NPs the shell thickness could be additionally taken into account to consider polydispersity, but it will make the computational simulations more complicated.

LIOAS signals recorded in EtOH of Au-NRs functionalized with SiO₂ were analyzed according to the approach proposed by Marti and co-workers.³³ Bare Au-NRs protected with CTAB bilayer cannot be studied using LIOAS method because of their poor stability in organic solvents. By gradually decreasing the energy of laser pulse (using a series of gray filters), we obtained the plot of H_{\max} versus E_{las} (Figure 2). The fraction of absorbed energy released promptly as heat (α) for Au-NRs can be calculated from the ratio of the slopes of linear dependencies of H_{\max} on E_{las} , obtained for the analyzed Au-

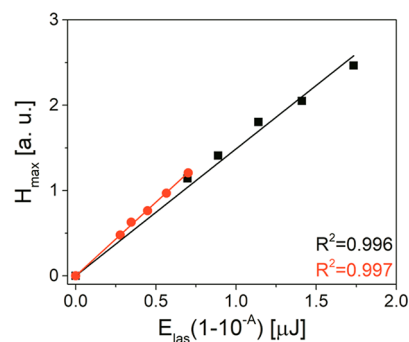


Figure 2. Exemplary dependence of the first maximum of the time-resolved laser-induced optoacoustic spectroscopy signal (H_{\max}) on the incident laser energy (E_{las}) multiplied by the fraction of absorbed energy ($1-10^{-A}$) for gold nanorods with 14 nm SiO₂ (black ■) and Ni²⁺ complex with pheophytin a³² (red ●).

NRs and reference.^{30,32} The UV–vis extinction spectra of Au-NRs were recorded before and after LIOAS measurements and no significant differences in them were observed. Therefore, it could be concluded that laser radiation and the pulse energy at extinction wavelength did not cause degradation of Au-NRs. It has been recently reported by Link et al.⁴⁵ that the change in Au-NRs shape could be induced by pulse laser radiation. They have observed melting of Au-NRs into spherical NPs upon high laser fluences ($\sim 1 \text{ J}\cdot\text{cm}^{-2}$). However, the energy range commonly used in time-resolved pulsed photoacoustic experiments is notably lower (about $\mu\text{J}/\text{pulse}$). Figure 3 presents a

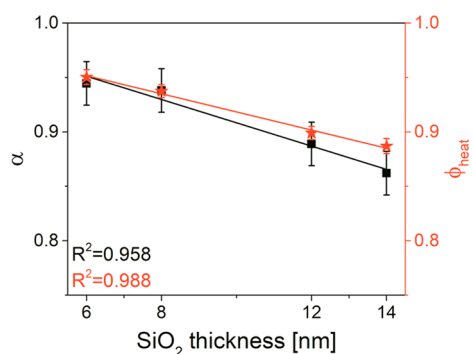


Figure 3. Comparison of experimentally determined fraction of excitation energy changed promptly into heat (α) and theoretically calculated light-to-heat conversion efficiency (ϕ_{heat}) versus the thickness of SiO_2 coating of gold nanorods.

comparison of experimentally determined α and theoretically calculated ϕ_{heat} versus SiO_2 coating thickness of Au-NRs. In the calculations of ACS and ECS spectra, a different φ angle was introduced to reduce the error of ϕ_{heat} .²⁹ The results of α and ϕ_{heat} obtained using LIOAS and FIT simulation, are in agreement. Moreover, α and ϕ_{heat} linearly decreased with increasing SiO_2 thickness. We have attributed the observed differences to variable size of Au-NRs and increased standard deviation of SiO_2 thickness with their increasing size. Because the differences between the experimental and theoretical results are small and the dependencies shown in Figure 3 are linear, for thicker SiO_2 shells the values of photothermal parameter could be extrapolated.⁴⁶ The slopes of the dependencies shown in Figure 3 were $(-1.07 \pm 0.12) \times 10^{-2} \text{ nm}^{-1}$ and $(-0.83 \pm 0.05) \times 10^{-2} \text{ nm}^{-1}$ for α and ϕ_{heat} , respectively. It is possible that other research groups in the future will use our results to assess the light-to-heat conversion efficiencies of functionalized Au-NRs with SiO_2 thickness above 14 nm. At the stage of biomaterials design these dependencies could be taken into account to obtain a single or bimodal theranostic system showing desired photothermal properties. The transducer in the LIOAS method integrates the heat released in the processes faster than 200 ns.⁴⁷ By means of the LIOAS method, we were able to observe efficient absorbed light-to-heat conversion of the Au-NRs with SiO_2 coating on the time scale below 200 ns. It seems that the LIOAS method is very precise and can be successfully applied for quantitative determination of the amount of absorbed energy changed promptly into heat by the functionalized metallic NPs. Nguyen et al.⁴⁸ have used recently time-resolved infrared spectroscopy for studies of heat-transfer dynamics of 30 and 90 nm SiO_2 -coated Au-NRs. Their results showed that in the case of Au-NRs coated with SiO_2 of about 30 nm (the smallest region of effective local heating) the heat-transfer time is about 600 ps

because the heat partly diffuses further from the SiO_2 shell to the water through the thermally resistant CTAB. In the case of very thick coated samples, of about 90 nm, the heat-transfer time is about 400 ps because of efficient heat diffusion just inside the SiO_2 shell.

Heat generated in NPs solution has been recently estimated using different techniques,^{26,29,49,50} but the results obtained by different authors vary significantly.^{49,50} Moreover, in most cases the relative heat generation was reported because the heat generator was unknown. Indirect techniques such as the method presented herein^{30,31} and photoacoustic imaging^{51,52} seem to offer new, more reliable approaches to study metallic NPs. The LIOAS method offers a higher sensitivity in comparison to that of photoacoustic spectrometry and the tunability of the excitation wavelength; therefore, different LSPR bands of NPs can be excited.

4. CONCLUSIONS

This work has a significant impact on biomedical applications of NPs such as PTT that require an accurate estimation of the amount of absorbed energy changed into heat upon NPs interaction with laser light.^{9,53} In conclusion, this study demonstrates the importance of LIOAS measurements in the quantification of the heat generated from metallic NPs in organic media.

■ ASSOCIATED CONTENT

Supporting Information

The Supporting Information is available free of charge on the ACS Publications website at DOI: 10.1021/acs.jpcc.9b09418.

Details concerning the materials and the synthesis used within this work (PDF)

■ AUTHOR INFORMATION

Corresponding Author

*E-mail: michal.kotkowiak@put.poznan.pl (M.K.). Tel.: +48 61 665 3177. Fax: +48 61 665 3178.

ORCID

Paulina Błaszkiwicz: 0000-0002-2355-8889

Michał Kotkowiak: 0000-0001-6611-0366

Emerson Coy: 0000-0002-4149-9720

Alina Dudkowiak: 0000-0001-5487-4051

Notes

The authors declare no competing financial interest.

■ ACKNOWLEDGMENTS

This work was supported by the Polish Ministry of Science and Higher Education (Project No. 06/62/SBAD/1921). E.C. acknowledges the partial support provided by the project H2020-MSCA-RISE-2017 (Project No. 778157). We also thank Prof. Leszek Fiedor from the Faculty of Biochemistry, Biophysics and Biotechnology at the Jagiellonian University in Poland for kindly providing the Ni^{2+} complex with pheophytin *a*.

■ REFERENCES

- (1) Evans, E. R.; Bugga, P.; Asthana, V.; Drezek, R. Metallic Nanoparticles for Cancer Immunotherapy. *Mater. Today* **2018**, *21* (6), 673–685.
- (2) Carbó-Argibay, E.; Rodríguez-González, B.; Pastoriza-Santos, I.; Pérez-Juste, J.; Liz-Marzán, L. M. Growth of Pentatwinned Gold

Nanorods into Truncated Decahedra. *Nanoscale* **2010**, *2* (11), 2377–2383.

(3) Wang, X.-W.; Gao, W.; Fan, H.; Ding, D.; Lai, X.-F.; Zou, Y.-X.; Chen, L.; Chen, Z.; Tan, W. Simultaneous Tracking of Drug Molecules and Carriers Using Aptamer-Functionalized Fluorescent Superstable Gold Nanorod–Carbon Nanocapsules during Thermo-Chemotherapy. *Nanoscale* **2016**, *8*, 7942–7948.

(4) Fang, S.; Li, C.; Lin, J.; Zhu, H.; Cui, D.; Xu, Y.; Li, Z. Gold Nanorods-Based Theranostics for Simultaneous Fluorescence/Two-Photon Luminescence Imaging and Synergistic Phototherapies. *J. Nanomater.* **2016**, *2016* (4), 1–10.

(5) El-Sayed, I. H.; Huang, X.; El-Sayed, M. A. Surface Plasmon Resonance Scattering and Absorption of Anti-EGFR Antibody Conjugated Gold Nanoparticles in Cancer Diagnostics: Applications in Oral Cancer. *Nano Lett.* **2005**, *5* (5), 829–834.

(6) He, S.; Kang, M. W. C.; Khan, F. J.; Tan, E. K. M.; Reyes, M. A.; Kah, J. C. Y. Optimizing Gold Nanostars as a Colloid-Based Surface-Enhanced Raman Scattering (SERS) Substrate. *J. Opt.* **2015**, *17* (11), 114013.

(7) Riley, R. S.; Day, E. S. Gold Nanoparticle-Mediated Photothermal Therapy: Applications and Opportunities for Multimodal Cancer Treatment. *WIREs Nanomed. Nanobiotechnol.* **2017**, *9* (4), e1449.

(8) Dong, Q.; Wang, X.; Hu, X.; Xiao, L.; Zhang, L.; Song, L.; Xu, M.; Zou, Y.; Chen, L.; Chen, Z.; et al. Simultaneous Application of Photothermal Therapy and an Anti-Inflammatory Prodrug Using Pyrene–Aspirin-Loaded Gold Nanorod Graphitic Nanocapsules. *Angew. Chem., Int. Ed.* **2018**, *57* (1), 177–181.

(9) (a) Iancu, C. Photothermal Therapy of Human Cancers (PTT) Using Gold Nanoparticles. *Biotechnol. Mol. Biol. Nanomed.* **2013**, *1* (1), 53–60. (b) Błaszkiwicz, P.; Kotkowiak, M. Gold-Based Nanoparticles Systems in Phototherapy - Current Strategies. *Curr. Med. Chem.* **2019**, *25* (42), 5914–5929.

(10) Kaneti, Y. V.; Chen, C.; Liu, M.; Wang, X.; Yang, J. L.; Taylor, R. A.; Jiang, X.; Yu, A. Carbon-Coated Gold Nanorods: A Facile Route to Biocompatible Materials for Photothermal Applications. *ACS Appl. Mater. Interfaces* **2015**, *7* (46), 25658–25668.

(11) Liu, Y.; Xu, M.; Chen, Q.; Guan, G.; Hu, W.; Zhao, X.; Qiao, M.; Hu, H.; Liang, Y.; Zhu, H.; et al. Gold Nanorods/Mesoporous Silica-Based Nanocomposite as Theranostic Agents for Targeting near-Infrared Imaging and Photothermal Therapy Induced with Laser. *Int. J. Nanomed.* **2015**, *10*, 4747–4761.

(12) Kertmen, A.; Torruella, P.; Coy, E.; Yate, L.; Nowaczyk, G.; Gapiński, J.; Vogt, C.; Toprak, M.; Estradé, S.; Peiró, F.; et al. Acetate-Induced Disassembly of Spherical Iron Oxide Nanoparticle Clusters into Monodispersed Core-Shell Structures upon Nanoemulsion Fusion. *Langmuir* **2017**, *33* (39), 10351–10365.

(13) Xu, Y.; He, R.; Lin, D.; Ji, M.; Chen, J. Laser Beam Controlled Drug Release from Ce6–Gold Nanorod Composites in Living Cells: A FLIM Study. *Nanoscale* **2015**, *7*, 2433–2441.

(14) Navarro, J. R. G.; Manchon, D.; Lerouge, F.; Blanchard, N. P.; Marotte, S.; Leverrier, Y.; Marvel, J.; Chaput, F.; Micouin, G.; Gabudean, A.-M.; et al. Synthesis of PEGylated Gold Nanostars and Bipyramids for Intracellular Uptake. *Nanotechnology* **2012**, *23* (46), 465602.

(15) Liu, L.; Ouyang, S.; Ye, J. Gold-Nanorod-Photosensitized Titanium Dioxide with Wide-Range Visible-Light Harvesting Based on Localized Surface Plasmon Resonance. *Angew. Chem., Int. Ed.* **2013**, *52* (26), 6689–6693.

(16) Abadeer, N. S.; Brennan, M. R.; Wilson, W. L.; Murphy, C. J. Distance and Plasmon Wavelength Dependent Fluorescence of Molecules Bound to Silica-Coated Gold Nanorods. *ACS Nano* **2014**, *8* (8), 8392–8406.

(17) Abadeer, N. S.; Murphy, C. J. Recent Progress in Cancer Thermal Therapy Using Gold Nanoparticles. *J. Phys. Chem. C* **2016**, *120* (9), 4691–4716.

(18) Oh, N.; Park, J. H. Endocytosis and Exocytosis of Nanoparticles in Mammalian Cells. *Int. J. Nanomed.* **2014**, *9*, 51–63.

(19) Wu, C.; Xu, Q. Stable and Functionable Mesoporous Silica-Coated Gold Nanorods as Sensitive Localized Surface Plasmon Resonance (LSPR) Nanosensors. *Langmuir* **2009**, *25* (16), 9441–9446.

(20) Stober, W.; Fink, A.; Bohn, E. Controlled Growth of Monodisperse Silica Spheres in the Micron Size Range. *J. Colloid Interface Sci.* **1968**, *26*, 62–69.

(21) Inose, T.; Oikawa, T.; Shibuya, K.; Tokunaga, M.; Hatoyama, K.; Nakashima, K.; Kamei, T.; Gonda, K.; Kobayashi, Y. Fabrication of Silica-Coated Gold Nanorods and Investigation of Their Property of Photothermal Conversion. *Biochem. Biophys. Res. Commun.* **2017**, *484* (2), 318–322.

(22) Jain, P. K.; Lee, K. S.; El-Sayed, I. H.; El-Sayed, M. A. Calculated Absorption and Scattering Properties of Gold Nanoparticles of Different Size, Shape, and Composition: Applications in Biological Imaging and Biomedicine. *J. Phys. Chem. B* **2006**, *110* (14), 7238–7248.

(23) Stefan Kooij, E.; Poelsema, B. Shape and Size Effects in the Optical Properties of Metallic Nanorods. *Phys. Chem. Chem. Phys.* **2006**, *8* (28), 3349–3357.

(24) Kessentini, S.; Barchiesi, D. Quantitative Comparison of Optimized Nanorods, Nanoshells and Hollow Nanospheres for Photothermal Therapy. *Biomed. Opt. Express* **2012**, *3* (3), 590–604.

(25) Phan, A. D.; Nga, D. T.; Viet, N. A. Theoretical Model for Plasmonic Photothermal Response of Gold Nanostructures Solutions. *Opt. Commun.* **2018**, *410*, 108–111.

(26) Chen, H.; Shao, L.; Ming, T.; Sun, Z.; Zhao, C.; Yang, B.; Wang, J. Understanding the Photothermal Conversion Efficiency of Gold Nanocrystals. *Small* **2010**, *6* (20), 2272–2280.

(27) Hernandez, P.; Tandler, P. J.; Govorov, A. O.; Carlson, M. T.; Richardson, H. H. Experimental and Theoretical Studies of Light-to-Heat Conversion and Collective Heating Effects in Metal Nanoparticle Solutions. *Nano Lett.* **2009**, *9* (3), 1139–1146.

(28) Maestro, L. M.; Camarillo, E.; Sánchez-Gil, J. A.; Rodríguez-Oliveros, R.; Ramiro-Bargueño, J.; Caamaño, A. J.; Jaque, F.; Solé, J. G.; Jaque, D. Gold Nanorods for Optimized Photothermal Therapy: The Influence of Irradiating in the First and Second Biological Windows. *RSC Adv.* **2014**, *4* (96), 54122–54129.

(29) Qin, Z.; Wang, Y.; Randrianalisoa, J.; Raeesi, V.; Chan, W. C. W.; Lipinski, W.; Bischof, J. C. Quantitative Comparison of Photothermal Heat Generation between Gold Nanospheres and Nanorods. *Sci. Rep.* **2016**, *6*, 29836.

(30) Kotkowiak, M.; Dudkowiak, A.; Fiedor, L. Intrinsic Photoprotective Mechanisms in Chlorophylls. *Angew. Chem., Int. Ed.* **2017**, *56*, 10457–10461.

(31) Staśkowiak, E.; Dudkowiak, A.; Wiktorowicz, K.; Cofta, J.; Frąckowiak, D. Spectral Properties of Stilbazolium Merocyanines - Potential Sensitizers in Photodynamic Therapy and Diagnosis. Part II. Merocyanines in Resting and Stimulated Lymphocytes. *J. Photochem. Photobiol., A* **2005**, *169* (2), 159–168.

(32) Pilch, M.; Dudkowiak, A.; Jurzyk, B.; Łukasiewicz, J.; Susz, A.; Stochel, G.; Fiedor, L. Molecular Symmetry Determines the Mechanism of a Very Efficient Ultrafast Excitation-to-Heat Conversion in Ni-Substituted Chlorophylls. *Biochim. Biophys. Acta, Bioenerg.* **2013**, *1827* (1), 30–37.

(33) Martí, C.; Nonell, S.; Nicolau, M.; Torres, T. Photophysical Properties of Neutral and Cationic Tetrapyrrolineporphyrazines. *Photochem. Photobiol.* **2000**, *71* (1), 53–59.

(34) Orendorff, C. J.; Murphy, C. J. Quantitation of Metal Content in the Silver-Assisted Growth of Gold Nanorods. *J. Phys. Chem. B* **2006**, *110*, 3990–3994.

(35) Weiland, T.; Timm, M.; Munteanu, I. A Practical Guide to 3-D Simulation. *IEEE Microw. Mag.* **2008**, *9* (6), 62–75.

(36) Kotkowiak, M.; Grześkiewicz, B.; Robak, E.; Wolarz, E. Interaction between Nanoprisms with Different Coupling Strength. *J. Phys. Chem. C* **2015**, *119* (11), 6195–6203.

(37) Grześkiewicz, B.; Ptaszyński, K.; Kotkowiak, M. Near and Far-Field Properties of Nanoprisms with Rounded Edges. *Plasmonics* **2014**, *9* (3), 607–614.

(38) *Handbook of Optical Constants of Solids*, 1st ed.; Palik, E. D., Ed.; Academic Press: 1997.

(39) Ali, M. R. K.; Wu, Y.; El-Sayed, M. A. Gold Nanoparticle-Assisted Plasmonic Photothermal Therapy Advances Towards Clinical Application. *J. Phys. Chem. C* **2019**, *123* (25), 15375–15393.

(40) Jaque, D.; Martínez Maestro, L.; del Rosal, B.; Haro-Gonzalez, P.; Benayas, A.; Plaza, J. L.; Martín Rodríguez, E.; García Solé, J. Nanoparticles for Photothermal Therapies. *Nanoscale* **2014**, *6* (16), 9494–9530.

(41) Zhao, J.; Xu, P.; Li, Y.; Wu, J.; Xue, J.; Zhu, Q.; Lu, X.; Ni, W. Direct Coating of Mesoporous Titania on CTAB-Capped Gold Nanorods. *Nanoscale* **2016**, *8*, 5417–5421.

(42) Li, J.; Zhu, B.; Zhu, Z.; Zhang, Y.; Yao, X.; Tu, S.; Liu, R.; Jia, S.; Yang, C. J. Simple and Rapid Functionalization of Gold Nanorods with Oligonucleotides Using an MPEG-SH/Tween 20-Assisted Approach. *Langmuir* **2015**, *31* (28), 7869–7876.

(43) Xiao, Q.; Lu, Y.; Chen, M.; Chen, B.; Yang, Y.; Cui, D.; Pan, B.; Xu, N. Antibody-Conjugated Silica-Modified Gold Nanorods for the Diagnosis and Photo-Thermal Therapy of *Cryptococcus Neoformans*: An Experiment In Vitro. *Nanoscale Res. Lett.* **2018**, *13*, 77.

(44) Scarabelli, L.; Sánchez-Iglesias, A.; Pérez-Juste, J.; Liz-Marzán, L. M. A “Tips and Tricks” Practical Guide to the Synthesis of Gold Nanorods. *J. Phys. Chem. Lett.* **2015**, *6* (21), 4270–4279.

(45) Link, S.; Burda, C.; Nikoobakht, B.; El-Sayed, M. A. Laser-Induced Shape Changes of Colloidal Gold Nanorods Using Femtosecond and Nanosecond Laser Pulses. *J. Phys. Chem. B* **2000**, *104* (26), 6152–6163.

(46) Chen, Y.-S.; Frey, W.; Kim, S.; Kruizinga, P.; Homan, K.; Emelianov, S. Silica-Coated Gold Nanorods as Photoacoustic Signal Nanoamplifiers. *Nano Lett.* **2011**, *11* (2), 348–354.

(47) Braslavsky, S. E.; Heibel, G. E. Time-Resolved Photothermal and Photoacoustic Methods Applied to Photoinduced Processes in Solution. *Chem. Rev.* **1992**, *92* (6), 1381–1410.

(48) Nguyen, S. C.; Zhang, Q.; Manthiram, K.; Ye, X.; Lomont, J. P.; Harris, C. B.; Weller, H.; Alivisatos, A. P. Study of Heat Transfer Dynamics from Gold Nanorods to the Environment via Time-Resolved Infrared Spectroscopy. *ACS Nano* **2016**, *10* (2), 2144–2151.

(49) Richardson, H. H.; Carlson, M. T.; Tandler, P. J.; Hernandez, P.; Govorov, A. O. Experimental and Theoretical Studies of Light-to-Heat Conversion and Collective Heating Effects in Metal Nanoparticle Solutions. *Nano Lett.* **2009**, *9*, 1139–1146.

(50) Roper, D. K.; Ahn, W.; Hoepfner, M. Microscale Heat Transfer Transduced by Surface Plasmon Resonant Gold Nanoparticles. *J. Phys. Chem. C* **2007**, *111*, 3636–3641.

(51) Cho, E. C.; Kim, C.; Zhou, F.; Cobley, C. M.; Song, K. H.; Chen, J.; Li, Z.-Y.; Wang, L. V.; Xia, Y. Measuring the Optical Absorption Cross Sections of Au-Ag Nanocages and Au Nanorods by Photoacoustic Imaging. *J. Phys. Chem. C* **2009**, *113*, 9023–9028.

(52) Okawa, S.; Hirasawa, T.; Sato, R.; Kushibiki, T.; Ishihara, M.; Teranishi, T. Numerical and Experimental Investigations of Dependence of Photoacoustic Signals from Gold Nanoparticles on the Optical Properties. *Opt. Rev.* **2018**, *25* (3), 365–374.

(53) Jang, B.; Park, J.; Tung, C.; Kim, I.; Choi, Y. Gold Nanorod - Photosensitizer. *ACS Nano* **2011**, *5* (2), 1086–1094.

Electronic Supplementary Information (ESI)

for

**Laser-Induced Optoacoustic Spectroscopy Studies
of Inorganic Functionalized Metallic Nanorods**

Paulina Błaszkiwicz[†], Michał Kotkowiak^{*,†}, Emerson Coy[‡], Alina Dudkowiak[†]

[†]Faculty of Technical Physics, Poznan University of Technology, Piotrowo 3, 60-965 Poznan, Poland

[‡]NanoBioMedical Centre, Adam Mickiewicz University, Wszechnicy Piastowskiej 3, 61-614 Poznan, Poland

To whom correspondence should be addressed:

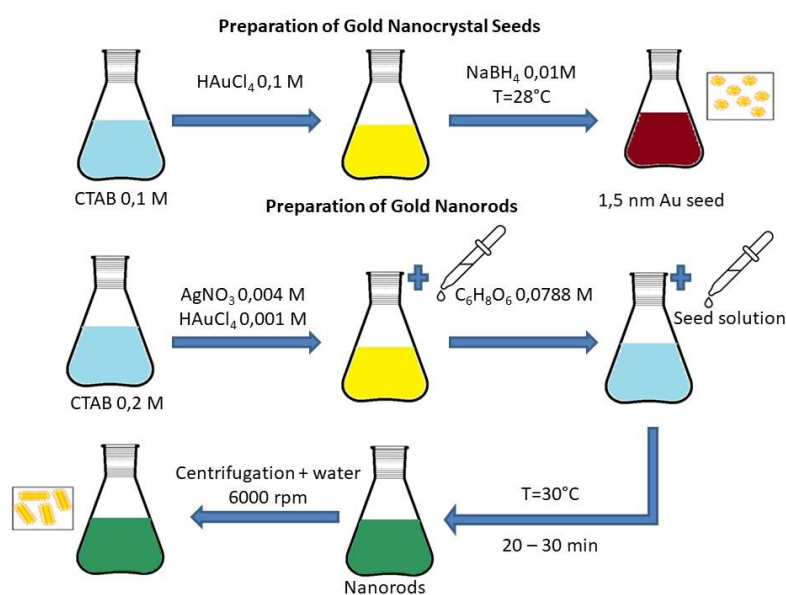
*e-mail: michal.kotkowiak@put.poznan.pl, Tel.: +48 61 665 3177, Fax: +48 61 665 3178.

1.1. Chemicals

Tetrachloroauric acid ($\text{HAuCl}_4 \cdot \text{H}_2\text{O}$) (99.99%) from Alfa Aesar, cetyltrimethylammonium bromide (CTAB) (99.00%), sodium borohydride (NaBH_4) (98.00%), silver nitrate (AgNO_3) (99.99%), ascorbic acid (AA) (99.00%), sodium hydroxide (NaOH) (99.99%), tetraethylorthosilicate (TEOS) (99.99%) were from Sigma Aldrich (USA). Ethanol (EtOH) 99.80% H_2O free was purchased from POCH S.A. (Poland).

1.2. Chemical synthesis of gold nanorods and silica coating of different shell thicknesses

All chemicals were dissolved in Mili-Q ultra-pure water in glass flasks treated with *aqua regia* prior to use. The synthesis of gold nanorods (Au-NRs) was performed by *in situ bottom-up* methods, which involves the reduction of chemical precursor by a reducing agent. Synthesis of Au-NRs was a two-step process as shown in Scheme S1. The Au-NRs were synthesized by the *seed-mediated growth* methods, in which the grains of colloidal gold are connected to the previously obtained spherical gold nanostructures, and then around the nanostructures Au-NRs are formed. The synthesis of Au-NRs based on that proposed by Nikoobakht et al.¹, was optimized and appropriately modified to meet the conditions of our lab. The first step gives a solution of spherical gold seeds (*seed solution*). By dissolving CTAB surfactant in deionized water we obtained a transparent solution, and then we added the precursor (HAuCl_4) and cooled reducing agent (NaBH_4). Upon vigorous stirring the colour of the solution changed to brownish-yellow. The reaction was performed in sterile conditions, while providing a constant temperature and humidity. The *seed solution* was stored at a temperature of approx. 28°C , which prevented the crystallization of CTAB surfactant. The second step of the synthesis was growth of the gold seed solution (growth of Au-NRs solution). Gold seeds were added to a growth solution containing CTAB, $\text{HAuCl}_4 \cdot x\text{H}_2\text{O}$, AgNO_3 and ascorbic acid. The seed solution should be added at a temperature of $27\text{--}30^\circ\text{C}$ so that the growth of Au-NRs could take place.



Scheme S1. Process of gold Au-NRs formation.

The CTAB bilayer on the surface of Au-NRs inhibits their agglomerations, and the presence of AgNO_3 in the growth solution encourages anisotropic Au-NRs growth. The Au-NRs with 2.25 ± 0.23 aspect ratio and maximum longitudinal plasmon resonance localized in the vicinity of 660 nm were studied. The TEM image of Au-NRs without SiO_2 coating is shown in Fig. S2. Au-NRs for functionalization were centrifuged in order to wash excess surfactant. SiO_2 coating was produced using the modified Stöber method.²⁻⁴ Concentration of CTAB surfactant must be controlled during the whole reaction process and tetraethyl orthosilicate solution (TEOS) was used for functionalization. The functionalization of Au-NRs coated with SiO_2 was realized according to Scheme S2.^{2,5} Au-NRs were twice centrifuged at 6000 rpm for 30 min. After, CTAB (0.2 M) was added in different volume (0.4, 0.6, 1.2 and 1.2 mL) and mixed 4 hours to equilibrate CTAB on the surface of Au-NRs. Then, NaOH (0.1 M) was added to the solution, that the pH value was obtained 10. If pH is below 9 then silica shell does not forms and if pH is higher than 10.5 it is heterogenous (Fig. S3). After 1 hour TEOS was added dropwise a 3 times in volume of 30 μl . TEOS was used in specific concentrations (20% in EtOH) to obtain SiO_2 shells of appropriate thicknesses. Solution was mixed overnight at 27-30°C and finally centrifugation twice times at 600 rpm for 30 min. and transferred to EtOH. In addition, SiO_2 coating reduces Au-NRs aggregation, increases solubility of Au-NRs in organic solvents, and makes functionalization by various silanes an easy task.



Scheme S2. Functionalization of Au-NRs with SiO_2 .

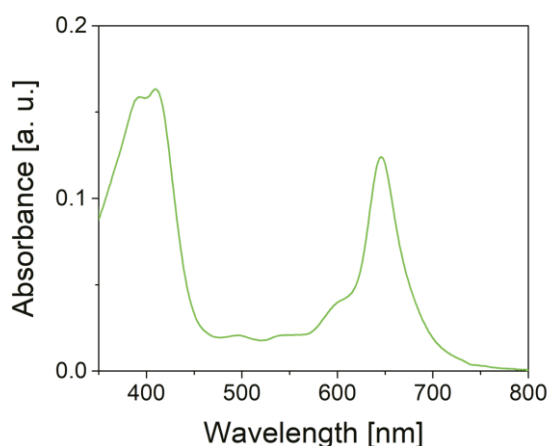


Fig. S1. UV-vis absorption spectrum of Ni-Phea in ethanol.

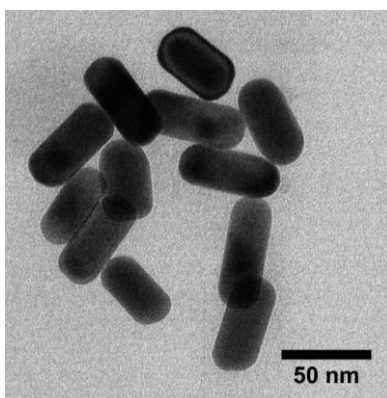


Fig. S2. TEM image of Au-NRs without SiO₂ coating.

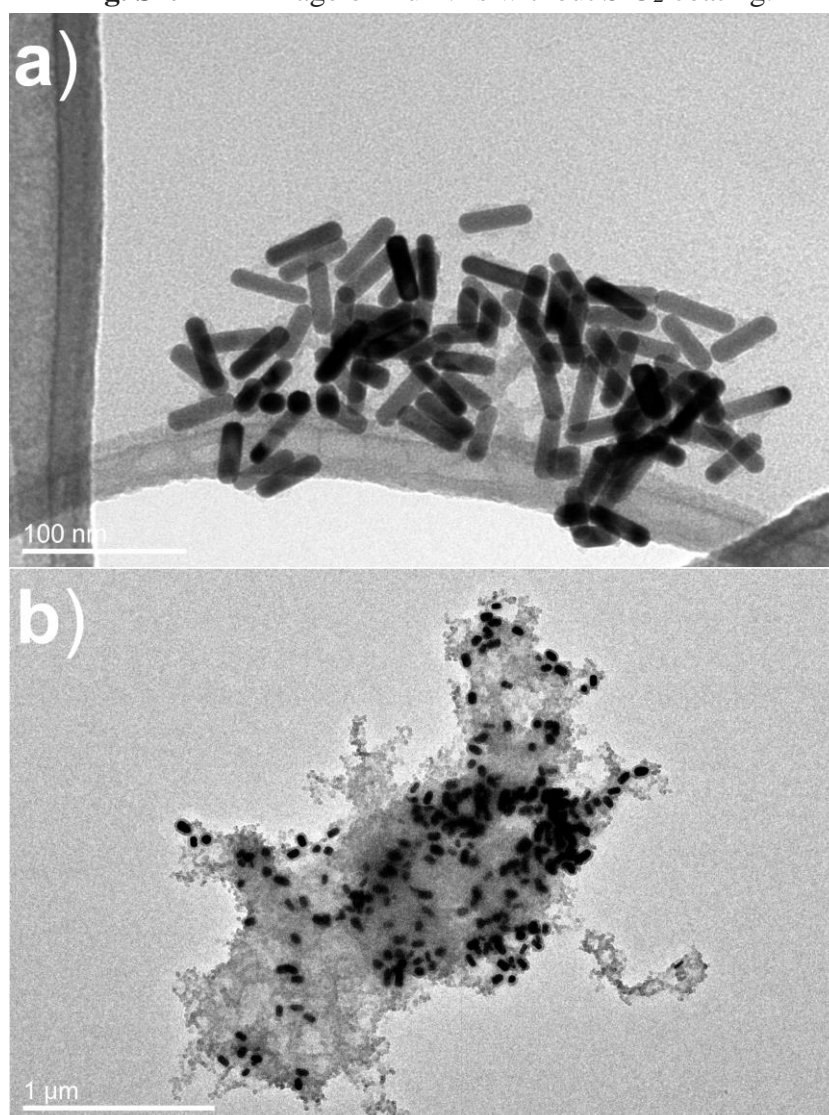


Fig. S3. TEM images of coated Au-NRs for pH below 9 (a) and at higher pH above 10.5 (b).

References

- (1) Nikoobakht, B.; Sayed, A. El. Preparation and Growth Mechanism of Gold Nanorods (NRs) Using Seed-Mediated Growth Method. *Chem. Mater.* **2003**, *15* (10), 1957–1962.
- (2) Gorelikov, I.; Matsuura, N. Single-Step Coating of Mesoporous Silica on Cetyltrimethyl Ammonium Bromide-Capped Nanoparticles. *Nano Lett.* **2008**, *8* (1),

369–373.

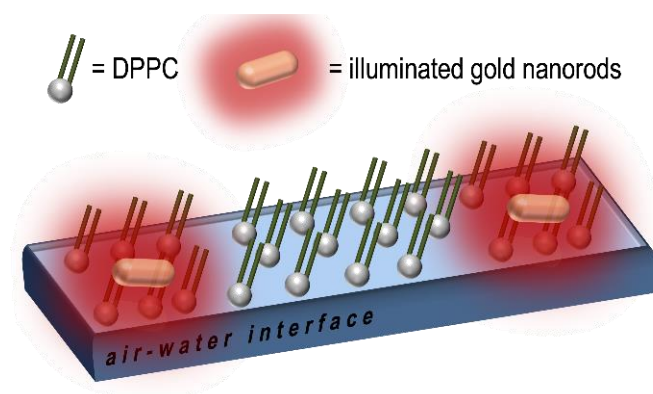
- (3) Hu, X.; Gao, X. Multilayer Coating of Gold Nanorods for Combined Stability and Biocompatibility. *Phys. Chem. Chem. Phys.* **2011**, *13* (21), 10028–10035.
- (4) Liz-Marzán, L. M.; Giersig, M.; Mulvaney, P. Synthesis of Nanosized Gold-Silica Core-Shell Particles. *Langmuir* **1996**, *12* (18), 4329–4335.
- (5) Abadeer, N. S.; Brennan, M. R.; Wilson, W. L.; Murphy, C. J. Distance and Plasmon Wavelength Dependent Fluorescence of Molecules Bound to Silica-Coated Gold Nanorods. *ACS Nano* **2014**, *8* (8), 8392–8406.

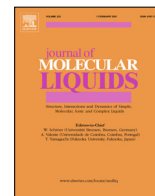
Przedruk publikacji [Tim, JML 2022]

B. Tim, P. Błaszkiwicz, M. Kotkowiak,

Altering model cell membranes by means of photoactivated organic functionalized gold nanorods,

Journal of Molecular Liquids 349 (2022), 118179-1-118179-7. (MEiN 100, IF 6,165)





Altering model cell membranes by means of photoactivated organic functionalized gold nanorods



Beata Tim, Paulina Błaszkiwicz, Michał Kotkowiak*

Faculty of Materials Engineering and Technical Physics, Poznan University of Technology, Piotrowo 3, 60-965 Poznan, Poland

ARTICLE INFO

Article history:

Received 25 August 2021

Revised 19 November 2021

Accepted 21 November 2021

Available online 25 November 2021

Keywords:

Plasmon heating

Langmuir monolayer

Surface plasmon resonance

Photothermal therapy

ABSTRACT

A possible non-invasive photothermal therapy employs photothermal agents with high light-to-heat conversion efficiency. Gold nanorods (Au-NRs) can be applied as photothermal agents because of their optical properties and specific tumor-targeting capability. The potential therapeutic applications and toxicological effects of photothermal agents depend on the interaction of the Au-NRs with the cell membrane, the understanding of which is of great importance. Although studies in this area have been performed, the interactions between model cell membranes and photoactivated Au-NRs have not yet been described. In this study, we explain how local excitation of the Au-NRs caused a local temperature increase in their vicinity that affected the properties of a model membrane composed of dipalmitoylphosphatidylcholine (DPPC). Our results showed that the illumination of the Au-NRs changed the DPPC's organization in the Langmuir monolayer. Upon photoactivation, the mutual distances between the DPPC molecules increased; however, the conformation of the lipid tails remained unchanged. Moreover, the illumination of the membrane at a surface pressure corresponding to that in a native cellular membrane caused a more stable and elastic behavior of the Langmuir monolayer. The results obtained corroborate the theory that photoactivation of Au-NRs influences the packing and phase behavior of mimetic cell membranes. In the long term, it may allow us to understand how the photoactivation of nanoparticles facilitates the transport of medicinal substances.

© 2021 The Authors. Published by Elsevier B.V. This is an open access article under the CC BY-NC-ND license (<http://creativecommons.org/licenses/by-nc-nd/4.0/>).

1. Introduction

As a result of the interaction of noble metal nanoparticles (NPs) with radiation, surface plasmons are excited, the oscillations of which generate a strong local increase in the intensity of the electromagnetic field [1–3]. This increase may generate a strong local temperature rise, and the use of the generated heat to destroy cancer cells is the basis of photothermal therapy [4]. The temperature increase is only local, as a result of which, in principle, only the tumor cells into which NPs were previously introduced are subjected to the influence of high temperature [5,6]. In the research conducted to explain the mechanism of the impact of NPs on the human body, an important role is assigned to the biological membranes that separate the individual structures of the body from the environment. Due to the structural and dynamic complexity of biological membranes, experimental studies on their properties are carried out on model systems using various types of membranes. In such studies, both single-component and multi-component membranes are used. Single-component membranes are most

often made of dipalmitoylphosphatidylcholine (DPPC), which is found, for example, in the erythrocyte membrane and is the main lipid component of pulmonary surfactant. Multicomponent membranes also contain other components that are either lipids or proteins [7–9]. The simplest biomimetic membrane systems are aggregates formed by surfactants, i.e., micelles, reverse micelles, monolayers, multilayers, and spherical objects. Model biological membranes created by phospholipids and the capabilities of current equipment have opened up new horizons for research in this field.

A commonly used method of producing stable lipid monolayers uses the Langmuir technique. Research has proved that the properties of real biological membranes and model Langmuir monolayers formed by phospholipid molecules, e.g., DPPC, are similar, which makes the Langmuir technique a frequently used method for research in the fields of medicine, drug chemistry, and nanotechnology [10–12]. Using the Langmuir technique, it is possible to assess the interactions of drugs, e.g., anti-cancer drugs or NPs, with the model cell membrane and to study the transport properties of pharmaceuticals or their manner of penetration through the membrane [4,13–17].

* Corresponding author.

E-mail address: michal.kotkowiak@put.poznan.pl (M. Kotkowiak).

The interaction of biomolecules with NPs at bio-nano interfaces is an important issue in scientific research [18]. Such studies have been performed using gold nanorods (Au-NRs) with various aspect ratios or other gold NPs, in combination with phospholipid monolayers made from dipalmitoylphosphatidyl glycerol (DPPG) or DPPC. The aspect ratio has been shown to influence interactions in lipid monolayers. These studies have also suggested that morphology and electrostatic forces regulate the interactions in the DPPG-Au-NRs, while, while van der Waals forces dominate in the DPPC-Au-NRs system. Van der Waals forces were associated with the formation of stable monolayers at the air–water interface, while electrostatic forces were involved in the formation of unstable monolayers. The size of the Au-NRs affected the expansion isotherms in both systems, but the lipid tails stayed ordered after expansion, which suggested phase separation between the lipids and nanomaterials at the interface [16,18,19]. It has also been shown that NPs have the potential to induce defects in the structure of DPPC monolayers [15,18]. Considering that DPPC is a component of lung surfactant and that nanotechnology is a rapidly developing field, the effect of NPs on respiratory function is a very interesting and important research area for scientists [13,16,20]. The interaction of NPs with lung surfactant had been unclear; therefore, the effect of shape on the penetration and degree of disruption of the monolayers was previously determined. Au-NRs showed the highest degree of penetration, but had the lowest side effects on the DPPC layer; these results may have a significant impact on the design of respiratory therapies [21]. The presence of hydrophobic alkylated NPs was also shown to modulate the processes of nucleation, growth, and morphology formation of condensed domains in DPPC monolayers [16]. Moreover, hydrophobic NPs inhaled with air remained on the alveolar surface for prolonged periods of time, which may affect respiratory function. Other scientific reports indicated that the addition of silica NPs changes the phase behavior, collapse time, and monolayer structure [13]. Hydrophilic silica NPs reduced the collapse pressure and stiffness of the DPPC monolayer and caused the monolayer to collapse earlier, as the steric hindrance led to compression resistance. In contrast, hydrophobic silica NPs had less effect on the monolayer in terms of collapse pressure or stiffness, but had greater effects on the texture of the monolayer, and the addition of hydrophobic NPs led to the formation of holes in the monolayer [13]. It is also important to understand the process of membrane penetration of functionalized NPs coated with polyethylene glycol (PEG). PEG-modified gold NPs had a nearly neutral surface and had little cytotoxicity *in vitro*. Functionalization of Au-NRs with thiol-terminated PEGs yielded PEGylated Au-NRs with a high stability and better biocompatibility, so the retention time of these Au-NRs in an aqueous medium was longer lasting. PEG-conjugated Au-NRs are circulated in the blood for prolonged periods, preventing the too-rapid inactivation of such systems (by the endoplasmic reticulum) and favoring their accumulation in tissues [22,23]. PEGylated Au-NRs are ideal candidates for studying their entry into the DPPC lipid layer and tracking the behavior of the system to investigate the consequences of this process [24].

There is a lack of data describing the properties of lipid monolayers and the manner of the penetration of NPs through model biological membranes as a result of their photoactivation. An important aspect is that DPPC is sensitive to temperature changes during the formation of a monolayer. Therefore, in this study we examined how the local excitation of Au-NRs, causing a local temperature increase in their vicinity, affected the properties of the model biological membrane. For this purpose, we performed thermodynamic, surface potential, and oscillating barrier studies of model cell membrane supported by Brewster angle microscopy. The results obtained may be helpful in understanding how the photoactivation of NPs facilitates the transport of medicinal substances.

2. Materials and methods

2.1. Chemicals

Tetrachloroauric acid ($\text{HAuCl}_4 \cdot \text{H}_2\text{O}$) (99.99%) was obtained from Alfa Aesar. Cetyltrimethylammonium bromide (CTAB) (99.00%), sodium borohydride (NaBH_4) (98.00%), silver nitrate (AgNO_3) (99.99%), ascorbic acid (99.00%), and O-(2-mercaptoethyl)-O'-methylpolyethylene glycol (PEG $M_w \approx 2000$) (99.99%) were purchased from Sigma Aldrich. Dipalmitoylphosphatidylcholine (1,2-dipalmitoyl-*sn*-glycero-3-phosphocholine, 16:0 PC, DPPC) was purchased from Avanti Polar Lipids (Alabama, USA). Spectrophotometric grade methanol was purchased from POCH S.A. (Poland). High purity chloroform for spectroscopy (CHCl_3) (>99.00%, Uvasol®), isopropanol ($\geq 99.80\%$), and acetone ($\geq 99.80\%$) were purchased from Merck.

2.2. Chemical synthesis of polymer coated gold nanorods

Ultrapure Milli-Q water ($18.2 \text{ M}\Omega \cdot \text{cm}$, $71.98 \pm 0.01 \text{ mN} \cdot \text{m}^{-1}$) was used for all aqueous solutions and as the Langmuir subphase. Au-NRs were prepared following the procedure of Nikoobakht et al. [25] with the modifications previously described by Błaszkiwicz et al. [26]. The functionalization of Au-NRs with PEG was carried out using the modified method described previously [22,27,28].

2.3. Langmuir and Langmuir-Blodgett thin film preparation and studies

A Langmuir-Blodgett (KSV Nima) balance was used, consisting of a Teflon trough ($304 \times 75 \text{ mm}$), two hydrophilic Delrin barriers, a surface potential sensor (KSV Nima SPOT), and a Brewster angle microscope (MicroBAM, KSV Nima). In order to measure the surface pressure, a platinum Wilhelmy plate (instrumental accuracy $0.01 \text{ mN} \cdot \text{m}^{-1}$) was used. Before each experiment, the trough surface was cleaned with isopropanol, acetone, and ultrapure water to obtain a surface pressure value for the pure subphase (Milli-Q water) below $0.2 \text{ mN} \cdot \text{m}^{-1}$ at the maximum compression. To obtain DPPC containing Au-NRs, we used the following procedure. A stock solution of Au-NRs ($2.5 \cdot 10^{-10} \text{ M}$, the concentration being calculated based on previous studies [29,30]) dispersed in methanol was mixed with DPPC ($0.1 \text{ mg} \cdot \text{mL}^{-1}$) so that the ratio of methanol to CHCl_3 was 1:4 (v:v). The volumes of solutions were as follows: 200 μL DPPC, 660 μL Au-NRs, and 2440 μL CHCl_3 . The Au-NRs and DPPC samples were spread at the subphase using a microliter syringe (Hamilton). After evaporation of CHCl_3 (approx. 25 min) from the dispersion of Au-NRs and DPPC, the layer was compressed by the symmetrical movement of the barriers at a constant speed of $5 \text{ mm} \cdot \text{min}^{-1}$, either in the presence of red light emitted from a power LED array (the mean light intensity was $115 \text{ mW} \cdot \text{cm}^{-2}$) or in its absence. During the compression, the changes in the surface pressure and surface potential on the surface of the trough were recorded.

In the next stage, relaxation experiments were performed to determine the stability of the monolayers, with Au-NRs and DPPC samples being spread at the air–water interface. After evaporation of the solvent (approx. 25 min), the monolayer was compressed (at a constant speed $5 \text{ mm} \cdot \text{min}^{-1}$) to a surface pressure of $30 \text{ mN} \cdot \text{m}^{-1}$, and the change of the relative surface area (A/A_0^{-1}) with time (t) was recorded. The measurements were carried out both in the presence and absence of light in order to determine the changes occurring at the surface film due to irradiation over time. While monitoring the change in the relative surface area (A/A_0^{-1}) over time (t), BAM images were also recorded, which allowed the structural changes occurring in the surface film due to the monolayer

irradiation to be noted. The dilatational viscoelasticity of the Langmuir films was studied using the oscillating barrier method. This experiment is based on recording the surface pressure response to a small-amplitude sinusoidal variation in the surface area. The Langmuir monolayers were first compressed on the surface by a pressure of $30 \text{ mN}\cdot\text{m}^{-1}$ and then allowed to relax for 20 min. The barriers were then set to oscillate, inducing small amplitude (1%) changes to the area available for the Langmuir films. The experiments were performed for several frequencies (f) from 30 to 140 mHz, at least 20 oscillation cycles being recorded for each frequency. A time interval of 60 s was preserved between subsequent cycles of oscillations. Each experiment was carried out at a constant temperature of $21\pm 1 \text{ }^\circ\text{C}$ and repeated three times to ensure reproducibility. A FLIR E5 thermal infrared camera was used to collect thermal images of Au-NRs solutions and Au-NRs monolayers.

3. Results and discussion

Au-NRs are promising materials for various biomedical applications, such as imaging, phototherapy, and drug delivery, due to their tunable localized surface plasmon resonance (LSPR) and photothermal effects [3,31]. The addition of AgNO_3 to the growth solution of Au-NRs encourages anisotropic growth and control of the aspect ratio [25,30], enabling the tuning of the position of the longitudinal LSPR maxima over different spectral ranges in order to manipulate tissue penetration depth. The penetration depth of light into a biological tissue is an important parameter for the biomedical application of Au-NRs. In our study, we synthesized polymer-functionalized Au-NRs with an aspect ratio of 2.25 and the maximum of the LSPR band at 660 nm. The extinction spectra of the synthesized Au-NRs functionalized with CTAB (aqueous solution) and PEG (methanol solution) are shown in Fig. S1 in the Supplementary Material. The polymer layers are non-toxic for living organisms and improve the stability of the Au-NRs, preventing aggregation in alcoholic/aqueous solutions. In a previous study, we reported high values of light-to-heat conversion efficiency for Au-NRs [26], which ensure an effective and large increase in their temperature under light illumination. Fig. 1 shows thermal images of Au-NRs in a Falcon tube and in an Au-NRs Langmuir monolayer upon 660 nm illumination. A higher increase in temperature was observed in the Falcon tube than in the Au-NRs Langmuir monolayer. Of course, in the case of the monolayer the effect is averaged due to the Au-NRs layer's thickness and also because of the thermal properties of water and heat conduction. At an early stage in our studies, we tried to alter the model cell membranes by means of photoactivated Au-NRs on a solid substrate, in order to stabilize the thermal properties more precisely and to minimize heat conduction. However, our previous studies for Au-NRs transferred to solid substrates showed specific dendritic-like aggregates of Au-NRs due to the polymer's presence at the surface of the NRs, which changed the position of the LSPR [32]. An example of a confocal microscopy image of Au-NRs Langmuir-Blodgett layers is shown in Fig. S2.

The localization of the NPs in a model cell membrane is strongly dependent on the shape of the NPs. Hydrophilic Au-NRs adsorb onto the hydrophilic head-groups of the DPPC monolayer after translocation across the lipid monolayer. Small disk NPs and barrel NPs could penetrate and separate from the DPPC monolayer [21]. Due to these previous results, we started our investigation on the influence of Au-NRs on the DPPC's arrangement after carefully selecting the concentration of the Au-NRs. A small quantity of Au-NRs was selected in order not to disturb the model cell membrane and the compression isotherm at its starting point (gaseous phase). Assuming a PEG layer thickness equal to 3 nm [27], the area

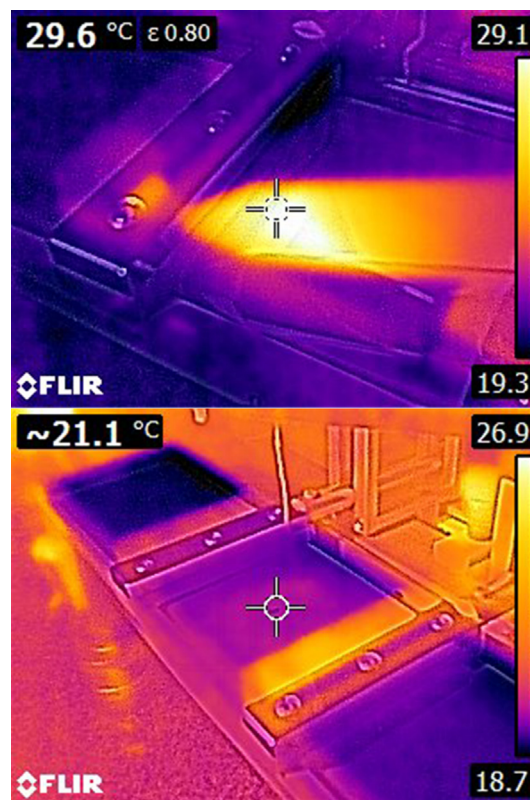


Fig. 1. Thermal images of Au-NRs in a Falcon tube (upper image) and in an Au-NRs Langmuir monolayer (lower image) upon 660 nm light illumination.

occupied by the Au-NRs (at a surface pressure equal to $30 \text{ mN}\cdot\text{m}^{-1}$) was 1.5% of the trough area.

In Fig. 2a-b, Langmuir isotherms and the compression modulus ($C_s^{-1} = -A \frac{d\pi}{dA}$) for the surface pressure of DPPC on its own and DPPC containing Au-NRs, with and without light illumination, are presented. It is well known that temperature has a strong influence on the properties of lipids [33]. The formation of a DPPC Langmuir monolayer depends on the temperature and is largely conditioned by the structural chain conformation of the DPPC lipid monolayer. The illumination of pure DPPC Langmuir monolayer did not heat up the air-water interface and thus did not influence the shape of the compression isotherm (results not shown). The presence of Au-NRs in the monolayer caused the disappearance of the characteristic phase transition, reflecting the coexistence of liquid-expanded (LE) and liquid-condensed (LC) phases. The maximum value of C_s^{-1} of the DPPC monolayer was $>250 \text{ mN}\cdot\text{m}^{-1}$, which meant that the phospholipid monolayer was in the solid phase (S). The addition of Au-NRs caused a decrease in the C_s^{-1} maximum value, proving that the physical properties of the DPPC monolayer had changed, because the obtained values of the C_s^{-1} maximum were located in the LC phase area. A similar effect was observed in studies of the effect of both nanoparticles and microparticles on the DPPC monolayer [16,34].

Many studies have demonstrated the disappearance or reduction of the LE-LC plateau and a shift to the right of the isotherm relative to the DPPC monolayer, suggesting the penetration of the NPs into the phospholipid layer [21,32,33]. Ye et al. [15] investigated the properties of systems consisting of DPPC and silica nanoparticles. These authors found that the addition of NPs had a great influence on the behavior of the monolayer, which was observed as the disappearance of the LE-LC coexistence region. Moreover, this effect was more pronounced with hydrophilic NPs, due to the fact

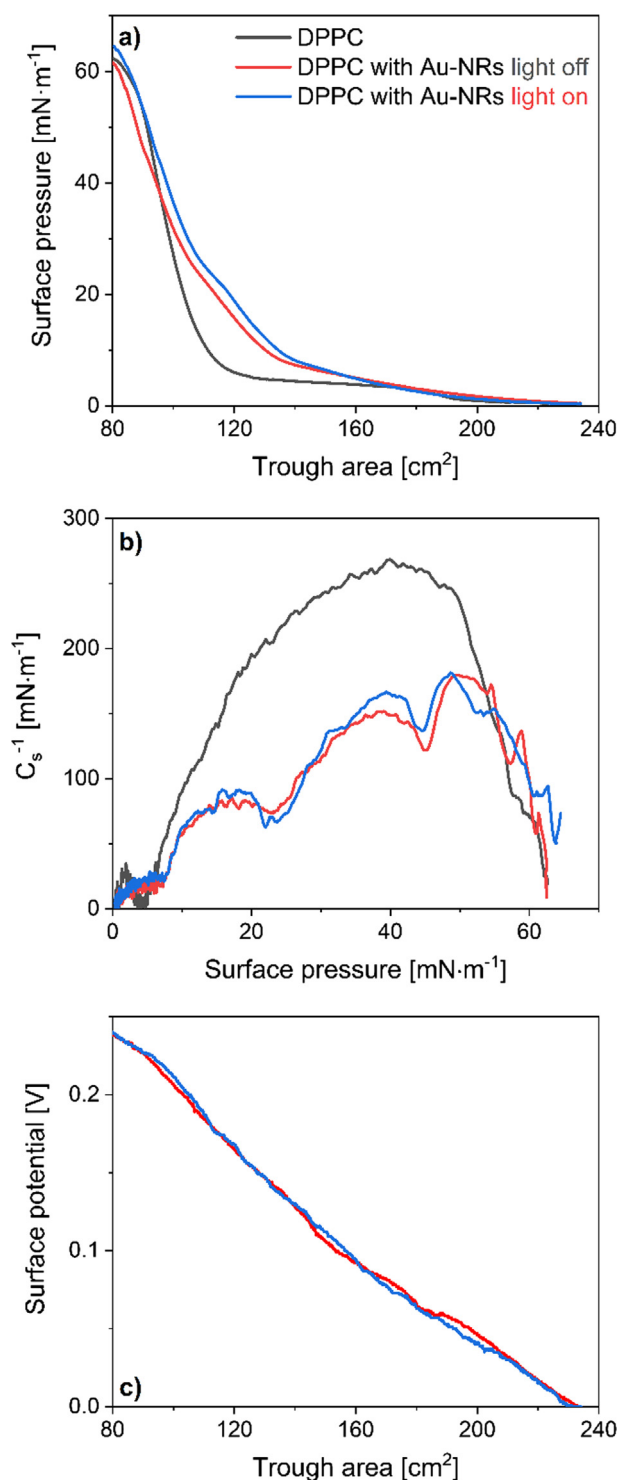


Fig. 2. The surface pressure versus trough area isotherm of DPPC (black line) and DPPC containing Au-NRs, with and without light illumination (blue and red line, respectively) (a), the dependence of surface compression modulus C_s^{-1} on surface pressure calculated based on (a) panel (b), and surface potential versus trough area of DPPC containing Au-NRs, with and without light illumination (c). (For interpretation of the references to colour in this figure legend, the reader is referred to the web version of this article.)

that they have a different affinity to DPPC molecules than do hydrophobic NPs. Consequently, the hydrophilic nature of the particles caused them to significantly affect the phospholipid monolayer. Our results showed that the C_s^{-1} values for the illuminated

model cell membrane seemed to be higher for surface pressures around 40 mN·m⁻¹. For the rest of the studied surface pressures, the C_s^{-1} values were comparable within experimental error. More importantly, the shapes of the isotherms for the DPPC containing Au-NRs with and without illumination were similar. However, for surface pressures above 8 mN·m⁻¹ the illuminated isotherm was shifted towards higher values of trough area, which remained constant once obtained. This phenomenon could be assigned to the induction of LSPR upon monolayer illumination and the high values of light-to-heat conversion efficiency of the Au-NRs. The shape of the isotherms with and without light illumination for surface pressures below 8 mN·m⁻¹ could be attributed to the small value of the aspect ratio of the Au-NRs [18]. This effect was recently discussed by Lins et al. [18]. These authors considered CTAB-functionalized Au-NRs dissolved in the subphase and their adsorption through a DPPC model membrane. In the case of aspect ratio values lower than 2.8, van der Waals interactions were predominant in the DPPC-Au-NRs system.

To obtain additional information about DPPC organization in the Langmuir monolayer, we measured surface potential curves of DPPC containing Au-NRs, with and without light illumination, as shown in Fig. 1c. NPs adsorbed onto the DPPC monolayer may change the local properties of lipids, which may initiate the structural disruption of the lipid monolayer [21,24]. It was found that hydrophobic NPs immerse themselves in the hydrophobic tails of the interfacial DPPC molecules, while hydrophilic NPs adsorb onto the hydrophilic head-groups of the interfacial DPPC molecules [21]. This finding is in good agreement with previous results from biological studies [20,35]. The illumination of the monolayer does not influence the shape of the surface potential curves. In other words, the value of the dipole moment is the same in both cases. The dipole moment could be changed by changes in the orientation of the alkyl chains of the DPPC. Therefore, the increased area occupied by DPPC molecules (Fig. 2a) in the case of monolayer illumination should not be attributed to structural changes in the DPPC orientation, but rather to changes in the mutual distances of the DPPC molecules.

Our observations are in good agreement with recent theoretical studies carried out by Lin et al. [21]. These authors studied the interactions between NPs of different shapes and a DPPC monolayer at the air-water interface during compression and expansion processes. During the film compression, NPs of different shapes showed various penetration abilities and degrees of structural disruption to the DPPC monolayer. More importantly, rod-like NPs showed the highest degree of penetration and the smallest side-effects to the DPPC monolayer. Experimental evidence of conformationally ordered lipid tails was presented in a previous study [18], which suggested phase separation between the lipids and NPs at the interface.

In the next step, a relaxation experiment was performed to determine the stability of the investigated systems. As a target surface pressure, 30 mN·m⁻¹ was selected, which corresponds to that in a native cellular membrane. The results of the relaxation experiments are shown in Fig. 3. Additionally, during relaxation experiments the BAM images shown in Fig. 4 of DPPC containing Au-NRs, with and without light illumination for various time intervals, were recorded. The course of the relaxation curve of the non-illuminated system was similar to that of DPPC. For both curves, a decrease in the value of $A \cdot A_0^{-1}$ to a value of about 0.75 was observed. However, in the case of the DPPC monolayer, in contrast to the DPPC monolayer containing Au-NRs without light illumination, the system stabilized after approx. 90 min. On the other hand, the illumination of the DPPC containing Au-NRs caused a more stable behavior of the Langmuir monolayer. This was confirmed by an increase in the $A \cdot A_0^{-1}$ value during the experiment.

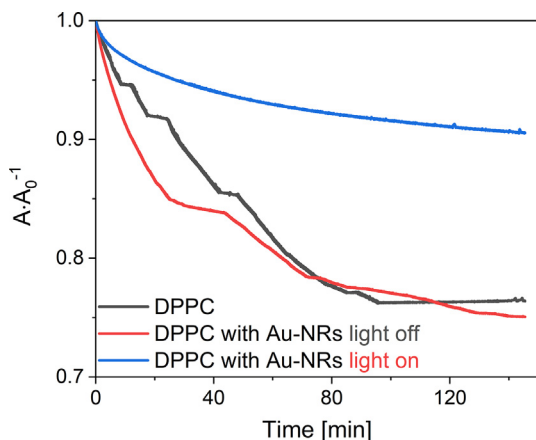


Fig. 3. Relative area changes versus time for DPPC (black line) and DPPC containing Au-NRs, with and without light illumination (blue and red line, respectively). The target surface pressure was $30 \text{ mN}\cdot\text{m}^{-1}$. (For interpretation of the references to colour in this figure legend, the reader is referred to the web version of this article.)

A similar situation was observed in the BAM images, which indicated significant differences in the morphology of the surface films with and without light illumination. Light bands were visible in the illuminated model cell membrane for the first 30 min (panels (a) to (e) in Fig. 4) of the process. After 40 min (panel (f) in Fig. 4) the monolayer became rigid, creating a homogeneous, viscous surface film. In the case of the system without light illumination (panels (k) to (t) in Fig. 4), bright bands were visible throughout the duration of the experiment, indicating the heterogeneity of the surface film. It can therefore be concluded that Au-NRs do not stabilize the monolayers over time by themselves,

while monolayer heating may induce repulsive interactions between DPPC molecules, and thus lead to the illuminated monolayer being stable over all time intervals.

The coexistence of lipid and NP regions affects the elasticity of the monolayer [18]. Therefore, the effect of the illumination of Au-NRs on the dilatational viscoelasticity of the DPPC containing Au-NRs was investigated under dynamic conditions by the oscillating barrier method, which allowed the determination of the dilatational viscoelasticity modulus (E) as a complex quantity. The dilatational modulus E was thus obtained, being a complex quantity composed of a real component, the elastic modulus (E'), and an imaginary component, the viscous modulus (E''). If the film is perfectly elastic, the imaginary part is equal to zero, while for a perfectly viscous material, the real part is zero. The ratio of E'' to E' is called the loss angle tangent. If $E''\cdot E'^{-1} > 1$, the monolayer has a more viscous character, while $E''\cdot E'^{-1} < 1$ implies an elastic behavior. The E' and E'' modulus and $E''\cdot E'^{-1}$ ratio as a function of f are shown in Fig. 5a and Fig. 5b, respectively. E' and E'' depended linearly on the frequency of oscillations in the studied range. In the case of the studied system, the values of the elastic modulus E' were higher than the values of the viscous modulus E'' , which indicated the formation of an elastic DPPC monolayer. The illumination of DPPC containing Au-NRs resulted in a decrease in both E' and E'' ; however, the values of E' remained higher than those of E'' , which indicated the formation of an elastic monolayer under illumination. The decrease in $E''\cdot E'^{-1}$ ratio increase elasticity of the illuminated monolayer, see Fig. 5b, was probably caused by a decrease in the number and size of the more rigid domains formed by the Au-NRs. The observed effect could be caused by the desorption of part of the Au-NRs from the air–water interface during Langmuir monolayer compression to a target surface pressure. However, our previous studies [32] for pure Au-NRs showed that the compression process of the Au-NRs was reversible. Moreover, the iso-

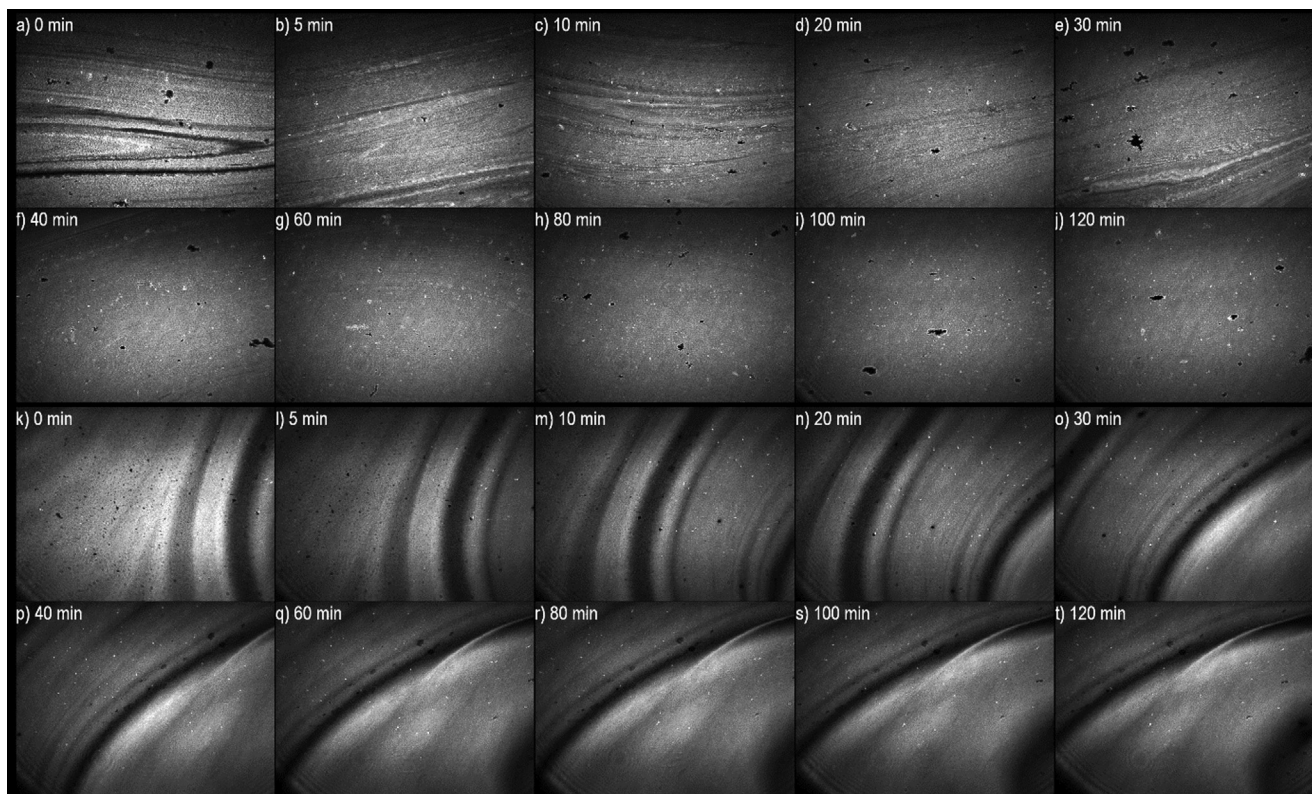


Fig. 4. Brewster angle microscope images of DPPC containing Au-NRs, with (a)–(j) and without (k)–(t) light illumination, collected during the relaxation experiments shown in Fig. 3 for the various times indicated on each panel.

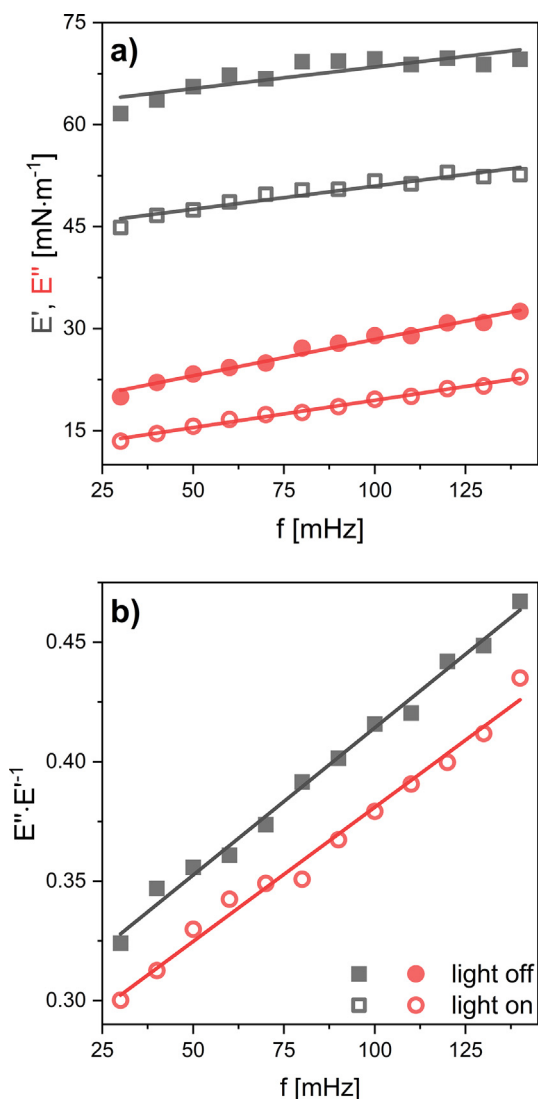


Fig. 5. Dependencies of the elastic (E') and viscous (E'') modulus (a) and $E''/E'-1$ ratio (b) on the oscillation frequency (f) of the Au-NRs with and without photoactivation. (For interpretation of the references to colour in this figure legend, the reader is referred to the web version of this article.)

therms recorded for both the compression and expansion of Au-NRs shown in Fig. S3 were characterized by an almost identical course, which proved the lack of aggregation of Au-NRs upon monolayer compression. Moreover, pegylated Au-NRs adsorb onto the hydrophilic head-groups of the interfacial DPPC molecules, thus the desorption of Au-NRs into the aqueous subphase was limited. Similar results were also obtained by Ruiz-Rincón et al. [36], who investigated the effect of local heating of NPs on model cell membranes. For this purpose, isolated iron oxide magnetic nanoparticles (MNPs) coated with oleic acid molecules were used. The model membrane produced in the research consisted of DPPC and cholesterol (Chol) in a 1:1 ratio, which play a significant role in biological membranes. DPPC:Chol 1:1 monolayer was deposited on a mica substrate using the Langmuir-Blodgett technique at a surface pressure of $35 \text{ mN}\cdot\text{m}^{-1}$. Then, MNPs were deposited on the prepared substrate at a surface pressure of $15 \text{ mN}\cdot\text{m}^{-1}$, which allowed to study the influence of the external magnetic field on the properties of the system. The authors conclude that the changes in the morphology of the model cell membrane result from the influence of the magnetic field on the MNPs. The deposited MNPs at the top of the model cell membrane are able

to penetrate the monolayer due to an increase in the film fluidity arising from the local temperature increase.

4. Conclusions

The aim of this study was to explain how excitation of Au-NRs affects the properties of a model cell membrane. Due to the high values of light-to-heat conversion efficiency of the investigated Au-NRs, the temperature of the monolayer gradually increased, causing a local temperature increase. The shape of the isotherms for the DPPC containing Au-NRs with and without illumination were similar. However, due to the induction of LSPR upon monolayer illumination for surface pressures above $8 \text{ mN}\cdot\text{m}^{-1}$, the illuminated isotherm was shifted towards higher trough area values, which remained constant once obtained. Surface potential studies proved that the increase in the occupied area of DPPC was not attributable to structural changes in DPPC, but rather to changes in the mutual distances between DPPC molecules. The illuminated monolayer, at a surface pressure corresponding to that in a native cellular membrane, was more stable and had more elastic character compared to the cell membrane without illumination. Furthermore, the membrane became rigid 40 min after reaching $30 \text{ mN}\cdot\text{m}^{-1}$. Our study showed that the packing and phase behavior of mimetic cell membranes could be changed upon the addition of small quantities of Au-NRs combined with monolayer illumination.

CRedit authorship contribution statement

Beata Tim: Investigation, Visualization, Methodology, Data curation, Writing – original draft. **Paulina Błaszkiwicz:** Investigation, Writing – original draft. **Michał Kotkowiak:** Conceptualization, Investigation, Methodology, Visualization, Data curation, Writing – original draft, Writing – review & editing, Supervision, Funding acquisition.

Declaration of Competing Interest

The authors declare that they have no known competing financial interests or personal relationships that could have appeared to influence the work reported in this paper.

Acknowledgment

This work was supported by the National Science Center in Poland by the project 2019/35/D/ST4/02037.

Appendix A. Supplementary material

Supplementary data to this article can be found online at <https://doi.org/10.1016/j.molliq.2021.118179>.

References

- [1] H. Gao, Y. Bi, X. Wang, M. Wang, M. Zhou, H. Lu, J. Gao, J. Chen, Y. Hu, Near-infrared guided thermal-responsive nanomedicine against orthotopic superficial bladder cancer, *ACS Biomater. Sci. Eng.* 3 (12) (2017) 3628–3634.
- [2] B. Zhang, I. Ahmed, P. Wang, Y. He, *Nanomaterials in the Environment and their Health Effects*, second ed., Elsevier, 2019.
- [3] P. Błaszkiwicz, M. Kotkowiak, Gold-based nanoparticles systems in phototherapy – current strategies, *Curr. Med. Chem.* 25 (42) (2019) 5914–5929.
- [4] F. Wang, P. Liu, L. Sun, C. Li, V.A. Petrenko, A. Liu, Bio-mimetic nanostructure self-assembled from Au@Ag heterogeneous nanorods and phage fusion proteins for targeted tumor optical detection and photothermal therapy, *Sci. Rep.* 4 (1) (2015).
- [5] P.K. Jain, M.A. El-Sayed, Plasmonic coupling in noble metal nanostructures, *Chem. Phys. Lett.* 487 (4-6) (2010) 153–164.

- [6] I.H. El-Sayed, X. Huang, M.A. El-Sayed, Surface plasmon resonance scattering and absorption of anti-EGFR antibody conjugated gold nanoparticles in cancer diagnostics: applications in oral cancer, *Nano Lett.* 5 (2005) 829–834.
- [7] M. Skrzypiec, M. Weiss, K. Dopierała, K. Prochaska, Langmuir-Blodgett films of membrane lipid in the presence of hybrid silsesquioxane, a promising component of biomaterials, *Mater. Sci. Eng., C* 105 (2019) 110090–110100.
- [8] M.J. Davies, J.W. Birkett, H. Bolton, A. Moore, The influence of cannabis smoke and cannabis vapour on simulated lung surfactant function under physiologically relevant conditions, *Surf. Interface Anal.* 51 (5) (2019) 558–565.
- [9] A.J. Sheridan, J.M. Slater, T. Arnold, R.A. Campbell, K.C. Thompson, Changes to DPPC domain structure in the presence of carbon nanoparticles, *Langmuir* 33 (39) (2017) 10374–10384.
- [10] M. Rojewska, M. Skrzypiec, K. Prochaska, The wetting properties of Langmuir-Blodgett and Langmuir-Schaefer films formed by DPPC and POSS compounds, *Chem. Phys. Lipids* 221 (2019) 158–166.
- [11] E. Piosik, M. Ziegler-Borowska, D. Chełminiak-Dudkiewicz, T. Martyński, Effect of aminated chitosan-coated Fe₃O₄ nanoparticles with applicational potential in nanomedicine on DPPG, DSPC, and POPC Langmuir monolayers as cell membrane models, *Int. J. Mol. Sci.* 22 (2021) 2467–2483.
- [12] E. Piosik, A. Zaryczniak, K. Mylkie, M. Ziegler-Borowska, Probing of interactions of magnetite nanoparticles coated with native and aminated starch with a DPPC model membrane, *Int. J. Mol. Sci.* 22 (2021) 5939–5963.
- [13] E. Guzmán, L. Liggieri, E. Santini, M. Ferrari, F. Ravera, Influence of silica nanoparticles on phase behavior and structural properties of DPPC-Palmitic acid Langmuir monolayers, *Colloids Surfaces A Physicochem. Eng. Asp.* 413 (2012) 280–287.
- [14] M. Pinheiro, J.J. Giner-Casares, M. Lúcio, J.M. Caio, C. Moiteiro, J.L.F.C. Lima, S. Reis, L. Camacho, Interplay of mycolic acids, antimycobacterial compounds and pulmonary surfactant membrane: a biophysical approach to disease, *Biochim. Biophys. Acta - Biomembr.* 1828 (2) (2013) 896–905.
- [15] X. Ye, C. Hao, J. Yang, R. Sun, Influence of modified silica nanoparticles on phase behavior and structure properties of DPPC monolayers, *Colloids Surfaces B Biointerfaces* 172 (2018) 480–486.
- [16] S. Tatur, A. Badia, Influence of hydrophobic alkylated gold nanoparticles on the phase behavior of monolayers of DPPC and clinical lung surfactant, *Langmuir* 28 (1) (2012) 628–639.
- [17] J. Hu, X. Li, M. Li, Y. Shang, Y. He, H. Liu, Real-time monitoring of the effect of carbon nanoparticles on the surface behavior of DPPC/DPPG Langmuir monolayer, *Colloids Surfaces B Biointerfaces* 190 (2020) 110922–110932.
- [18] P.M.P. Lins, V.S. Marangoni, T.M. Uehara, P.B. Miranda, V. Zucolotto, J. Cancino-Bernardi, Differences in the aspect ratio of gold nanorods that induce defects in cell membrane models, *Langmuir* 33 (50) (2017) 14286–14294.
- [19] M. Dwivedi, R. Harishchandra, O. Koshkina, M. Maskos, H.-J. Galla, Size influences the effect of hydrophobic nanoparticles on lung surfactant model systems, *Biophys. J.* 106 (1) (2014) 289–298.
- [20] X. Lin, T. Bai, Y.Y. Zuo, N. Gu, Promote potential applications of nanoparticles as respiratory drug carrier: insights from molecular dynamics simulations, *Nanoscale* 6 (2014) 2759–2767.
- [21] X. Lin, Y.Y. Zuo, N. Gu, Shape affects the interactions of nanoparticles with pulmonary surfactant, *Sci. China Mater.* 58 (1) (2015) 28–37.
- [22] F. Schulz, W. Friedrich, K. Hoppe, T. Vossmeier, H. Weller, H. Lange, Effective PEGylation of gold nanorods, *Nanoscale* 8 (13) (2016) 7296–7308.
- [23] V. Bouzas, T. Haller, N. Hobi, E. Felder, I. Pastoriza-Santos, J. Pérez-Gil, Nontoxic impact of PEG-coated gold nanospheres on functional pulmonary surfactant-secreting alveolar type II cells, *Nanotoxicology* 8 (8) (2014) 813–823.
- [24] P.A. Oroskar, C.J. Jameson, S. Murad, Rotational behaviour of PEGylated gold nanorods in a lipid bilayer system, *Mol. Phys.* 115 (9–12) (2017) 1122–1143.
- [25] B. Nikoobakht, M.A. El-Sayed, Preparation and growth mechanism of gold nanorods (NRs) using seed-mediated growth method, *Chem. Mater.* 15 (10) (2003) 1957–1962.
- [26] P. Błaszkiwicz, M. Kotkowiak, E. Coy, A. Dudkowiak, Laser-induced optoacoustic spectroscopy studies of inorganic functionalized metallic nanorods, *J. Phys. Chem. C* 123 (44) (2019) 27181–27186.
- [27] K. Rahme, L. Chen, R.G. Hobbs, M.A. Morris, C. O'Driscoll, J.D. Holmes, PEGylated gold nanoparticles: polymer quantification as a function of PEG lengths and nanoparticle dimensions, *RSC Adv.* 3 (2013) 6085–6094.
- [28] P. Szustakiewicz, N. Kolsut, A. Leniart, W. Lewandowski, Universal method for producing reduced graphene oxide/gold nanoparticles composites with controlled density of grafting and long-term stability, *Nanomaterials* 9 (2019) 1–16.
- [29] A. Gole, C.J. Murphy, Seed-mediated synthesis of gold nanorods: role of the size and nature of the seed, *Chem. Mater.* 16 (2004) 3633–3640.
- [30] P. Błaszkiwicz, M. Kotkowiak, E. Coy, A. Dudkowiak, Tailoring fluorescence and singlet oxygen generation of a chlorophyll derivative and gold nanorods via a silica shell, *J. Phys. Chem. C* 124 (3) (2020) 2088–2095.
- [31] X. Huang, M.A. El-Sayed, Plasmonic photo-thermal therapy (PPTT), *Alexandria J. Med.* 47 (1) (2011) 1–9.
- [32] B. Tim, P. Błaszkiwicz, A.B. Nowicka, M. Kotkowiak, Optimizing SERS performance through aggregation of gold nanorods in Langmuir-Blodgett films, *Appl. Surf. Sci.* 573 (2022) 151518–151527.
- [33] A.G. Bykov, E. Guzmán, R.G. Rubio, M.M. Krycki, O.Y. Milyaeva, B.A. Noskov, Influence of temperature on dynamic surface properties of spread DPPC monolayers in a broad range of surface pressures, *Chem. Phys. Lipids* 225 (2019) 104812–104818.
- [34] M. Rojewska, B. Tim, K. Prochaska, Interactions between silica particles and model phospholipid monolayers, *J. Mol. Liq.* (2021) 116999, 11709.
- [35] A.K. Sachan, R.K. Harishchandra, C. Bantz, M. Maskos, R. Reichelt, H.-J. Galla, High-resolution investigation of nanoparticle interaction with a model pulmonary surfactant monolayer, *ACS Nano* 6 (2) (2012) 1677–1687.
- [36] S. Ruiz-Rincón, A. González-Orive, V. Grazú, R.M. Fratila, J.M.d.I. Fuente, P. Cea, Altering model cell membranes by means of localized magnetic heating, *Colloids Surfaces B Biointerfaces* 196 (2020) 111315–111323.

Supplementary material

for

**Altering model cell membranes by means of photoactivated
organic functionalized gold nanorods**

Beata Tim, Paulina Błaszczewicz, Michał Kotkowiak*

Faculty of Materials Engineering and Technical Physics, Poznan University of Technology,
Piotrowo 3, 60-965 Poznan, Poland

To whom correspondence should be addressed:

*E-mail: michal.kotkowiak@put.poznan.pl (M.K.)

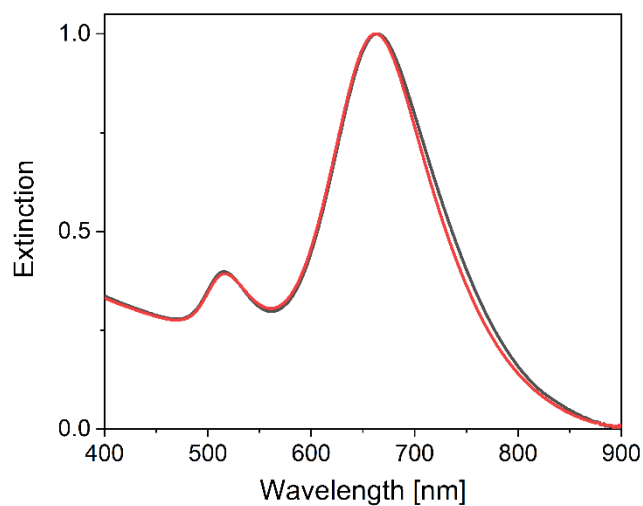


Fig. S1. Extinction spectra of Au-NRs functionalized with CTAB (black line) and PEG (red line).

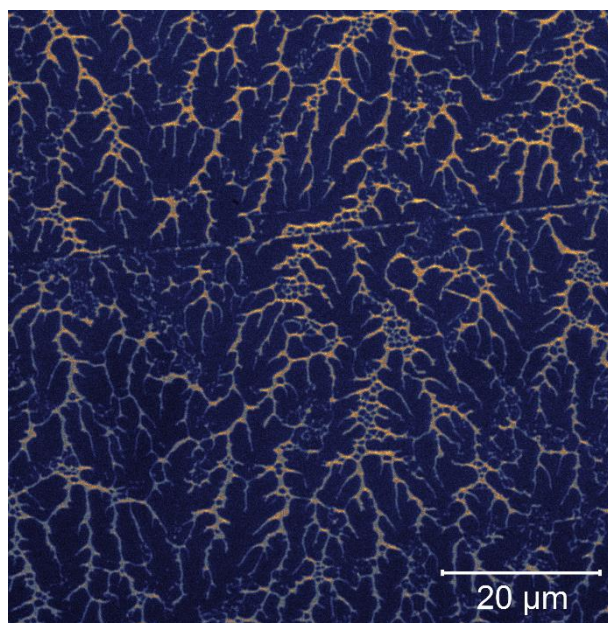


Fig. S2. Example of confocal microscopy image of Au-NRs Langmuir-Blodgett layers deposited on quartz substrates for surface pressures of $12 \text{ mN}\cdot\text{m}^{-1}$ [1].

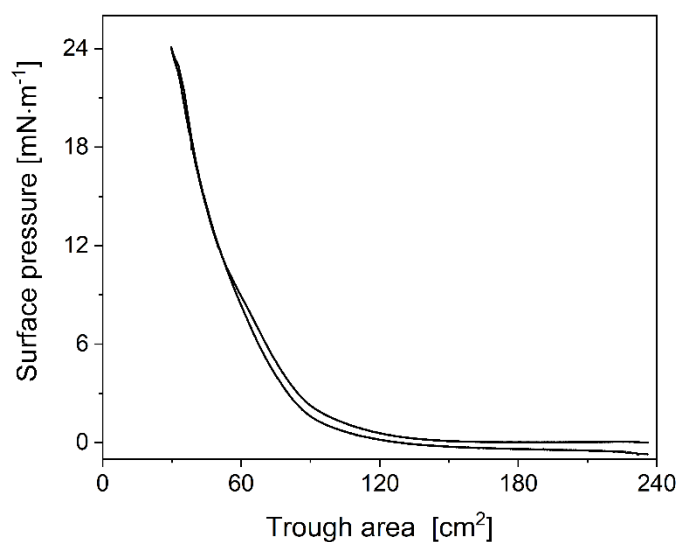


Fig. S3. The surface pressure *versus* trough area hysteresis of Au-NRs Langmuir monolayer [1].

References

- [1] B. Tim, P. Błaszkiwicz, A.B. Nowicka, M. Kotkowiak, Optimizing SERS performance through aggregation of gold nanorods in Langmuir-Blodgett films, *Appl. Surf. Sci.* 573 (2022) 151518–151527.